X-ray Spectroscopic Study of Tungsten Compounds

THESIS SUBMITTED FOR THE DEGREE OF

DOCTOR OF PHILOSOPHY

IN THE FACULTY OF SCIENCE

GOA UNIVERSITY

GOA 403 205

BY

SHANTANU A. GAUNS

UNDER THE GUIDANCE OF

PROFESSOR P. R. SARODE

DEPERTMENT OF PHYSICS

GOA UNIVERSITY

GOA 403 205

October, 1996

To

My Papa and Ayi

DECLARATION

The author declares that this thesis hereby submitted represents work which has been carried out by him and that it has not been submitted to any other University or Institution for the award of any Degree, Diploma, Associateship, Fellowship or any other such title.

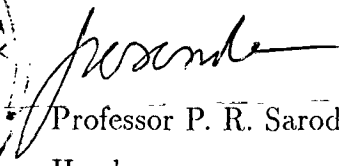Place: Taleigao Plateau.

Date : October, 1996

(Shantanu A. Gauns)

CERTIFICATE

I hereby certify that the above Declaration of the candidate Shantanu A. Gauns is true and that this thesis represents his independent work.

Professor P. R. Sarode

Head

Department of Physics

Goa University, Goa

October 24, 1996

T-126

Contents

List of Figures

List of Tables

Chapter 1

Introduction

1.1 Introduction

The element tungsten (W) with atomic number 74 is one of the so-called "less-common metals" and occurs in the periodic group VIa with chromium (atomic number 24) and molybdenum (atomic number 42). In all its properties it closely resembles the latter element. In the pure metallic state tungsten has a lustre somewhat like that of steel.

The chemistry of tungsten is very vast [1-3] covering nine oxidation states from -2 to +6. Tungsten has been studied since the characterization of tungstic acid by Woulffe in 1779 and Scheele in 1781. Further studies on its oxychlorides [4], halides [3, 5]; their derivatives [6] and cynide complexes [7] were carried out by different researchers. The discovery of metal-sandwitch type of compounds e.g., cyclopentadienyl compounds, led opening to the vast field [3] for research on tungsten compounds.

The synthesis of cyclopentadienyl compounds and use of tungsten metal in many technological applications is because of its characteristic physical properties like high melting point, electrical conductivity, mechanical properties, etc. This has renewed the interest in studies of compounds of tungsten in recent years [8]. Its mechanical properties are unusually influenced by small additions of contaminations thus resulting in changes in its microstructure has been exploited in recent years.

A number of inorganic compounds of tungsten like binary and complex halides have been prepared [8]. Several techniques like NMR [9], NQR [10], IR and Raman [11, 12] spectroscopies, X-ray and electron diffraction have been used for studying the properties of these compounds. These compounds mostly have monomeric structure and show weak paramagnetism. EPR studies [7] have been carried out on organometallic complexes of tungsten.

While tungstates of the composition MWO_4 (M = Sr, Ba, Pb) have the scheelite $CaWO_4$ structure, sodium tungstate, Na_2WO_4 crystallizes into spinel structure, and lithium tungstate and lithium molybdate are isostructural with beryllium silicate. All of these contain WO_4 tetrahedra. The tungstates MWO_4 (M = Ni, Mn, Co, Mg, Zn) are isostructural (space group C_{2h}^4) and are character-

ized by WO_6 octahedra [13]. Some of these tungstates find their use in making fluorescent materials and for laser crystals. Fusion of the alkali tungstates have also been studied in connection with molten tungstate baths used for electroplating with tungsten [14]. Tungstates of lead, zinc and sodium find their use in chemicals, paint-enamel, and textile industries [1]. The compounds formed in BaO-WO_3 system are of great importance because of their use as oxide cathodes [15]. $Bi_2(WO_4)_3$ has been frequently used as a catalyst in the process of dehydrogenation of butene to butadiene.

Infrared and NMR studies of the tungstic acid, the hydrated form of the trioxide have been carried out in order to confirm the presence of hydroxyl groups. These hydrated forms appear to contain only lattice water and not the OH groups [16]. The oxo anions of tungsten(VI) range from the simple WO_4^- tetrahedra and WO_6^{6-} octahedra to a highly polymeric species such as $W_{24}O_{72}(OH)_{12}^{12-}$ [2]. The salts of tungstic acid can be distinguished into three kinds, normal, meta and paratungstates and their chemistry has been reviewed in greater details by Aveston [17] and Glemser et al [18]. Sodium paratungstate is sometimes used in the dyeing industry as a mordant. Mild reduction of heteropolytungstates produces characteristic and very intense blue colour ("heteropoly blues"), which find application commercially as dyes and pigments [5].

Tungsten dioxide and tungsten trioxide are the well known oxides in the W-O system [19]. Two mixed valence phases, $W_{18}O_{49}(WO_{2.72})$ and $W_{20}O_{58}(WO_{2.90})$ also exist in the range $WO_2 - WO_3$, and substoichiometric phases of WO_3, viz. $WO_{2.96}(W_{50}O_{148})$ and $WO_{2.98}(W_{40}O_{119})$ have been characterized in the literature [20]. Measurements of resistivity and Seebeck coefficient indicate that some of the oxides show metallic behaviour. Sienko and coworkers [21] have investigated in detail the mechanism of electrical conduction in stoichiometric and oxygen-deficient oxides of tungsten. WO_3 in combination with other metal oxides forms very interesting mixed oxides called "tungsten bronzes". The physical properties of these bronzes have been examined in great detail and have been discussed in the literature [22]. A number of catalytic compounds of tungsten have also been synthesized and characterized. The mixed oxides of tungsten and $\gamma - Al_2O_3$ have found their use as industrial catalyst.

However since the work reported in this thesis deals mainly with studies on tungsten oxide bronzes and the catalytic compounds of tungsten, a brief account of these complex systems is given below.

1.2 Tungsten Bronzes

The oxide bronzes have chemical formula $M_x TO_n$ in which the electropositive M metal atoms are inserted into covalent network TO_n of oxygen and transition metal T atoms. Insertion of the M atoms reduces the covalent network, thereby introducing d state electrons which may be either localised at the transition elements T imparting it a semiconductor character, or delocalosed over the TO_n subarray, giving to it metallic properties.

The structure of the oxide bronzes obviously reflects the character of TO_n subarray. It also depend upon the choice of the element M, its concentration x and the temperature of preparation. With increase in concentration x, the crystallographic sites available to the M atoms approach saturation. However, the value of x for which the phase $M_x TO_n$ stops being thermodynamically stable is generally less than the concentration of crystallographically available sites.

It has recently also been shown that more complex oxide bronzes may exist. For example, two transition elements may simultaneously occupy the covalent subarray, or on the other hand, M atoms may be introduced giving a more complex substitutional mechanism in which the TO network expands with the loss of M atoms. At a given temperature, the compositional ranges of such phases are given by a two-divisional region in the equilibrium diagram. The mean oxidation state (2n-x) of the transition element is intermediate between maximum value p and (p-1) because of a structural constraint. History reveals that the best studied of the bronzes are those of tungsten. These tungsten bronzes have general formula $M_x WO_3$, (x < 1); where M may be a rare-earth or an alkali [23]. The covalent WO_3 array consists of tungsten-occupied oxygen octahedra, distorted or regular, sharing common corners as hinges. The W-O-W angles may be varied so as to create a variety of tunnels into which the foreign M atoms like barium, lead, thallium, copper or silver can be inserted [24].

4

Ostertag [24], in 1966, prepared a large number of lanthanide bronzes of the composition $M_{0.1}WO_3$ (M = Ce, Pr, Nd, Sm, Eu, Gd, Tb, Dy, Ho, Er, Tm and Lu) by the solid state reaction of metallic tungsten with a mixture of WO_3 and a trivalent rare-earth oxide. Single crystals of these bronzes several millimeters in length are generally synthesized by electrolytic reduction at 1200^0C containing a mixture of (WO_3 + tungstate) or (WO_3 + chloride). Two types of phases are found : cubic perovskite and pseudocubic tetragonal. Each phase has a compositional range ($0.085 < x < 0.16$ for the cubic phase, and $x < 0.085$ for the tetragonal phase, as in europium and gadolinium). For the lanthanum and yttrium bronzes [24] the upper concentration limit become smaller as the ionic radius decreases : $x=0.19$ for La^{3+} (1.14 Å), $x=0.16$ for Gd^{3+}(0.97 Å), $x=0.15$ for Y^{3+}(0.91 Å) similar to alkali bronzes. Increase in the charge of the insertion cation appreciably reduces the stability of the tungsten bronzes. The physical and chemical properties of rare-earth tungsten bronzes have been studied by several researchers [25, 26]. The magnetic susceptibility measurements [27] of these compounds indicate that the rare-earth ions account for the magnetic moment.

1.3 Tungsten Catalysts

A catalyst is a substance which increases the rate of a chemical reaction without being consumed in the process. In general, catalytic process may be classified as homogeneous or heterogeneous. In homogeneous catalysis, the reactants are present in a single phase, commonly a liquid solution. In heterogeneous catalysis, the reactants and catalyst are present as separate phases. Many a times the reactants are in the form of vapour while the catalyst is a solid. However, other combinations of phases such as liquid-liquid are also possible. Both types of catalytic processes are of considerable scientific interest and are important technologically [28].

Solid catalysts may be classified in two broad categories metals and nonmetals. The later are frequently oxides. Solid catalysts of practical interest are generally high surface area materials. In some cases the catalyst is highly porous material.

Most of the surface area then resides in the walls of the pores, and is often termed the "internal surface" of the solid. For highly porous solids, the internal surface area of a particle is frequently several orders of magnitude higher that the external surface area. Activated alumina is a highly porous material of this type with surface areas commonly in the range 100-300 m^2/gm. It is employed as a catalyst for dehydration of alcohols or for the skeletal isomerization of olefins. Often the active component of a catalyst is supported on a carrier to achieve high dispersion. The carrier is usually a high surface area refractory material such as silica or alumina.

Supported metal catalysts are highly important in industries. A method commonly employed in the preparation of such catalysts is called impregnation. The method involves contacting of a carrier with a solution of a salt of the metal of interest. The solute deposits on the carrier, and the resulting material is then dried and often calcined at higher temperature. The material dispersed on the carrier is then reduced to the metallic form, usually by contact with a stream of hydrogen at elevated temperature forming small metal clusters or crystallites dispersed over the carrier surface.

Nonmetallic catalysts of interest are frequently oxides such as alumina, chromia, titania or molybdena. Such catalysts are commonly prepared by procedures involving precipitation or gel formation method. The use of a carrier in a nonmetallic catalyst, as in the case of metal catalysts, is a common method of improving the degree of dispersion of the active catalytic component. Such catalysts are generally prepared by impregnation or coprecipitation procedures. The coprecipitated material is then dried and calcined at higher temperature. Amongst different catalysts, titania supported tungsten oxide catalysts are very important [21-32]. These catalysts are known to be very efficient for various acid-catalyzed heterogeneous reactions [29], preferentially for the disproportionation of propane [30, 31]. For the selective catalytic reduction of NO by NH_3, they are of interest in the industrial application because of their activity at high temperature, their thermal stability and low oxidation activity for SO_2 [32, 33]. Similarly the nickel-tungsten-alumina catalysts are also very useful in industries due to their catalytic action in many catalytic reactions such as hydrodesulphurization,

6

hydrocracking and hydrogenation processes [34, 35].

To a considerable extent our understanding of the properties of chemical systems like catalysts or complex oxides at the microscopic level comes from probes of structure. Of the many structure probes that have been developed, the most useful would be X-ray diffraction. Information, at the atomic or molecular level can be obtained by various spectroscopies, spanning the electromagnetic spectrum. Amongst many structure probes, X-ray absorption spectroscopy is frequently used to study local atomic environment around the absorbing ions in complex systems. In the following section the principles involved in the X-ray absorption process and different spectral features in the X-ray absorption spectra and their relation to various physico-chemical parameters are briefly described.

1.4 The Process of X-ray Absorption

The interaction of X-rays with matter [36, 37] results in a number of interesting phenomena such as, scattering, photoelectron absorption, pair production (in the case of X-rays of energy > 1.02 MeV), secondary emission, Auger emission etc. The analysis of the attenuation, generally logarithmic of X-ray intensity requires, therefore, the segregation of the various processes involved, of which the photoelectric absorption is usually the most important and is referred to as the true absorption.

When an X-ray beam passes through a medium, the intensity of the transmitted beam I is attenuated logarithmically. According to the classical absorption equation, if the incident beam of intensity I_o has travelled a distance x, then the absorption coefficient

$$\mu_l = -\left(\frac{1}{x}\right) \ln \frac{I}{I_o} \qquad (1.1)$$

It follows from equation(1.1) that the dimensions of μ_l are reciprocal centimetres so that it represents the attenuation of the beam per unit length travelled and is called the linear absorption coefficient. It turns out to be dependent on the energy (wavelength) of the X-rays, the atomic numbers of the constituent atoms, and on their state of aggregation.

Calculation of the linear absorption coefficient is complicated by this last fact so that it is more convenient to use a *mass* absorption coefficient

$$\mu_m = \frac{\mu_l}{\rho} \tag{1.2}$$

where ρ is the density of the absorbing medium and μ_m is the absorption cross section of the mass unit.

In the analysis of the dependence of μ on wavelength and atomic number, it is most convenient to define an *atomic* absorption coefficient

$$\mu_a = \frac{A}{N_o}\mu_m \tag{1.3}$$

where A is the atomic weight of the element and N_o is Avogadro's number. A plot of μ_a against wavelength, for any element, has the general appearance of the curve shown in Fig.1.1. The absorption increases with increasing wavelength (decreasing energy of incident X-rays) until an abrupt discontinuity occurs. After this discontinuity, called an *absorption edge*, the absorption increases with wavelength until new discontinuities are encountered. An empirical study of the relation between the atomic absorption coefficient and the X-ray wavelength and atomic number (Z) of the absorbing atoms shows that curve like that in Fig.1.1 can be described by

$$\mu_a = CZ^m\lambda^n + \sigma_a(Z,\lambda) \tag{1.4}$$

where the coefficient C takes on different values on each side of an absorption edge and the "best" values for the two exponents are m = 4 and n = 3. The second term in equation(1.4) is called the *atomic scattering cross section* σ_a and represents the intensity lost due to the scattering in directions other than that of the incident beam. For wavelengths that are large compared to electron-electron distances in atoms $\lambda > 0.5$ Å, σ_a is nearly independent of wavelength and increases in proportion to Z. Since the first term in equation(1.4) increases with both Z and λ much more rapidly, the second term may be neglected by comparison. At shorter wavelengths, the λ dependence becomes more complex but, because of severe experimental difficulties in measuring the scattering part of equation(1.4), an accurate dependence has not been established. Since the second

8
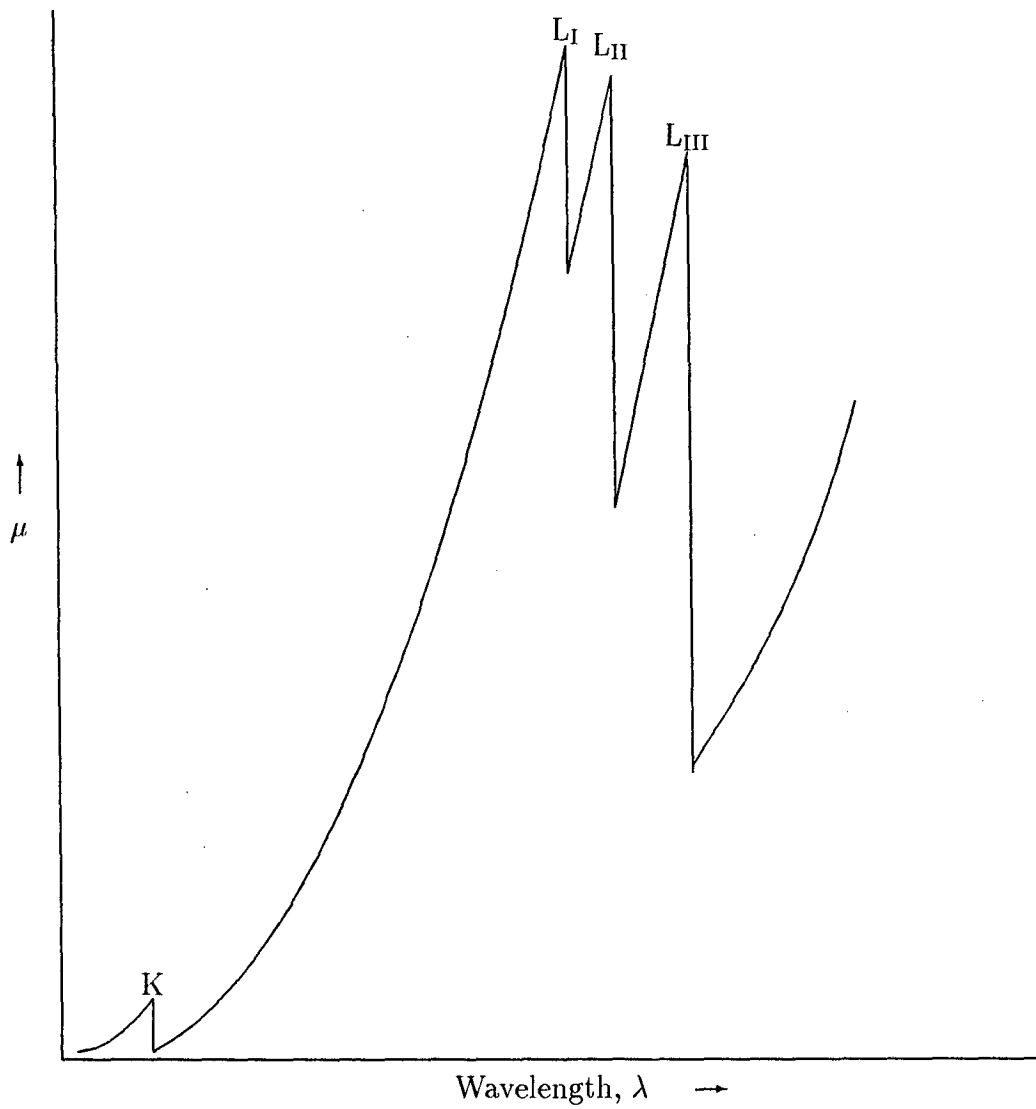
Fig. 1.1: Schematic illustration of the variation of the atomic absorption coeffi-
cient, μ with wavelength, λ

term is small (typically, $\sigma/\rho \sim 0.10$ to 0.20 cm^2/gm), it is normally neglected in the discussion of absorption coefficients. This is an acceptable practice for all but for the lightest elements, for which the total absorption coefficient may have commensurate magnitudes (For carbon, $\mu_m < 4.0$ cm^2/gm for $\lambda < 1.5$ Å).

The first term in equation(1.4) is of primary interest, not only because it is relatively much larger but also because it represents the wavelength and Z dependence of the photoelectric absorption process for X-rays. As can be seen in Fig.1.1, as the wavelength of the transmitted X-rays increases, the photoelectric absorption increases proportionally to λ^3, until a critical wavelength is reached. For wavelengths longer than that at the absorption edge, the incident X-rays have insufficient energy to knock out a particular kind of bound electron in the atom, and the photoelectric ejection of such electrons no longer contributes to the absorption process. The absorption edges in Fig.1.1 are called the K, L_I, L_{II}, and L_{III} edges, respectively, according to the inner electron whose binding energy equals the energy at the absorption edge. Following the photoelectron ejection of an inner electron, the excited atom typically emits an X-ray photon, as an outer electron falls into the newly created hole, so that the first term in (1.4) is called the *fluorescence term.*

For free atoms [38], such as in the case of monoatomic gases, the processes of X-ray emission and absorption are simple and are well understood. However, these processes become rather complex when the atom is no more free, such as in solids and chemical compounds. The mechanism of X-ray emission and absorption in a solid [39, 40] is shown in Fig.1.2. In a solid the valence electrons of the neighbouring atoms interact with each other and the energy levels are no longer discrete as in the case of free atoms but are broadened, the outer ones being more broad than the inner ones and from quasi-continuous valence and conduction bands. The X-ray emission band spectrum results from the transition of the electrons from the valence band to an inner level. It provides information about the distribution of the occupied electron states in the valence band, since the inner level is generally sharp and well-defined. The X-ray absorption spectrum, on the other hand, corresponds to the transitions of the ejected photoelectron to empty states, bound or unbound of proper symmetry, and provides complemen-

10
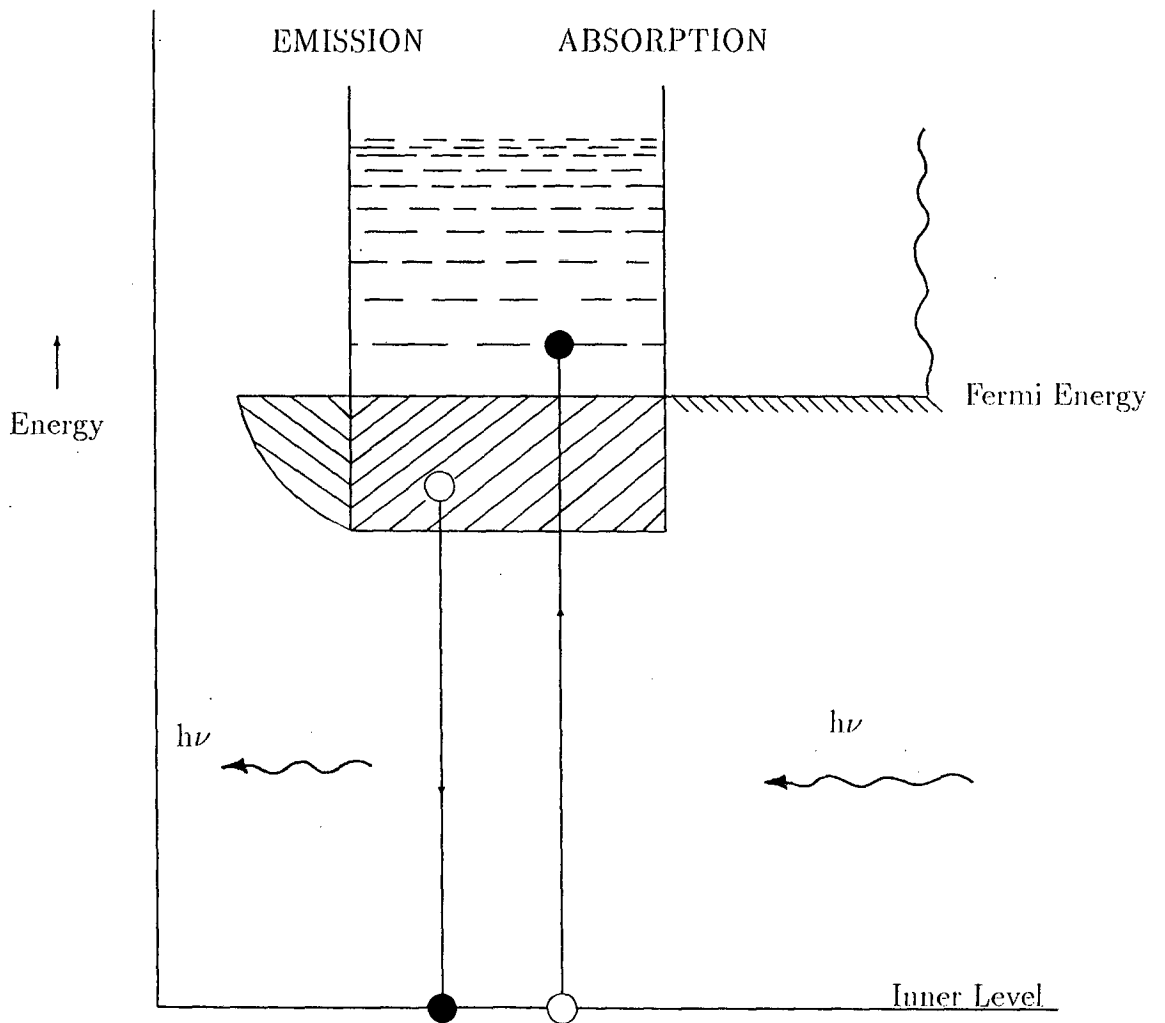
Figure 1.2: The mechanism of X-ray Absorption and Emission

tary information about the density of unoccupied electronic energy states.

1.4.1 The Position, Shape and Fine Structure of an X-ray Absorption Discontinuity

In the X-ray emission process, if $I(\nu)$ denotes the intensity per unit frequency range, then $I(\nu)d\nu$ is the intensity of X-rays emitted with frequencies in the range $d\nu$ corresponding to the energy range dE and the expression for $I(\nu)$ is given [40] as

$$I(\nu) = \frac{ne^2h^3\Omega\nu^2}{3\pi^3m^2c^3} \int_s \frac{|M_{fi}|^2}{|grad\ E|} ds \qquad (1.5)$$

where Ω is the volume of the unit cell, n is the number of radiators per unit volume, M_{fi} is the matrix element or the transition probability, subscript i and f correspond to the initial and the final states respectively and the integration is carried out over a constant energy surface in k-space. Equation (1.5) represents the observed frequency distribution within an emission band.

In the X-ray absorption process, if $A(\nu)d\nu$ denotes the energy absorbed per unit time by an atom in the electron transition from a sharp inner level to a band of empty states in an energy range dE and $I_o(\nu)d\nu$ is the incident intensity (energy per unit area per unit time), then the linear absorption coefficient (in cm^{-1}) is given by

$$\mu_A(\nu) = n \frac{A(\nu)d\nu}{I_o(\nu)d\nu} \qquad (1.6)$$

where n represents the number of atoms per cm^3.

On the basis of Dirac's radiation theory, the energy absorbed per second per unit frequency range by one atom may be expressed as

$$\alpha(\nu) = \frac{e^2h}{2\pi m^2c\nu}|M_{fi}|^2 I_o(\nu) \qquad (1.7)$$

Furthermore, $E = h(\nu - \nu_0)$, where $h\nu$ is the energy of the incident photon and $h\nu_0$ is the energy interval between the initial X-ray level and the unoccupied state of lowest energy. Upon averaging over the three directions of the electron momentum, the power absorbed in transitions into a number of closely grouped

12

states spread over an energy interval $hd\nu$ becomes

$$A(\nu)d\nu = \frac{e^2\hbar^2\Omega I_o(\nu)d\nu}{6\pi^2 m^2 c\nu} \int_s \frac{|M_{fi}|^2}{|gradE|} ds \qquad (1.8)$$

Hence from equation (1.8)

$$\mu(\nu) = \frac{ne^2\hbar^2\Omega}{6\pi^2 m^2 c\nu} \int_s \frac{|M_{fi}|^2}{|gradE|} ds \qquad (1.9)$$

The above expression can be approximated [41] to

$$\mu(E) \propto \nu P(E)N(E) \qquad (1.10)$$

where N(E) is the density of unoccupied states at energy E and P(E) is the transition probability for a transition involving the two states concerned, with the initial state being the core state and the final state being one in which an electron is excited to a normally unoccupied level in the valence or conduction band. It is very difficult to calculate theoretically P(E) for such transitions in the case of solids. However, the selection rules often help in giving a rough estimate of the transition probability. Assuming the dipole approximation to be valid for solids, one can assume the K, L_I, ... absorption spectra to reflect the density of unoccupied p like states in the conduction band, and the L_{II}, L_{III}, M_{III}, ... spectra to reflect the density of d and s electron states. In a given band the transition probability is generally assumed [42] to be a monotonous function of energy.

The first significant attempt towards the explanation of the shape of an X-ray absorption discontinuity in a solid was that of Richtmyer, Barnes and Ramberg [43] who described the absorption edge in terms of a series of absorption lines with equal widths and having equal transition probabilities. In their work, Richtmyer et al. employed the following expression for the intensity distribution function $J_{AB}(\nu)d\nu$ for an absorption line, given by Weisskopf and Wigner [44].

$$J_{AB}(\nu)d\nu = \frac{\Gamma_A + \Gamma_B}{2\pi} \cdot \frac{d\nu}{\left(\nu_{AB} - \nu\right)^2 + \left[\frac{(\Gamma_A+\Gamma_B)}{2}\right]^2} \qquad (1.11)$$

where A and B refer to the initial and final states involved in the electronic transition, ν_{AB} is the frequency corresponding to the transition and is

$$\nu_{AB} = \nu_A - \nu_B = (E_A - E_B)/h \qquad (1.12)$$

13

and Γ_A and Γ_B are related to the mean life-times τ_A and τ_B of the states A and B respectively through the relations

$$\Gamma_A = \frac{1}{2}\pi\tau_A \quad \text{and} \quad \Gamma_B = \frac{1}{2}\pi\tau_B \tag{1.13}$$

Richtmyer et al have discussed using the relation (1.11) the shape of the L_{III} absorption discontinuity of gold and have shown that the variation of the absorption coefficient in the vicinity of the absorption discontinuity follows an arc-tan curve given by the formula

$$\mu(E) = constant \left[\frac{1}{2} - \frac{1}{\pi} \arctan\left[\frac{\nu_{E_oA} - \nu}{\Gamma_E/2}\right]\right] \tag{1.14}$$

where Γ_E is the full width at the half maximum of each absorption line and ν_{E_oA} is the frequency difference between the initial state in the absorption process and the first one of the final states.

It is difficult to assess the exact importance of the above formula because of the absence of experimental verification of the assumptions leading to it and the lack of the knowledge of the transition probabilities. In spite of it, it has been found that in many cases there exists rather a close similarity between the theoretical arc-tan curve and the experimentally observed curves. Whenever such a close fit exists, the calculations leading to the above formula for $\mu(E)$ show that the inflection point on the absorption curve corresponds to a transition of the inner electron to the first available empty level in the solid.

A detailed study by Parratt [45] of the K-absorption discontinuity of gaseous argon (Z=18) has led to a further step in the understanding of the X-ray absorption process. He has decomposed the observed absorption curve, duly corrected for experimental distortions, into a series of resonance absorption lines corresponding to the transitions 1s $\rightarrow$ np, where n > 3. The wavelength positions of these absorption lines were calculated with the help of the optical terms of potassium (Z=19), since an ionized argon atom can be considered to be similar to a potassium atom. This study has been extended to the other inert gases by Brogren [46]. The approximation was further examined by Mitchell [47] for neon who cautioned that this model may not hold for very light atoms. In a different approach, Vainshtein and Narbutt [48] have calculated the relative intensities of

the various absorption lines assuming hydrogenic wavefunctions for the initial and final states for the inert gases.

Soules and Shaw [49] have studied the K-absorption spectrum of solid argon and have found that it differs very much from that obtained in the gaseous state. The absorption edge for the solid closely follows the theoretical arc-tan curve except in the region of maximum absorption. The first absorption maximum in the curve of the gas has approximately the same wavelength as the inflection point on the absorption curve of the solid. These results, together with Nilsson's [50] measurements of the absorption coefficients with different excitation voltages, confirm the view that the inflection point on an X-ray absorption discontinuity corresponds to the transition of an inner electron to the first unoccupied level in the conduction band of the solid.

Breinig et al. [51] have proposed a theoretical model for absorption edges and derived the following expression for the absorption cross section near the edge :

$$\sigma_{nlj}(E) = \sum_{n'l'j'} \frac{\Gamma/2\pi}{\left[E - (E_{n'l'j'} - E_{nlj})\right]^2 + \left(\frac{\Gamma}{2}\right)^2} + a\left[\frac{1}{2} + \frac{1}{\pi}tan^{-1}\frac{2}{\Gamma}\left(E + E_{nlj} + \epsilon'\right)\right]$$

(1.15)

for $E_{n'l'j'} < \epsilon'$. Here E_{nlj} and $E_{n'l'j'}$ are initial and final states in the transition, E denotes the photon energy, Γ is the width of the excited state and $\epsilon'(-0.5eV)$ the constant energy used for inclusion with the continuum the highest bound states whose widths exceed their separation. It is clear from this expression that the profile of the X-ray absorption discontinuity is nothing but a Lorentzian of appropriate height and width superimposed on an arc-tan curve. Breinig et al. have studied the K-absorption edge spectra of argon and krypton and L-absorption spectra of xenon. These workers decomposed their spectra into Lorentzians and an arc-tan curve. They found a good agreement between the peak position of Lorentzian corresponding to a particular electronic transition and the optical energy obtained from experiments.

Although rigorous calculations of the shapes of absorption discontinuity have been done by Breinig et al., for argon, krypton and xenon, these have not been to date (to our knowledge) for different absorption edges in solids. Nevertheless, it has been found useful and practical to perform numerical analysis on the absorp-

tion data in terms of the positions, widths and oscillator strengths of bound-state and resonance peaks and of an edge position, width, and height for the principal continuum edge. Cramer and Hodgson [52] have done such type of analysis by decomposing the Mo K-edge spectrum in $[Mo_7O_{24}]^{6-}$. These authors have shown that by fitting the absorption edge with several Lorentzians and an arctangent function, the positions and intensities of edge features may be quantitated. In the case of $Co/Mo/Al_2O_3$ catalysts, the Mo K-edge position was resolved into three Gaussians by least-squares fitting of nine parameters by Chiu et al [53] in order to find the extent of distortion of the octahedron of oxygen atoms in the first coordination shell. In this laboratory [54] also, the decomposition of K-edge profiles of transition metal ions in various compounds into Lorentzians and arctangent function has been done and it has been shown that the areas under different Lorentzians give a measure of extent of tetrahedral to octahedral clusters.

It has been often found that the position of an X-ray absorption discontinuity changes with the physicochemical environment of the absorbing atom. It was Bergengren [55] who first demonstrated the dependence of X-ray absorption discontinuities on chemical combination. He investigated the K-absorption edge of phosphorus in its various allotropic forms and found slight variations in the wavelength of the edge. Lindh [56], who carried out a number of experiments to study the effect of chemical combination on the wavelengths of the K-absorption discontinuities of chlorine, phosphorus and sulphur in various compounds, demonstrated that the wavelength of the X-ray absorption spectrum of an atom varies with its chemical state in the compound. Stelling [57] using spectrograph with higher dispersion than that used by Lindh has studied the K-absorption limit of chlorine in various chlorides. Aoyama et al [58] have studied the K-absorption limit of chlorine in various organic compounds. Coster [59] has studied the K-absorption edges of first row-transition metals in their different oxides and lent support to the earlier observations. These investigations were soon followed by many researchers who extended the study of chemical shifts to all sorts of compounds, complexes, alloys, solutions and glasses.

Considering the various factors which may affect the energy necessary to re-

move an electron from an ion in a crystal, Pauling [60] has discussed the dependence of the wavelength of an absorption discontinuity on the chemical environment of the absorbing atom and has emphasized the importance of electrostatic potential seen by the absorbing ion due to its environment and the external screening caused by the valence electrons. The experimentally observed chemical shifts of the K-absorption edges of chlorine in LiCl, NaCl, KCl and RbCl seem to be in accordance with the theory proposed by Pauling, but the results obtained for some other compounds, e.g. NH_4Cl, CuCl and AgCl do not agree with it.

Kunzl [61] made a critical examination of the experimental work concerning the displacement of the K-absorption discontinuities of atoms present in different oxidation states in their oxides. He formulated a law according to which the displacement of an absorption edge in a series of compounds depends directly upon the valency of the element in the compound under consideration. This dependence is given by the relation $\Delta\nu/R \propto V$, where $\Delta\nu$ denotes the change in the frequency of the absorption edge for a given compound with respect to that for the pure element, R is the Rydberg constant and V is the valency of the absorbing atom. This dependence of the chemical shift on valence has been supported by the work of Zinn [62], Barton [63], Manescu [64], Glenn and Dodd [65] and many others. Assuming the dependence of the position of the K-absorption limit on valency Boehm et al [66] have reported the valence of cobalt in vitamin B_{12} to be three. Kirichock and Karalnik [67], Vainshtein [68], Miller [69], Mande and Chetal [70] and Sarode et al. [71] have determined the valency of transition metal ions in different compounds and complexes, making use of the Kunzl's law. However, several investigations [72-74] have pointed out the limitations of the Kunzl's law. The effect of electronegativity and character of the ligands, type of hybridization, nature of chemical bond, coordination number and the other structural parameters [75] seem to affect the chemical shift. Agarwal and Verma [76] have given an empirical rule which states that "in general, the chemical shift is towards the high energy side of the metal edge and it increases progressively with the increase in the valence of the cation, unless the shift is either suppressed by the covalent character of the bond or enhanced by the formation of metal-metal bonding." Dey and Agarwal [77] have further attempted to demonstrate a linear

17

variation of the chemical shift with the product of the ionicity of the bond and square of the valency.

Several workers [78, 79] have tried to correlate the chemical shift with effective charges on the absorbing atoms calculated by different methods. Batsanov and Ovsyannikova [80] have investigated the position of the K-absorption discontinuity of manganese in some of its compounds and have observed its dependence on the coordination charge on the absorbing ions. Barinskii and Nadzhakov [81] have attempted to determine the effective charges in some transition metal compounds by this method. These attempts have been critically reviewed by Barinskii and Nefedow [82]. Through somewhat involved reasoning Böke [83] also has tried to deduce the effective charges on the absorbing metal atoms in various complexes. Srivastava et al. [84] have also shown that the variation in the K-edge shifts of copper in some complexes involving Cu^I and Cu^{II} ions follows a parallel variation in the calculated effective nuclear charge. In 1973 Mande and Sapre [85] have shown that the absorption discontinuity in a compound shifts towards the higher or lower energy side with respect to the corresponding discontinuity in the pure element depending upon whether the absorbing atom is a cation or an anion and that the magnitude of the chemical shift depends upon the effective charge on the absorbing ion. These authors determined the effective charges in the case of gallium selenide and gallium telluride using the X-spectroscopic technique. Mande and Kondawar [86] have calculated the effective charges on cobalt ions in some of their intermetallic compounds and a correlation between the X-ray absorption shifts and the effective charges has been found. Sarode [87] has investigated the L_{III}-absorption edges in bismuth halides and observed a variation of position of the absorption discontinuity with the partial ionic charge, calculated on the basis of Sanderson's method. Sarode et al. [88] have examined the K-absorption spectra of several oxides and pervoskites of manganese, iron and cobalt. These authors have found a functional relationship between chemical shifts and effective atomic charges.

It is not always easy to locate the position of the X-ray absorption discontinuities unequivocally because their shapes often appear complicated and do not always follow [89] the simple arctangent curve. Moreover, the discontinuities are

18

frequently accompanied by [90] fluctuations in the absorption coefficient on the low as well as high energy sides. These complexities in X-ray absorption spectra can be roughly classified in the following groups :

Pre-absorption :

This is the structure observed on the low energy side of the absorption edge. It is usually attributed [91] to the availability of localized unoccupied electronic levels below the conduction band. In the case of some rare earths and their systems one observes in the L and M spectra such preabsorption peaks corresponding to transitions to the unfilled atomic levels. Preabsorption structures in some insulators like CuO, ZnO, RbCl etc. have also been observed by Cauchois and Mott [91], who have interpreted their results on a model suggested earlier by Frenkel [92]. According to Frenkel in the non-metallic solids the hole formed in an inner atomic level can trap the free electron in the lattice by virtue of its Coulomb field, forming a bound electron hole pair (exiton), which forms free atomic like levels in the forbidden gap. Transitions of the inner electron to these levels give rise to the preabsorption maximum on the low energy side of the absorption discontinuity.

Pre-absorption peaks have also been observed [93-97] in compounds wherein the metal ions have tetrahedral, square planar and square pyramidal coordination. The intensities of these peaks are found to depend on the coordination geometry of the metal site [94, 95]. For example, in compounds like Ag_3VO_4, where vanadium ion is tetrahedrally coordinated by four oxygen ligands, the intensity of pre-edge peak is large [96], whereas in $GdVO_3$, the vanadium ion being in octahedral coordination. the intensity is very small. The metal ions, which have square pyramidal coordination in compounds, show the pre-absorption peak whose intensity is slightly smaller than those observed for tetrahedrally coordinated compounds [96]. Shulman et al. [98] have explained that vibronic mixing of np and nd characters makes the low energy transitions allowed. Theoretical considerations [93, 99] also support this view.

Splitting of Discontinuity and the Near Edge Structure :

In the X-ray absorption spectra, it has been found [90,100-103] that the discontinuity often splits into two or more components and that their appears some fine structure in its immediate vicinity (upto about 30 eV) on its high energy side. Kossel [104] has observed this structure initially in the case of gases and had suggested a model of single electron transitions to the empty atomic states for the interpretation of such structure. This type of structure was later found [105] to appear in the liquids and solids also. This near edge structure in the case of metals, alloys and highly covalent compounds is usually attributed [90] to the distribution of unoccupied states of appropriate symmetry in the conduction band. For gaseous molecules, molecular solids and transition metal coordination complexes it is attributed [106-109] to the transitions of core electrons to the states formed due to molecular formation. In the K-absorption spectra of transition metal compounds several workers [94, 98, 102, 109] have observed a weak low energy peak at the threshold followed by a shoulder on a rising absorption that culminates in a strong peak. The occurrence of low energy peak corresponding to inner electron transition to nd state, has already been discussed above. The shoulder peak and strong absorption maxima are generally assigned to ns and np states. The transition to the outer states created due to capture of another atom's electron [110] (cross-over transition) as well as the creation of multiple inner vacancies [111] may also give rise to some small peaks near the absorption edge.

White Line :

The appearance of a strong peak just above the X-ray absorption edge for some elements and compounds has been an interesting subject in X-ray spectroscopy for many years. The strong peak is referred to as a "white line" (or "raie blanche" in French), because such a little amount of radiation at certain wavelengths would penetrate the absorber relative even to the radiation transmitted above the edge, giving a white line on the photographic film used in the early experiments. For example, white lines have been observed at the K-edges of elements, Ga and

As, Ni in Ni_2O_3, Cu in CuO, and Zn in Zno [91], but not in the 3d transition elements [100]. White lines have also been observed at the L_{II} and L_{III} edges (but not at the L_I edge) of Fe, Co, Ni [112, 113], Cu in CuO [114], Ru, Rh, Pd [115, 116], Sm, Gd through Lu [117], Ta, W, Re [118-121], compounds of Hg and Tl [122] and U [118]. The list is by no means complete; in fact, with the enhanced intensity and improved resolution from synchrotron radiation sources [123, 124], white lines have been observed in a large number of substances. Although the origin of the strong absorption has not been analyzed in detail, it is generally believed [91] to be associated with an atomic like electric-dipole-allowed transition from an inner shell to an unoccupied level with a high density of states in the vicinity of the absorbing atom. In this regard, the white line also depends on the chemical bonding because Cu in metal or Cu_2O does not have white line [114] while W in WO_3 exhibits a broader white line than the one metallic W [121].

Wei and Lytle [125] have studied the L_{II} and L_{III} edges of tantalum metal. These authors have associated the white line with an atomic like allowed transition from $2p_{1/2}$ and $2p_{3/2}$ states to the vacant 5d states of a high density. However, a quantitative comparison with the calculated band structure was not possible because none of the existing band structure calculations has included the effect of a core hole. In an attempt to understand the white lines, Wei and Lytle presented two least-squares analyses of the Ta L_{III}-edge in terms of (a) a Lorentzian profile and (b) a Breit-Wigner-Fano type formula. They found that the latter, which was first suggested by Cauchois and Mott, appeared to provide a better fit to the asymmetric line shape.

Brown et al. [126] have done rigorous theoretical calculations of white lines and shown that the calculated weight of the absorption in the white line corresponding to a $2p_{3/2}$ to $5d_{5/2}$ transition is consistent with the experimentally determined value in platinum metal. However, experimental results for Ni and Ti do not fit into their theoretical framework.

21

Extended X-ray Absorption Fine Structure:

The extended X-ray absorption fine structure (EXAFS) refers to oscillations in the X-ray absorption coefficient observed on the high-energy side of an X-ray absorption edge. Such oscillations can extend up to 1000 eV above the edge and may have a magnitude of 10% or more.

This phenomenon of EXAFS has been known since 1930, and the basic physical explaination has been provided by Kronig [127], who says that these oscillations are due to modification of the final state of the photoelectron by the crystal or in the case of gaseous molecules, by atoms surrounding the excited atom. Since then there have been various further attempts to theoretically understand the EXAFS, but without complete success [128-132]. The various theories can be classified into two categories, long-range order (LRO) and short-range order(SRO). The LRO theories require the existence of long-range order to explain the fine structure. Because EXAFS is found experimentally in amorphous solids and molecules the experimental evidence favours the SRO theoretical approach. For this reason during 1970 and later the theoretical interest had centered on the SRO theories. In these theories only the environment in the vicinity of the excited atom is held responsible for EXAFS. Most SRO theories of EXAFS agree on the basic physics. The differences occur in the various approximations made in the calculations.

However, there has never been detailed theoretical investigation of the relationship between the LRO and SRO theories although one knows that both approaches must give the same results if correctly formulated. It is shown by Stern [133] that the LRO theories as usually formulated are incorrect because they neglect the dominant effects. In 1970, Sayers, Lytle and Stern [134] derived the first successful working theory of EXAFS. This was subsequently modified by Stern [133] to a more general form and further refined by others [135, 136]. According to these theories, EXAFS is regarded as resulting from interference between the photoelectron wave propagating from the X-ray absorbing atom and the wave backscattered by neighbouring atoms. Depending on whether the scattered wave returns to the origin in phase or out of phase with the outgoing wave,

there is an increase or decrease in absorption.

Sayers et al. [137] have shown that the structural information can be obtained most directly from EXAFS by taking the Fourier transform of EXAFS data. With highly symmetrical structures involving only a single absorber nearest neighbour distance in the first coordination sphere, one can use Fourier transform to obtain such distances to an accuracy of about 0.01 Å.

Besides giving radial distance information, EXAFS also contains information about the type and number of scattering atoms and their motion relative to the absorber. The atom type reveals itself through the absolute phase of the fine structure oscillations and through the EXAFS amplitude envelope. This amplitude is also affected by the static and thermal disorder of absorber-scatterer distances. Moreover, simple theory predicts that the magnitude of the fine structure will be linearly proportional to the number of scattering atoms and inversely proportional to the square of the absorber-scatterer distance. During 1975-1977, much of the amplitude information has been discarded, but in late 1978, Cramer et al. [138] has demonstrated that using a known phase shifts and amplitude functions, one can estimate the number and identity of near-neighbours at a particular distance.

Sometimes one observes that in the fine structure there exists certain peaks which cannot be attributed [139] to the states created in the above fashion. There is evidence to suggest that these peaks can be ascribed to plasmons excited during the X-ray absorption process.

Since most of the experimental work presented in this thesis is done by using X-ray absorption spectroscopy, it would be appropriate here to mention briefly the special advantages of this technique that makes it a versatile probe for electronic structure determination.

1.5 Some Special Advantages of X-ray Absorption Spectroscopy

The X-ray absorption technique has found wide applicability in many diverse areas as a tool to determine the local atomic environment in many classes of materials whose structures defied analysis by standard techniques such as diffraction or diffuse scattering [140-144]. The properties of X-ray absorption technique that make it so useful for structure determination are :

1. The local atomic arrangement can be determined about each type of atom in a sample separately. By tuning the X-rays to the absorption edge energy of an atom, only its environment is probed.

2. Since EXAFS measures only short range order, there is no fundamental distinction between crystals with long range order and samples without, such as amorphous solids, liquids, and solutions. Thus aperiodic systems can be studied with the same ease as crystals.

3. In principle, the kinds of surrounding atoms can be distinguished by the energy dependence of their contributions to the EXAFS.

4. The number of atoms at a given average distance and the disorder in their location about the average can be quantified by EXAFS.

5. In unoriented samples only the radial distance between the centre atom and its neighbouring atoms is determined, but in oriented samples which have less than cubic symmetry, angular positions are discernible.

6. Structural information is obtained from X-ray absorption spectroscopy by a simple and direct analysis.

7. The X-ray absorption measurements are relatively easy and rapid.

8. Determination of the chemical state of atom is possible by determining absorption edge shift and the near-edge structure.

9. Information regarding the empty states in the conduction band as well as the low-lying continuum states can be obtained from the absorption spectrum by making use of a relatively narrow inner state as a scanning probe.

10. It is a non-destructive technique and comparatively small quantities of materials are required in the investigation.

11. The site symmetry of the absorbing ions i.e., the geometrical distribution of atoms around the absorbing atom can be obtained simply by studying the profiles of X-ray absorption edges in the model compounds and in the unknown systems.

It is because of these properties and advantages that X-ray absorption spectroscopy occupies an important place amongst the different techniques of investigating electronic structure of materials.

1.6   Purpose and Scope of the present study

Amongst the transition metal compounds, the compounds of tungsten, in particular, tungsten bronzes and tungsten oxides having catalytic properties have attracted attention of many researchers because of their many technical applications. Goodenough [145] and others [1, 2, 4, 22, 23, 34] have discussed theoretically the nature of chemical bonding in these compounds, However, not much systematic experimental work seems to have been done on their electronic and structural properties. A few year ago, Horsley et al [146] and Hilbrig et al [147] had studied, using X-ray spectroscopic method, some complex oxides of tungsten in order to obtain structural information on the chemical liason in these compounds. We thought it worthwhile to extend this study to some binary and ternary inorganic compounds, organometallic complexes, supported tungsten oxide catalysts and rare earth tungsten oxide bronzes, with an aim to see if the correlation between the chemical shifts of the X-ray absorption discontinuities and the oxidation states/effective charges of the absorbing atoms, demonstrated by Sarode et al [88] is valid in the case of compounds of tungsten.

In this thesis we report our investigations on :

1. the position and profile of tungsten L absorption edges in WI_2, $K_3W_2Cl_9$, WO_2, WS_2, WSe_2, WCl_4Pyr_2, $C_{11}H_{14}N_2O_{12}BaW_2.6H_2O$, $[WCl_4L_2]Cl$ (L = 2,4,6 trimethylpyridine), $K[WO_2(C_2O_4)].xH_2O$, $(NH_4)_2WS_4$, $Fe_2(WO_4)_3$, $Al_2(WO_4)_3$, $CaWO_4$, $Eu_2(WO_4)_3$, $Na_2WO_4.2H_2O$, WO_2Br_2, $WOCl_4$, WCl_6, WO_2Cl_2, $NiWO_4$, $ZnWO_4$, $H_3PW_{12}O_{40}.5H_2O$, $(NH_4)_6H_2W_{12}O_{40}.5H_2O$, WO_3, $WO_3.H_2O$ and WV_2O_6 and;

2. the position and profile of tungsten L absorption edges in rare-earth tungsten oxide bronzes namely, $Eu_{0.1}WO_3$, $Sm_{0.1}WO_3$, $La_{0.1}WO_3$, $Na_{0.15}WO_3$ and $In_{0.21}WO_3$;

3. the position and profile of tungsten L absorption edges in the calcined air exposed and reduced alumina and titania supported tungsten oxide catalysts containing 4, 6, 8, 10 and 12 % by weight of WO_3 on the surface and 20% calcined and reduced $Ni - W/Al_2O_3$;

4. the extended X-ray absorption fine structure at the tungsten L_{III}-edge in some catalytic samples mentioned in (3) and

5. Rietveld Refinement of the structural parameters of few representative bronzes, wherein no detailed crystal structure data are available.

References

[1] G. D. Rieck, Tungsten and Its Compounds, Pergamon Press, Oxford (1967).

[2] R. V. Parish, "The Inorganic Chemistry of Tungsten", in Advances in Inorganic Chemistry and Radiochemistry, $\underline{9}$, Academic Press, New York pp.315-354 (1966).

[3] C. L. Rollinson in "Chromium, Molybdenum and Tungsten" in Comprehensive Inorganic Chemistry, Eds. J. C. Bailar, H. J. Emeleus, R. Nyholm and A. F. Trotman-Dickenson, Pergamon Press, New York, Vol.3 (1973).

[4] A. F. Wells, Structural Inorganic Chemistry, Oxford Univ. Press, London and New York (1962).

[5] D. L. Kepert, "Isopolyanions and heteropolyanions, Chapt. 51 in Comprehensive Inorganic Chemistry, $\underline{4}$, pp.607-672, Pergamon Press, Oxford (1973).

[6] B. Cohen, A. J. Edwards, M. Mercer and R. D. Peacock, Chem. Commun., p.322 (1965).

[7] B. R. Mc Garvey, Inorg. Chem., $\underline{5}$, 476 (1966).

[8] P. Hagenmuller in "Tungsten Bronzes, Vanadium Bronzes and Related in Compounds" in Comprehensive Inorganic Chemistry, Eds. J. C. Bailar, H. J. Emeleus, R. Nyholm and A. F. Trotman-Dickenson, Pergamon Press, New York, Vol.4 (1973).

[9] G. H. Cady and G. B. Hargreaves, J. Chem. Soc., P.1563 (1961).

[10] K. J. Shimomura, Sci. Hiroshima Univ., Ser. A21, 241 (1958).

[11] T. G. Burke, D. F. Smith and A. H. Nielsen, J. Chem. Phys., 20, 447 (1952).

[12] K. N. Tanner and A. B. F. Duncan, J. Am. Chem. Soc., 73, 1164 (1951).

[13] G. M. Clark and W. P. Doyle, Spectrochim. Acta, 22, 1441 (1966).

[14] J. A. M van Liempt, Z, Electrochem., 31, 249 (1925).

[15] E. S. Rittner, Phillips Res. Rep., 8, 184 (1953).

[16] O. Glemser and H. Ackermann, Z. Anorg. Allgem. Chem., 325, 281 (1963).

[17] J. Aveston, Inorg. Chem., 3, 981 (1964).

[18] O. Glemser, W. Holznagel, W. Hoeltje and E. Schwarzmann, Z. Natur-
forsch., 20b, 725 (1965).

[19] C. N. R. Rao, "Transition Metal Oxides" in Solid State Chemistry, Ed. C.
N. R. Rao, Marcel Dekker, Inc., New York, pp.526-533 (1974).

[20] E. Gebart and R. J. Ackermann, Inorg. Chem., 5, 136 (1966).

[21] J. M. Berak and M. J. Sienko, J. Solid State Chem., 2, 109 (1970).

[22] M. J. Sienko, in "Non-Stoichiometric Compounds", Adv. Chem. Ser., Amer-
ican Chemical Society (R. F. Gould ed.), 39, 224 (1963).

[23] F. Kupka and M. J. Sienko, J. Chem. Phys., 18, 1296 (1950).

[24] W. Ostertag, Inorg. Chem., 5, 758 (1966) and references cited therein.

[25] P. G. Dickens and M. S. Whittingham, Quart. Rev., 22, 30 (1968).

[26] M. T. Shipunova, V. V. Kozik and V. V. Serebrenkov, Zh. Neorg. Khim.,
33, 2732 (1988).

[27] E. Bialkowska, E. Polaczkowa, A. Polaczek and A. Gesci, Bull. Acad. Pol.
Sci. Ser. Sci. Chim., 21-2, 137 (1973).

[28] J. H. Sinfelt, Annu. Rev. Nat. Sci., 2, 641 (1972).

[29] Ai. M., J. Catal., 49, 305 (1977).

[30] T. Yamaguchi, Y. Tanaka, K. Tanabe, J. Catal., 65, 442 (1980).

[31] T. Yamaguchi, S. Nakamura and H. Nagumo, In Proceedings of the International Congress on Catalysis, 8th; Verlag Chemie : Weinheim, Germany, 1984; 5, p.579.

[32] M. Imanari, Y. Watanabe, S. Masuda and F. Nakajima, In Proceedings of the 7th International Congress on Catalysis, p.841 (1981).

[33] S. Morikawa, K. Takahashi, J. Mogi and S. Kurita, Bull. Chem. Soc. Jpn., 55, 2254 (1982).

[34] O. Weisser and S. Landa, "Sulphide Catalysts, Their Properties and Applications", Pergamon Press, New York, N.Y. (1973).

[35] K. T. Ng and D. M. Hercules, J. Phys. Chem., 80, 2094 (1976).

[36] M. Siegbahn, The spectroscopy of X-rays, (Oxford University Press, London) (1925).

[37] E. F. Kaelble, Handbook of X-rays (McGraw-Hill Book Company, New York) (1967).

[38] A. E. Sandström, Handbuch der Physik, edited by S. Flügge (Springer-Verlag, Berlin) 30, 78 (1957).

[39] C. Kunz, Comments on Solid State Physics, 5, 31 (1973).

[40] D. H. Tomboulian, Encyclopedia of Physics edited by S. Flugge (Springer-Verlag, Berlin) 30, 246 (1957).

[41] D. J. Fabian, L. M. Watson and C. A. W. Marshall, Rep. Prog. Phys., 34, 601 (1972).

[42] G. A. Rooke, Soft X-ray Band Spectra and the Electronic Structure of Metals and Materials, edited by D. J. Fabian (Academic Press, London) p.3, (1968).

[43] F. K. Richtmyer, S. W. Barnes and E. Ramberg, Phys. Rev., 46, 843 (1934).

[44] V. Weisskopf and E. Wigner, Z. Physik, 63, 54 (1939).

[45] L. G. Parratt, Phys. Rev., 56, 295 (1939).

[46] G. Brogren, Nova Acta. Reg. Soc. Sc., Uppasala 14(4th Series), 4 (1948).

[47] G. R. Mitchell, Develop. Appl. Spectry., 4, 109 (1965).

[48] F. E. Vainshtein and K. I. Narbutt, Dokl. Akad. Nauk. SSSR, 105, 1196 (1955).

[49] J. A. Soules and C. H. Shaw, Tech. Rep. No.2, Ohio State University, Res. Found 1954.

[50] A. Nilsson, Ark. Physik, 6, 513 (1953).

[51] M. Breinig, M. H. Chen, G. E. Ice, F. Parente and B. Crasemann, Phys. Rev., A 22, 520 (1980).

[52] S. P. Cramer and K. O. Hodgsen, Prog. of Inorg. Chem., 25, 4069 (1978).

[53] N. -S. Chiu, S. H. Bauer and M. F. L. Johnson, J. Catalysis, 89, 226 (1984).

[54] P. R. Sarode, X-ray Spectrometry (submitted).

[55] J. Bergengren, Compt. Rend., 172, 1175 (1925); Z. Physik, 3, 247 (1920).

[56] A. E. Lindh, Z. Physik, 6, 303 (1921); Z. Physik, 31, 210 (1925).

[57] O. Stelling, Z. Anorg. Allg. Chemie, 131, 1023 (1927).

[58] S. Aoyama, K. Kimura and Y. Nishina, Zeit. F. Physik, 44, 810 (1927); 46, 150 (1927).

[59] D. Coster, Z. Physik, $\underline{25}$, 83 (1924).

[60] L. Pauling, Phys. Rev., $\underline{34}$, 954 (1929) .

[61] V. Kunzl, Coll. Trav. Chim Techecoslovaquie, $\underline{4}$(S), 213 (1932).

[62] W. H. Zinn, Phys. Rev., $\underline{46}$, 659 (1934).

[63] V. P. Barton, Phys. Rev., $\underline{71}$, 406 (1947).

[64] I. Manescu, Compt. Rend., $\underline{255}$, 537 (1947).

[65] G. L. Glenn and C. G. Dodd, J. Appl. Phys., $\underline{39}$, 5372 (1968).

[66] G. Boehm, A. Faesseler and G. Rittmayer, Z. Naturforschung, $\underline{96}$, 509 (1954).

[67] P. P. Kirichok and S. M. Karalink, Bull. Acad. Sci. USSR. Phys. Ser., $\underline{31}$, 1043(1967).

[68] E. Vainshtein, R. M. Ovrutskaya and B. I. Kotlyar, Sov. Phys. Solid State, $\underline{5}$. 2935(1963).

[69] A. Miller, J. Phys. Chem. Solids, $\underline{29}$, 633(1968).

[70] C. Mande and A. R. Chetal, Int. Conf. X-ray Spectra and Chem. Binding (Karl Marx University, Leipzig) 194, (1966).

[71] P. R. Sarode, G. Sankar, A. Srinivasan, S. Vasudevan, C. N. R. Rao and J. M. Thomas, Angewandte Chemie, $\underline{23}$, 323 (1984).

[72] W. W. Beeman and J. A. Bearden, Phys. Rev., $\underline{61}$, 455 (1942).

[73] D. Coster and S. Kiestra, Physica, $\underline{14}$, 175 (1948).

[74] E. W. White and H. A. Mckinstry, Advances in X-ray Analysis, edited by G.R.Mallett et.al. (Plenum Press, New York), $\underline{9}$, 376 (1966).

[75] A. Faesseler, Proc. X Colloquim Spectroscopium Internationale, University of Marylands, 307 (1962).

[76] B. K. Agarwal and L. P. Verma, J. Phys. C : Solid State Phys., $\underline{3}$, 535 (1970).

[77] A. K. Dey and B. K. Agarwal, J. Chem. Phys., $\underline{59}$, 1397 (1973).

[78] S. M. Karalnik, Bull. Acad. Sci. USSR Phys. Ser., $\underline{21}$, 1432 (1957).

[79] M. V. Becker, Naturwissenscaften, $\underline{51}$, 633 (1964).

[80] S. S. Batsanov and J. A. Ovsyannikova, Akad. Nauk. Beloruss SSR, 93 (1966). Chemical Bonds in Semiconductors and Thermodynamics, edited by N. N. Sirota (Consultant's Bureau New York) 65 (1968).

[81] R. L. Barinski and B. G. Nadzhakov, Bull. Acad. Sci. USSR Phys. Ser., $\underline{24}$, 419 (1960).

[82] R. L. Barinski and W. I. Nefedow, Röntgenenspektroskopische Bestimmung der Atomladungen in Molekulen (Akademische Verlagsgellschaft geest and Portig K.G.Leipzig).

[83] K. Böke, Z. Physik Chem. Neue Folge, $\underline{10}$, 45 (1957).

[84] U. C. Shrivastava, H. L. Nigam and A. N. Vishnoi, Indian J. Pure Appl. Phys., $\underline{10}$, 61 (1972) and refernces therein.

[85] V. B. Sapre and C. Mande, J. Phys. C: Solid State Phys., $\underline{5}$, 793 (1972); J. Phys. Chem. Solids, $\underline{34}$, 1331 (1973).

[86] V. K. Kondawar and C. Mande, X-ray Spectrometry $\underline{5}$, 2 (1975); J. Phys. C : Solid State Phys., $\underline{9}$, 1351 (1976).

[87] P. R. Sarode, Z. Naturfursch, (a)$\underline{33}$, 946 (1978).

[88] P. R. Sarode, S. Ramasesha, W. H. Madhusudan and C. N. R. Rao, J. Phys. C : Solid State Phys., $\underline{12}$, 2439 (1979).

[89] R. A. Van Nostrand, Int. Conf. X-ray Spectra Chem. Binding (Karl Marx University Leipzig), 255 (1955).

[90] L. V. Azaroff and D. M. Pease, X-ray Spectroscopy, edited by L. V. Azaroff (McGraw Hill Book Company, New York) 284 (1974).

[91] Y. Cauchois and N. F. Mott, Phil. Mag., 40, 1260 (1949).

[92] J. Frenkel, Physik Z. Sowj., 9, 158 (1936).

[93] F. W. Kutzler, C. R. Natoli, D. K. Misemer, S. Doniach and K. O. Hodgson, J. Chem. Phys., 73, 3274 (1984).

[94] G. Sankar, P. R. Sarode and C. N. R. Rao, Chem. Phys., 76, 435 (1983).

[95] J. Wong, F. W. Lytle, R. P. Messmer and D. H. Maylotte, Phys. Rev., B30, 5596 (1984).

[96] B. H. Sonaye, Ph.D. Thesis, Goa University (1995).

[97] L. Kau, D. J. Spira-Solomon, J. E. Penner-Hahn and K. O. Hodgson, J. Am. Chem Soc., 109, 6433 (1987).

[98] R. G. Shulman, Y. Yaffet, P. Eisenberger and W. E. Blumberg, Proc. Natl. Acad. Sci. USA, 73, 1384 (1976).

[99] R. A. Bair and W. A. Goddard, Phys. Rev., B22, 2267 (1980).

[100] W. W. Beeman and H. Friedman, Phys. Rev., 56, 392 (1939).

[101] I. B. Borovskii and V. A. Batyrev, Bull. Acad. Sci. USSR, Phys. Ser., 24, 449 (1960).

[102] M. Belli, A. Scafati, A. Bianconi, S. Mobilio, L. Palladino, A. Pease and E. Burattini, Solid State Commun., 35, 355 (1980).

[103] L. A. Grunes, Phys. Rev., B 27, 2111 (1983).

[104] W. Kossel, Z. F. Physik, 1, 119 (1920).

[105] F. Babonneau, S. Doeuff, A. Leaustic, C. Sanchez, C. Cartier and M. Verdaguer, Inorg. Chem., 27, 3166 (1988).

[106] D. W. Fischer, Band Structure Spectroscopy of Metals and Alloys, edited by D. J. Fabian and L. M. Watson (Academic Press, London) p.669 (1973).

[107] D. S. Urch, Advances in X-ray Analysis, edited by C. S. Barret (Plenum Press, New York) 14, 250 (1971).

[108] A. V. Pendharkar and C. Mande, Chemical Analysis, 7, 244 (1975).

[109] W. Seka and H. P. Hanson, J. Chem. Phys., 50, 344 (1969).

[110] D. W. Fischer, Advances in X-ray Analysis, edited by C. S. Barret et.al. (Plenum Press, New York) 13, 159 (1970).

[111] L. G. Parratt, Rev. Mod. Phys., 31, 616 (1959).

[112] Y. Cauchois and C. Bonnelle, C. R. Acad. Sci. Paris, 245, 1230 (1957).

[113] P. Hanzely and R. J. Liefeld, in Electronic Density of States, Natt. Bur. Stand. Spec. Publ. No. 323, edited by L. H. Bennett, p. 319 (1971).

[114] C. Bonnelle, C. R. Acad. Sci. Paris, 248, 2324 (1959).

[115] I. G. Shveitser and M. A. Blokhin, Bull. Acad Sci. USSR, 31, 962 (1967).

[116] M. F. Sorokina and S. A. Nemnonov, Bull. Acad Sci. USSR, 31, 1039 (1967).

[117] P. R. Sarode, Ph.D. Thesis, Nagpur University (1977).

[118] Y. Cauchois and I. Manescu, C. R. Acad. Sci. Paris, 210, 172 (1940).

[119] D. Coster and H. deLong, Physica, 13, 385 (1947).

[120] S. N. Gupta and B. D. Padalia, J. Phys., F1, L16 (1971).

[121] J. A. Bearden and T. M. Snyder, Phys. Rev., 59, 1626 (1941).

[122] B. K. Agarwal and L. P. Verma, J. Phys., C2, 104 (1969).

[123] B. M. Kincaid and P. Eisenberger, Phys. Rev. Lett., 34, 1361 (1979).

[124] M. L. Perlman, E. M. Rowe and .E. Watson, Phys. Today, 27, July 30 (1974).

[125] P. S. Wei and F. W. Lytle, Phys. Rev., B19, 679 (1979).

[126] M. Brown, R. E. Peierls and E. A. Stern, Phys. Rev., B15, 738 (1977).

[127] R. de L. Kronig, Z. Physik, 70, 317 (1931); 75, 468 (1932).

[128] A. Peterson, Z. Physik, 80, 258 (1933).

[129] A. L. Kostarev, Zh. Eksp. Teor. Fiz., 11, 60 (1941); 19, 413 (1949).

[130] T. Hayasi, Sci. Rep. Tôhoku Univ., 33, 123 (1949); 34, 185 (1950).

[131] T. Shiraiwa, T. Ishimura and M. Sawada, J. Phys. Soc. Japan., 13, 847 (1958).

[132] A. I. Kozlenkov, Bull. Acad. Sci. USSR Phys. Ser., 25, 968 (1961).

[133] E. A. Stern, Phys. Rev., B10, 3027 (1974).

[134] D. E. Sayers, F. W. Lytle and E. A. Stern, Advan. X-ray Anal., 13, 248 (1970).

[135] C. Ashley and S. Doniach, Phys. Rev., B11, 1279 (1975).

[136] P. A. Lee and J. B. Pendry, Phys. Rev., B11, 2795 (1975).

[137] D. E. Sayers, E. A. Stern and F. W. Lytle, Phys. Rev. Lett., 27, 1204 (1971).

[138] S. P. Cramer, K. O. Hodgson, E. I. Stiefel and W. E. Newton, J. Am. Chem. Soc., 100, 2748 (1978).

[139] Mande C. and N. V. Joshi, Proc. Int. Conf. X-ray Spectroscopy and Structure of Matter, Kiev Institute of Metal Physics, Ukr. SSR, p.57 (1968).

[140] E. A. Stern, Contemp. Phys., 19, 289 (1978).

[141] P. M. Eisenberger and B. M. Kincaid, Science, <u>200</u>, 1441 (1978).

[142] D. R. Sandström and F. W Lytle, Ann. Rev. Phys. Chem., <u>30</u>, 215 (1979).

[143] L. Powers, Biochem. Biophys. Acta, <u>683</u>, 1 (1982).

[144] P. A. Lee, P. H. Citrin, P. Eisenberger and B. M. Kincaid, Rev. Mod. Phys., <u>53</u>, 769 (1981).

[145] J. B. Goodenough, Magnetism and the Chemical Bond, Wiley InterScience, New York (1963).

[146] J. A. Horsley, I. E. Wachs, J. M. Brown, G. H. Via and F. D. Hardcastle, J. Phys. Chem., <u>91</u>, 4014 (1987).

[147] F. Hilbrig, H. E. Göbel, H. Knözinger, H. Schmelz and B. Lengeler, J. Phys. Chem., <u>95</u>, 6973 (1991).

Chapter 2

Experimental Techniques

2.1 Introduction

This Chapter is divided into three parts, viz. preparation of materials, its characterization by X-ray diffraction and X-ray absorption spectroscopic measurements.

2.2 Preparation of Materials

This section describes the preparation of the compounds of tungsten, tungsten oxide bronzes and the catalytic compounds of tungsten.

2.2.1 Preparation of Tungsten Compounds

Most of the compounds were obtained commercially and a few were prepared in the laboratory.

$K_3W_2Cl_9$ was obtained [1] by crystallizing the electrolytically reduced acidic solution of potassium tungstate.

The pyridine complex, WCl_4py_2 is prepared [2] by the reaction of pyridine with the tungsten chloride.

$[WCl_4L_2]Cl$ where L = 2,4,6-trimethylpyridine was prepared by standard method of Brown and Ruble [2]. $Ba[W_2(O)(\mu - O)(\mu - R - pdta)].6H_2O$, where R-pdta = R-propylenediamine-N,N,N',N'-tetraacetate was synthesized according to the procedure of Ikari et al [3].

$K_2[WO_2(C_2O_4)].xH_2O$ was prepared [4] by reducing potassium tungstate with tin in a solution containing oxalic acid and potassium oxalate. The colour of the solution changes from blue to green to red. Tin was removed as tin sulphide from the red solution from which red crystals of the oxalato complex were then slowely deposited.

WO_2Br_2 was made [5] by heating WO_3 with CBr_4 in a sealed Pyrex tube at $200°C$.

WV_2O_6 was synthesized [6] from equimolar mixture of high purity samples of V_2O_3 and WO_3 oxides heated after melting at $1000°C$ in an evacuated quartz tube for 72 hrs., and then by slow-cooling to room temperature.

2.2.2 Preparation of Tungsten Oxide Bronzes

$Eu_{0.1}WO_3$ was prepared [7] by mixing the high purity powder samples of Eu_2O_3, WO_3 and W in appropriate molar ratio. The reagents were carefully grounded and pelletised and then were enclosed in the evacuated sealed silica tube and heated for 100 hours at $1270^\circ K$. To achieve homogeneity in the product, the process was repeated thrice. The sample thus formed was rapidly cooled to room temperature. The bronzes $Sm_{0.1}WO_3$, $La_{0.1}WO_3$ and $In_{0.2}WO_3$ were made by similar method.

$Na_{0.15}WO_3$ was prepared [8] by mixing appropriate proportions of WO_3, WO_2 and Na_2WO_4. This mixture was sealed in an evacuated quartz tube and was heated slowly in the begining and then abruptly to a temperature of $800^\circ C$ which was kept constant for 10 hrs.

2.2.3 Preparation of Supported Tungsten Oxide Catalysts

Catalytic samples of $WO_3/\gamma - Al_2O_3$ were prepared by impregnation to incipient wetness using $\gamma - Al_2O_3$ as the support. $\gamma - Al_2O_3$ was first dried at $110^\circ C$ for 12 hrs. before impregnation. An appropriate volume of an aqueous $(NH_4)_6H_2W_{12}O_{40}.xH_2O$ solution was added to the pre-heated alumina in two equal portions and mixed well after each addition. These were allowed to stand for 30 min. in a covered beaker and dried for 12 hrs. at $110^\circ C$. Samples were then calcined in a furnace at $550^\circ C$ for 12 hrs.

Catalysts containing nickel were prepared by sequentially impregnating a calcined WO_3/Al_2O_3 (1-2 hrs.) catalyst with an solution of nickel nitrate. The impregnation procedure was the same as that described for WO_3/Al_2O_3 catalysts. The compound thus obtained was dried overnight at $110^\circ C$ and calcined at $500^\circ C$ for 16 hrs.

WO_3/TiO_2 samples were made in a manner similar to the above. They were prepared by dissolving ammonium tungstate in water and impregnating the support carrier TiO_2. These were then dried at $100^\circ C$ and calcined at $450^\circ C$ for 2 hrs.

2.3 Powder X-ray Diffraction

The characterization of compounds synthesized was done using X-ray diffraction (XRD) technique for checking and identifying the formation of phases in the compounds. The XRD measurements on powdered samples were performed using Rigaku X-ray diffractometer system (D/Max II-C). The intensity of Cu K_α radiation diffracted from the powder specimen was detected by a scintillation counter and recorded as a function of 2θ, where θ is the Bragg angle. Diffraction peaks were indexed and the unit cell parameters were calculated using the Powder Diffraction package PDP11 [9]. It is found that all the inorganic and organometallic compounds prepared are single phase. The calculated lattice parameters from the program PDP11 agrees well with these reported in JCPDS Powder Diffraction File [10]. The stoichiometries of the compounds were established from performing the chemical analysis of all the compounds prepared. A typical diffractogram recorded in this work is shown in Fig. 2.1.

2.4 X-ray Absorption Measurements

We describe below the apparatus used in this investigation to record the X-ray L-absorption spectra of pure tungsten, several tungsten compounds, tungsten oxide bronzes and the alumina and titania supported tungsten oxide catalysts. It is to be noted here that some of the spectra were recorded using very high-intensity X-ray source. This is particularly important where the concentration of the absorbing metal ion is low.

2.4.1 X-ray Spectrometer

Our basic X-ray spectrometer is a horizontal Rigaku wide angle diffractrometer with attached tube stand. The major modification is an improved crystal (monochromator) support for optimum alignment of the diffracting crystal (Fig.2.2). This spectrometer is used with a conventional X-ray diffraction generator and X-ray tubes (Fe, Mo or Cu target) chosen to provide a high intensity continuum in the region of the absorption edge to be measured, while missing
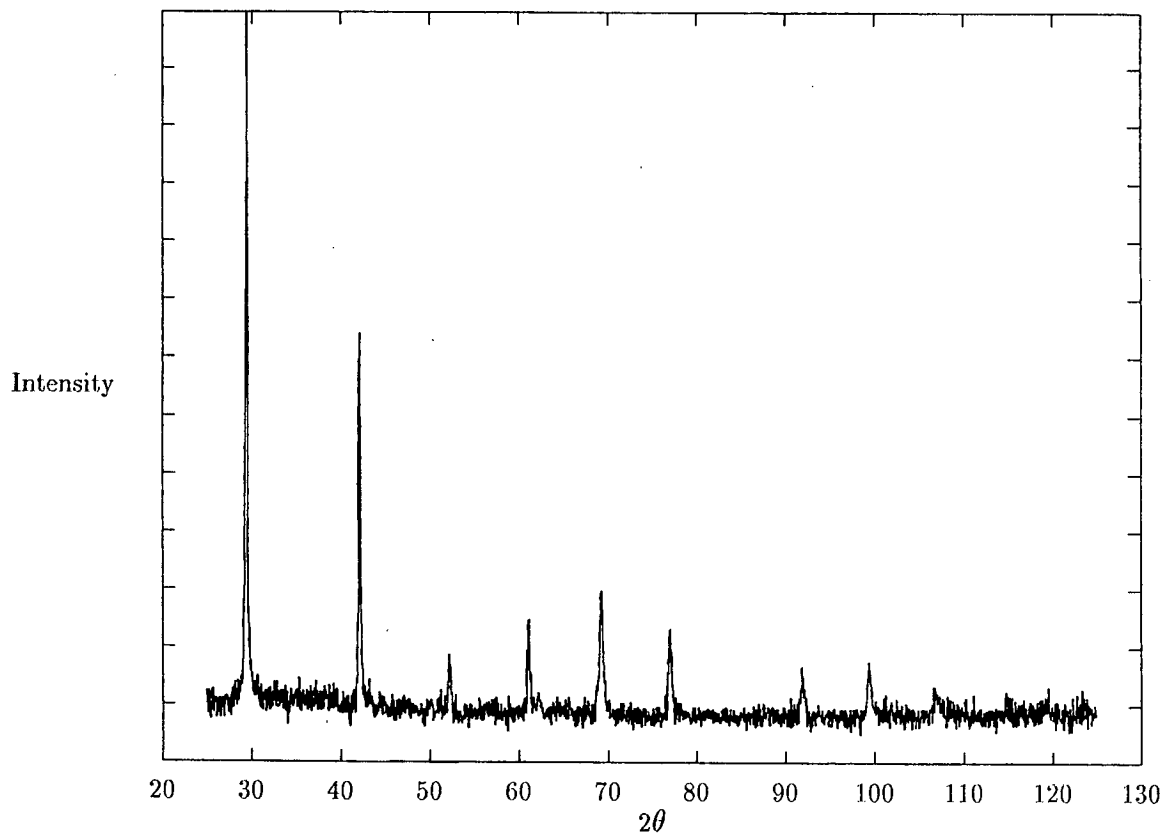
Fig. 2.1: X-ray diffraction pattern for $Eu_{0.1}WO_3$.
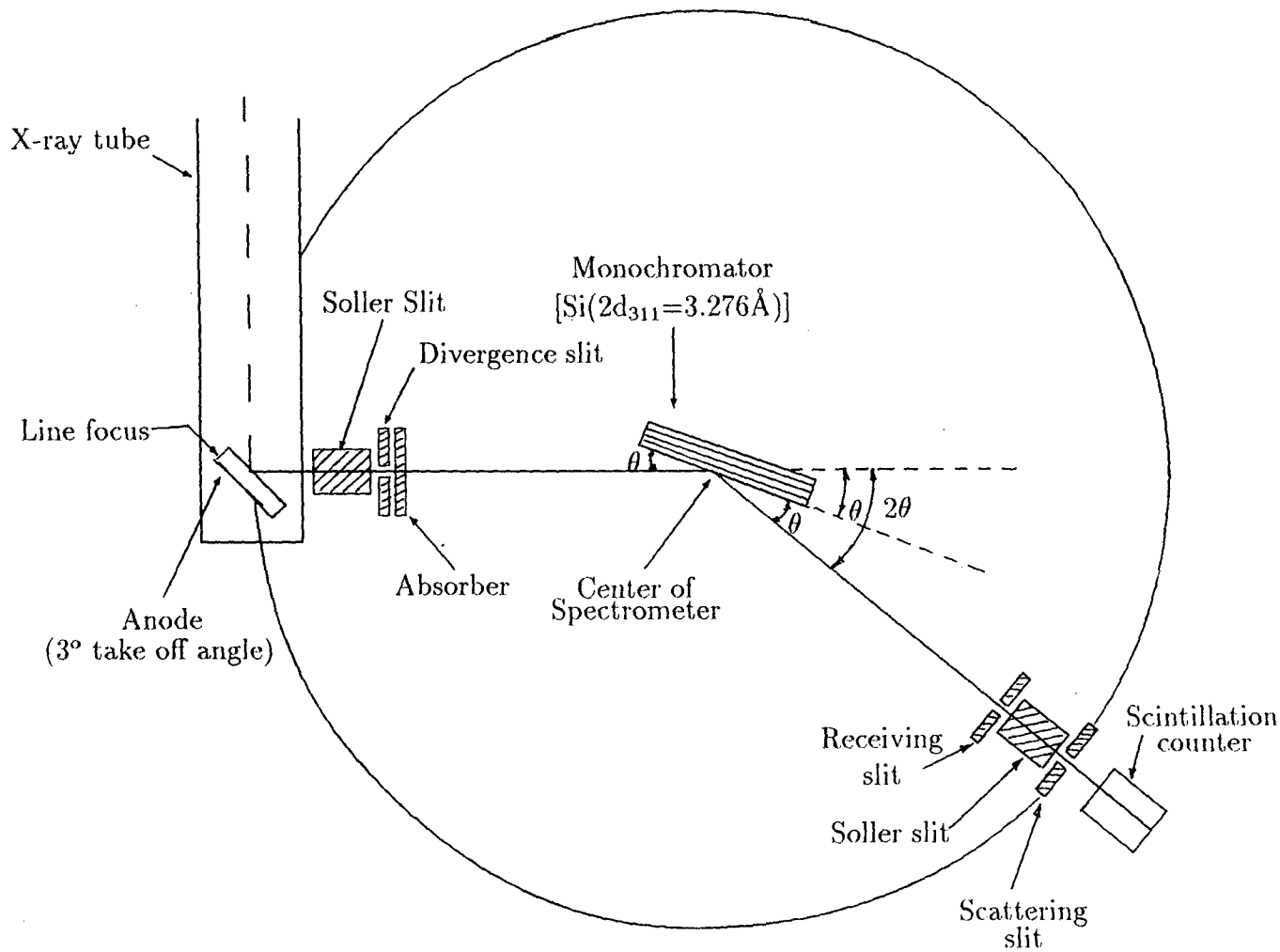
Fig. 2.2: Schematic diagram of X-ray absorption spectrometer

the intense characteristic X-ray emission lines. The spectrometer is used with a goniometer radius of 18.75 cm using simple set-back brackets and an X-ray tube takeoff angle of approximately 3° (adjusted for maximum diffracted intensity). The first slit is used to limit the angular divergence of the X-ray beam, and the Bragg-Brentano parafocussing conditions and slit position require the focusing (exit) slit to be approximately the same size. Between the two slits, a single-crystal monochromator Bragg diffracts a narrow band of the incident X-rays and adds its diffraction pattern to the divergence of the beam. The vertical divergence is limited to ±2° by a Soller slit located before the exit slit. Thus the resolution function depends primarily on the size of the slits and crystal diffraction pattern [11]. Our usual method of operation employs 0.05 mm slits (0.025° divergence) in the 2θ range from 15° to 45° and 0.1 mm (0.5° divergence) slits for angles greater then 45° with overlap as experimentally required. Hence resolving power defined as $(\tan\theta)/\Delta\theta$ (or $\lambda/\Delta\lambda$) (is approximately 1000 - 2000. The diffracted intensity from the continuum operating at full recommended tube power is typically $(1 - 10)\times10^3$ photons per second before passing through the sample. For the case of 0.05 mm slits at $2\theta = 45°$ and a LiF crystal ($2d = 4.026\text{Å}$) the energy-band width, assuming a rectangular response function, received at the exit slit would be $\sim 4\text{eV}$ ($\Delta E = E\cot\theta\Delta\theta$); however, the intensity distribution of the radiation filling the exit slit has the usual diffraction profile and the Rayleigh resolution criterion suggests that the spectrometer should be advanced in angular increments of 1/2 the angular width of the exit slit, i.e., $\Delta2\theta = 0.01°$ for 0.05 mm slits.

The measurements are carried out 0.5° 2θ below the absorption edge corresponding to ~ 120 eV and 3° 2θ above the edge corresponding to ~ 800 eV. The actual mode of operation is as follows: For each spectrometer position, I, transmitted intensity through the absorber and I_0, the incident X-ray intensity are measured (preset count mode) and stored on a floppy disc, the spectrometer is advanced to the next 2θ position, and the sequence is repeated. A separate scaler is used to generate a running number for each subsequent pair (I, I_0). Knowledge of the start position (See Table 2.1 and 2.2) and the 2θ stepping increment allows calculation of X-ray wavelength for any data pair. The usual experiments involves

43

500-1000 data pairs. The spectrometer stepping motor and absorber changer are activated and synchronized by the X-ray scaler print-out command. It was found that the mechanical accuracy of the absorber placement mechanism limited the precision to $\sim 0.3\%$; thus 10^5 photons were recorded for each I, I_o, and increased precision to 0.1% was achieved by averaging multiple passes. The problem of coincidence loss in the X-ray detecting electronics was corrected using the method of Short [12] and Burbank [13]. If uncorrected, intense emission lines from the X-ray tube leave an image in the data, which can be mistaken for EXAFS.

The flanged tube stand attached to the spectrometer allowed the X-ray tube to be translated, rotated and inclined with respect to the spectrometer circle. The alignment procedure consisted of locating (by means of these adjustments) the most intense spot on the X-ray tube target so that it was directed through narrow aligned entrance and exit slits at $2\theta = 0°$ as measured by a protected X-ray detector. The crystal monochromator was then inserted and a suitable characteristic line chosen for final crystal adjustment. At the calculated 2θ the translation, tilt and rotation (θ) adjustments of the crystal holder were used to obtain peak diffracted intensity of standard line which located the diffracting volume of the crystal at the centre of the spectrometer. Further refinement of the alignment was not necessary if the procedure described in the section on precision and accuracy of the energy scale was followed.

2.4.2   Monochromator Crystals

The usual discussion of monochromators for X-ray spectrometers emphasizes high resolution with narrow crystal rocking curves and multicrystal spectrometers. Our requirement stresses high X-ray intensity at moderate resolution for good statistical accuracy of measured EXAFS. Although better resolution would probably show more details particularly near the edge, there is an inherent width ($\sim 20eV$) in the EXAFS due in part to temperature smearing as well as lifetime broadening [14] e.g., 1.5 eV for the Cu K edge.

Given the flat crystal geometry, this experiment is intensity limited by the inherent luminosity of the X-ray tube and the diffraction efficiency of the monochro-

mator. A given monochromator has a diffractive dispersion called its "rocking curve" which is the angular width of the diffracted beam. When the crystal is exposed to a continuum of diverging radiation, it selects from the total flux just that angular range of wavelength $\Delta\lambda$, which is its rocking curve width, and diffracts a narrow band toward the exit slit, thus a crystal with very a narrow rocking curve will diffract comparatively few photons. A crystal with a wider rocking curve than the divergence of the slit system will smear the diffracted beam over the exit slits. The optimum condition is obtained when the divergence of the slit system and rocking curve of monochromator are approximately equal.

The efficiency of diffraction and the rocking curve width of diffraction crystals may be modified by appropriate treatment. LiF(200) or Si(311) is particularly workable crystal in this respect. The integrated reflection coefficient for non-polarised radiation, which is the area under the crystal rocking curve, has been calculated as a function of wavelength for the two extremes of the crystal perfection, a perfect crystal and an ideal mosaic crystal [15, 16]. The measured values of selected cleaved and treated crystals are also shown [16]. This helps to increase the photons diffracted by a factor of 3. The time necessary to obtain a precision measurement was reduced proportionately. The treatment consisted of vigorous sanding on rough paper to drive dislocations into the crystal followed by successively finer paper to 600 grit to provide a smooth surface. Part of the damaged surface layer was then removed by an etching procedure [17].

2.4.3 Preparation of Absorbers

The absorbers were prepared in a variety of ways: malleable metals were rolled (2-5 μm); some materials were evaporated onto mylar or thin Al foil, soluble materials were dissolved and then absorbed and dried on filter paper, many materials were ground to 400 mesh, mixed with a vacuum grease and then cast on a smooth substrate. After drying, the casts were sandwiched between thin transparent adhesive tapes for support and attached to the sample holder. The optimum absorber thickness considering contrast, measurement time and counting error problem was attained when $I/I_o \sim 1/3$ on the high absorption side of

the edge. For dilute solutions absorber thickness was kept such that $I/I_o \sim 1/10$.

2.4.4 Precision and Accuracy of the Energy Scale

The kinetic energy of the ejected photoelectrons E must be established accurately in order to evaluate the natural EXAFS variable k. For every experiment, characteristic and/or impurity lines from the X-ray tube occurred and were used as standard reference points to calculate an effective lattice constant for the monochromator to establish the energy scale at the accuracy to which they were known [18]. Many elements were present as an impurities on the X-ray tube anode; eg., Cu, Ni, Fe and Mn are usually present, plus the characteristic line from the primary anode element in multiple orders of diffraction. Replicate experiments established a presicion of $\sigma = 75$ ppm ($\pm$ 0.7 eV at the Cu K edge) as compared to 40 ppm typical calibration lines. By using the calibration lines to calculate the lattice constant for every set of data, the requirement was removed for corrections involving the diffraction process in the monochromator crystal such as temperature correction, lorentz-polarization correction, refraction and various errors due to misalignment. The value of E associated with each data pair was calculated from [19]

$$E = \frac{12398.52}{2d \sin \theta} eV \qquad (2.1)$$

The data collected from the EXAFS apparatus consisted of number of counts with the absorber in (I) and out (I_o) of the beam along with the corresponding angular position of the spectrometer. The preliminary data processing programs developed in this laboratory [20], (i) tabulated the initial data and calculated the X-ray photon energy and the total absorption, (ii) removed the oscillatory part of the X-ray absorption from the smooth monotonic background, and (iii) normalized the data to a per-atom scale.

References

[1] H. B. Jonassen, A. R. Tarsey, S. Cantor and G. F. Helferich, Inorg. Syn., 5, McGraw-Hill, New York, p.39 (1957).

[2] T. M. Brown and B. Ruble, Inorg. Chem., 6, 1335 (1967).

[3] S. Ikari, Y. Sasaki and T. Ito, Inorg. Chem., 29, 53 (1990)

[4] G. W. A. Fowles, "Halide and Oxyhalide Complexes", in Preparative Inorganic Reactions., 1, Interscience, New York, p.137 (1964).

[5] M. Pouraud and M. Chaigneau, Compt. Rend., 249, 2568 (1959).

[6] G. Pourroy, M. Drillon, L. Padel and J. C. Bernier, Physica B 123, 21 (1983).

[7] R. J. Bouchard and J. L. Gillson, Inorg. Chem., 7, 969 (1968).

[8] E. Polaczkowa, Bull. Acad. Polon Sci., Ser. sci. chim., 17, 445 (1969).

[9] M. Calligaris, Powder Diffraction Package (Version 1.1), Departimento di Scienze Chimiche, Universitat di Trieste, Italy (1989).

[10] Powder Diffraction File, published by JCPDS International Centre for Diffraction Data, Swarthmore (USA) (1988).

[11] H. P. Klug and L. E. Alexander, X-ray Diffraction Procedures, Wiley, New York, p.235 (1954).

[12] M. A. Short, Rev. Sci. Instrum., 31, 618 (1960).

[13] R. D. Burbank, Rev. Sci. Instrum., 32, 368 (1961).

[14] L. G. Parratt, Rev. Mod. Phys., 31, 616 (1959).

[15] R. W. James, The Optical Principles of the Diffraction of X-rays, Bell, London, p.268 (1958).

[16] J. Vierling, J. V. Gilfrich and L. S.Birks, Appl. Spectros., 23, 342 (1969).

[17] J. J. Gilman and R. Johnston, Dislocations and Mechanical Properties of Crystals, Wiley, New York, p.119 (1957).

[18] J. A. Bearden, Rev. Mod. Phys., 39, 78 (1967).

[19] E. R. Cohen and B. N. Taylor, J. Phys. Chem. Ref. Data, 2, 663 (1973).

[20] P. R.Sarode, Computer Programs For the Analysis of X-ray Absorption Spectra (1990) (Unpublished).

Table 2.1: Crystal and Detector angles for tungsten L$_I$-absorption edges.

Edge	λ Å	Energy in eV	Crystal plane	2d (Å)	Crystal	Detector angle
W L$_I$	1.02467	12099.6	Si(111)	6.276	9°23'48"	18°47'36"
			Si(220)	3.825	15°32'19"	31°4'38"
			Si(311)	3.276	18°13'37"	36°27'14"
			Si(400)	2.715	22°10'24"	44°20'48"
			LiF(200)	4.026	14°44'41"	29°29'22"

Table 2.2: Crystal and detector angles for tungsten L$_{III}$-absorption edges.

Edge	λ Å	Energy in eV	Crystal plane	2d (Å)	Crystal	Detector angle
W L$_{III}$	1.21550	10199.9	Si(111)	6.276	11°10'2"	22°20'5"
			Si(220)	3.825	18°31'43"	37°3'26"
			Si(311)	3.276	21°46'45"	43°33'31"
			Si(400)	2.715	26°35'46"	53°11'32"
			LiF(200)	4.026	15°28'45"	30°57'31"

Chapter 3

Tungsten L-Absorption Edges

3.1 Introduction

It is well known[1-6] that tungsten compounds have interesting chemistry as a consequence of 5d and 6s electrons present in the valence band. The nature of bonding in these compounds varies widely. For example, ionic contributions to the bondings in tungsten(IV) halides reach a maximum with WF_4 and minimum in an unstable compounds like WI_2 [7].

A feature of fundamental importance which influences the structure and bonding in W compounds is that the 5d, 6s and 6p levels are sufficiently close and hybridization of these orbitals is energetically favourable in several tungsten compounds. Hybridization alters the character of otherwise pure and partially vacant 5d and empty 6p levels of polyvalent covalently bonded W compounds. In the absence of hybridization, like in ionically bonded W^{4+} or W^{6+} compounds, the same 5d and 6p levels are subject to strong crystal field effects of the coordination spheres of ligands and depending on the point group symmetry of the tungsten atom, degeneracies of the p and d manifolds are lifted up. Hence it suggests that in either situation XANES spectroscopy should prove to be very strong informative experimental approach to study the coordination geometry and bonding relations in tungsten compounds. Since the near-edge features involve the transition from some core states to allowed lowest unoccupied empty states in the valence region of a given atomic center, XANES spectra should reveal not only the allowedness or otherwise of these transitions, but also the mixing or splitting of the final state-orbitals[8,11]. In this Chapter, we report XANES investigations of selected divalent, trivalent, tetravalent, pentavalent and hexavalent tungsten compounds, where, using the known structural data, informative deductions on structural bonding relations have been made. Both W L_I and $L_{II,III}$ edge XANES spectra have been used since they probe 2s $\rightarrow$ 6p and 2p $\rightarrow$ 5d transitions respectively.

Also since X-ray spectra probe dominantly the effect of local coordinations, we have extended the investigations to the tungsten oxide bronzes and industrially important tungsten oxide catalytic materials. We may expect on reasonable grounds that the near-edge analysis of these bronzes and catalytic compounds

51

will provide us the information on atomic environment of tungsten ions.

As mentioned above, since tungsten shows valences varying between 2^+ to 6^+, it would be therefore interesting to see whether the loading of WO_3 on Al_2O_3 or on TiO_2 in the catalysts or doping of rare-earth oxide in WO_3 forces tungsten to change its atomic environment. It is with this aim, we have undertaken the study of W L_I, L_{II} and L_{III}-edges in some model compounds, tungsten oxide bronzes and catalytic compounds of tungsten. In particular, we have measured the L_I, L_{II} and L_{III} absorption spectra of tungsten in WI_2, $K_3W_2Cl_9$, WO_2, WS_2, WSe_2, WCl_4Pyr_2, $C_{11}H_{14}N_2O_{12}BaW_2.6H_2O$, $[WCl_4L_2]Cl$ (L = 2,4,6 trimethylpyridine), $K[WO_2(C_2O_4)].xH_2O$, $(NH_4)_2WS_4$, $Fe_2(WO_4)_3$, $Al_2(WO_4)_3$, $CaWO_4$, $Eu_2(WO_4)_3$, $Na_2WO_4.2H_2O$, WO_2Br_2, $WOCl_4$, WCl_6, WO_2Cl_2, $NiWO_4$, $ZnWO_4$, $H_3PW_{12}O_{40}.5H_2O$, $(NH_4)_6H_2W_{12}O_{40}.5H_2O$, WO_3, $WO_3.H_2O$ and WV_2O_6 and tungsten oxide bronzes, $Eu_{0.1}WO_3$, $Sm_{0.1}WO_3$, $La_{0.1}WO_3$, $Na_{0.15}WO_3$ and $In_{0.21}WO_3$. We have examined the L-edge spectra of calcined air exposed and reduced alumina and calcined titania supported tungsten oxide catalysts. We have chosen catalysts containing 4, 6, 8, 10 and 12 % by weight of WO_3 on the surface. L-edge spectra of calcined and reduced $Ni - W/Al_2O_3$ catalysts of tungsten are also studied.

3.2   Results and Discussion

In Figs.3.1-14 are presented the normalized L_I and L_{III}-absorption edge spectra of representative tungsten compounds, tungsten oxide bronzes, calcined and reduced alumina and calcined titania supported tungsten   oxide catalysts and nickel-tungsten alumina catalysts. As mentioned in Chapter 2, the X-ray absorption spectra were recorded at room temperature on single crystal X-ray spectrometer using Si(311) as monochromator.

The energy scale for the edge spectra given in these figures were calibrated relative to tungsten metal foil. The first derivative of the L_I-edge spectrum shows two peaks : the first peak gives the inflection point of the edge. The energy scale was set in such a way that the first peak in the derivative spectrum corresponds to the W L_I energy (12099.6 eV) and the energies of the peak positions of all the
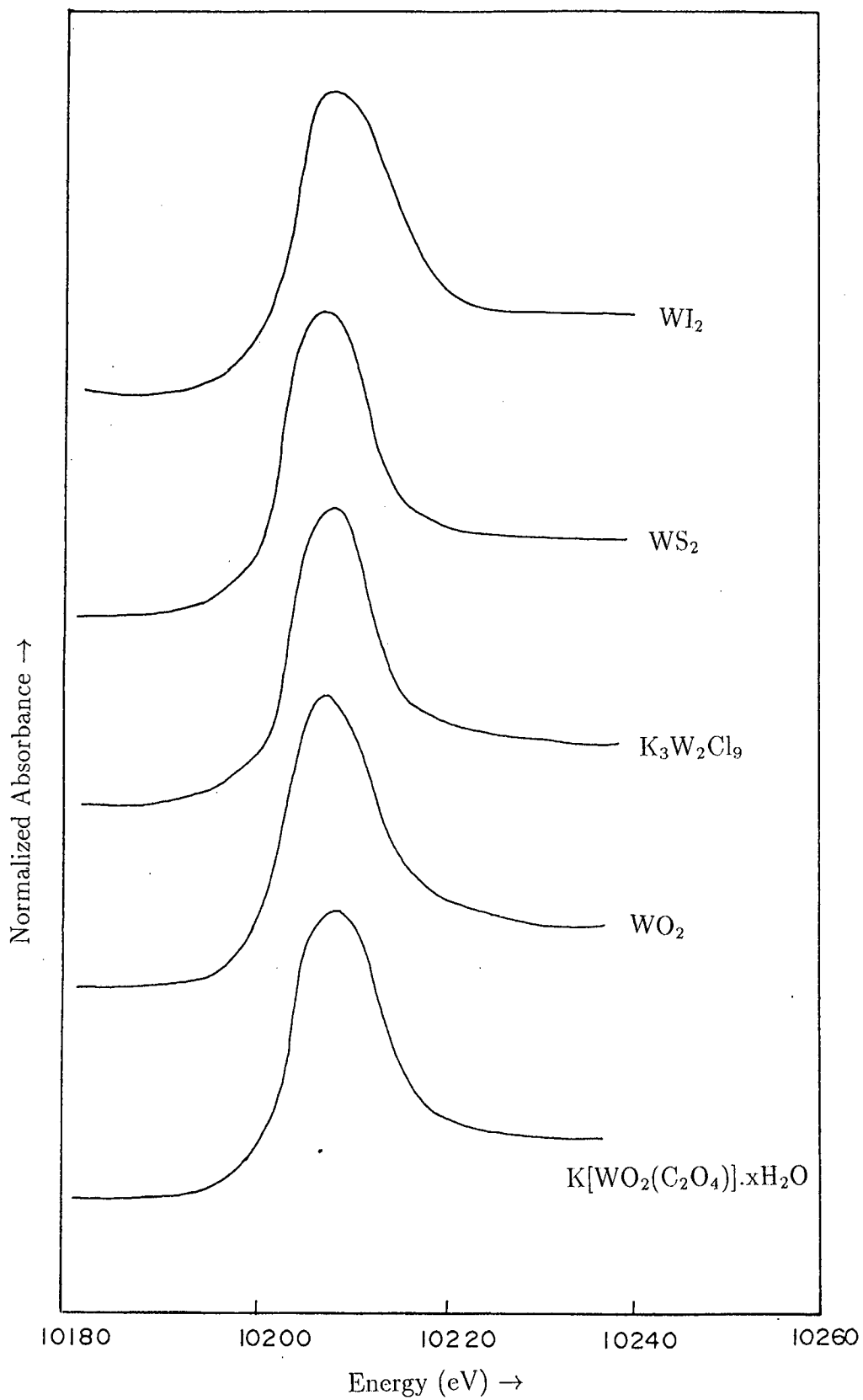
Figure 3.1: L_{III}-edge spectra in octahedral compounds of tungsten.
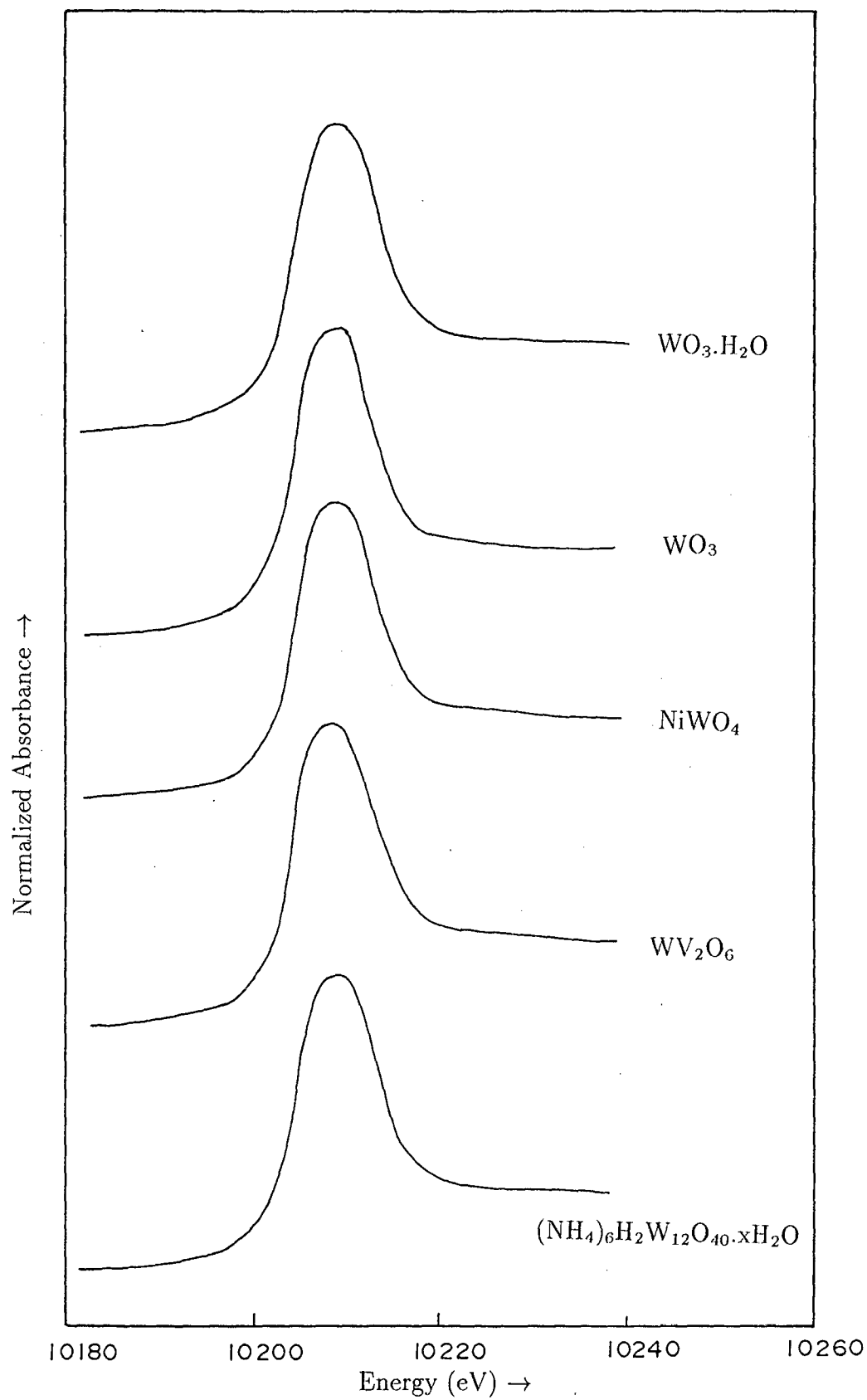
Figure 3.2: L_{III}-edge spectra in octahedral compounds of tungsten.
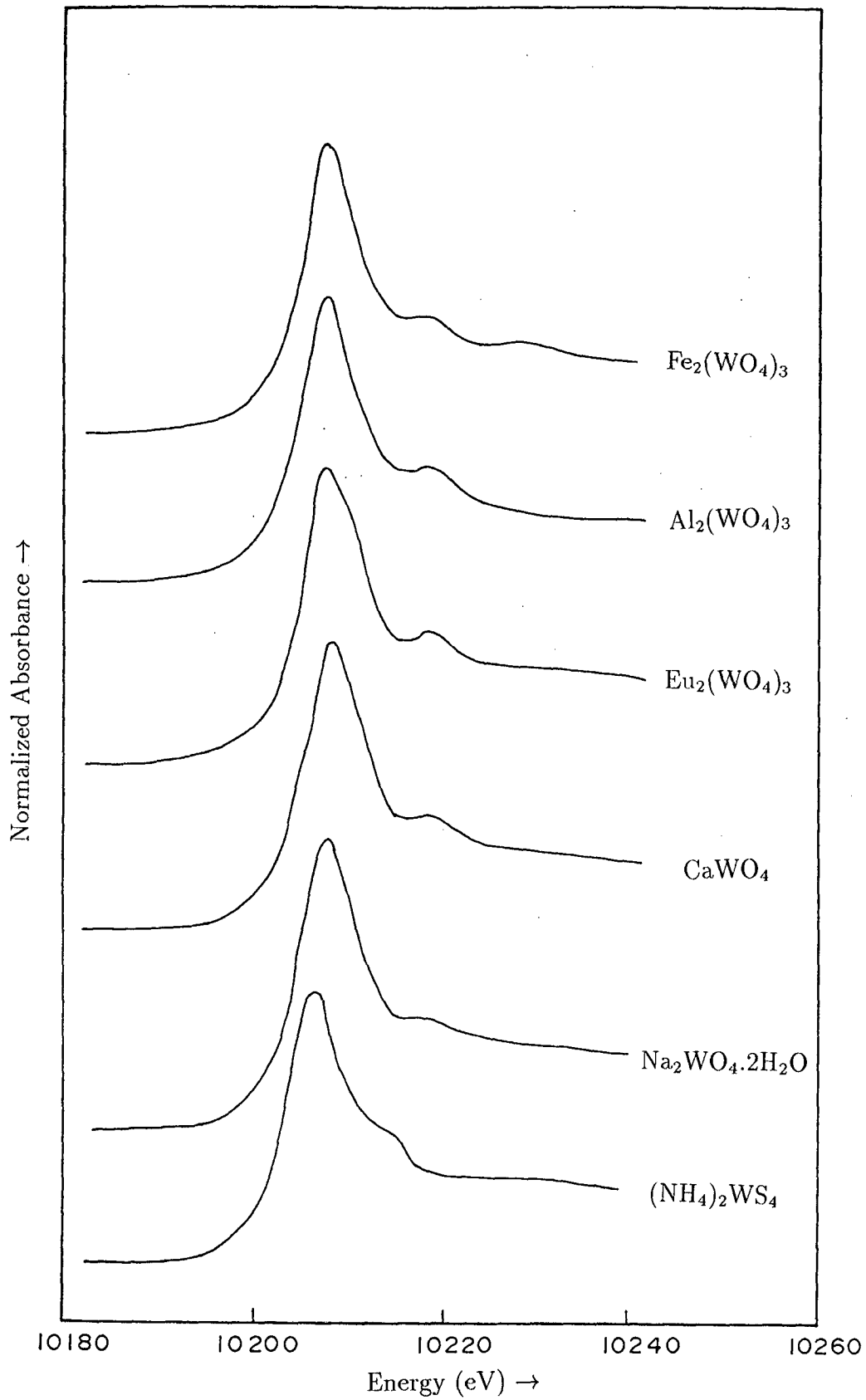
Figure 3.3: L_{III}-edge spectra in tetrahedral compounds of tungsten.
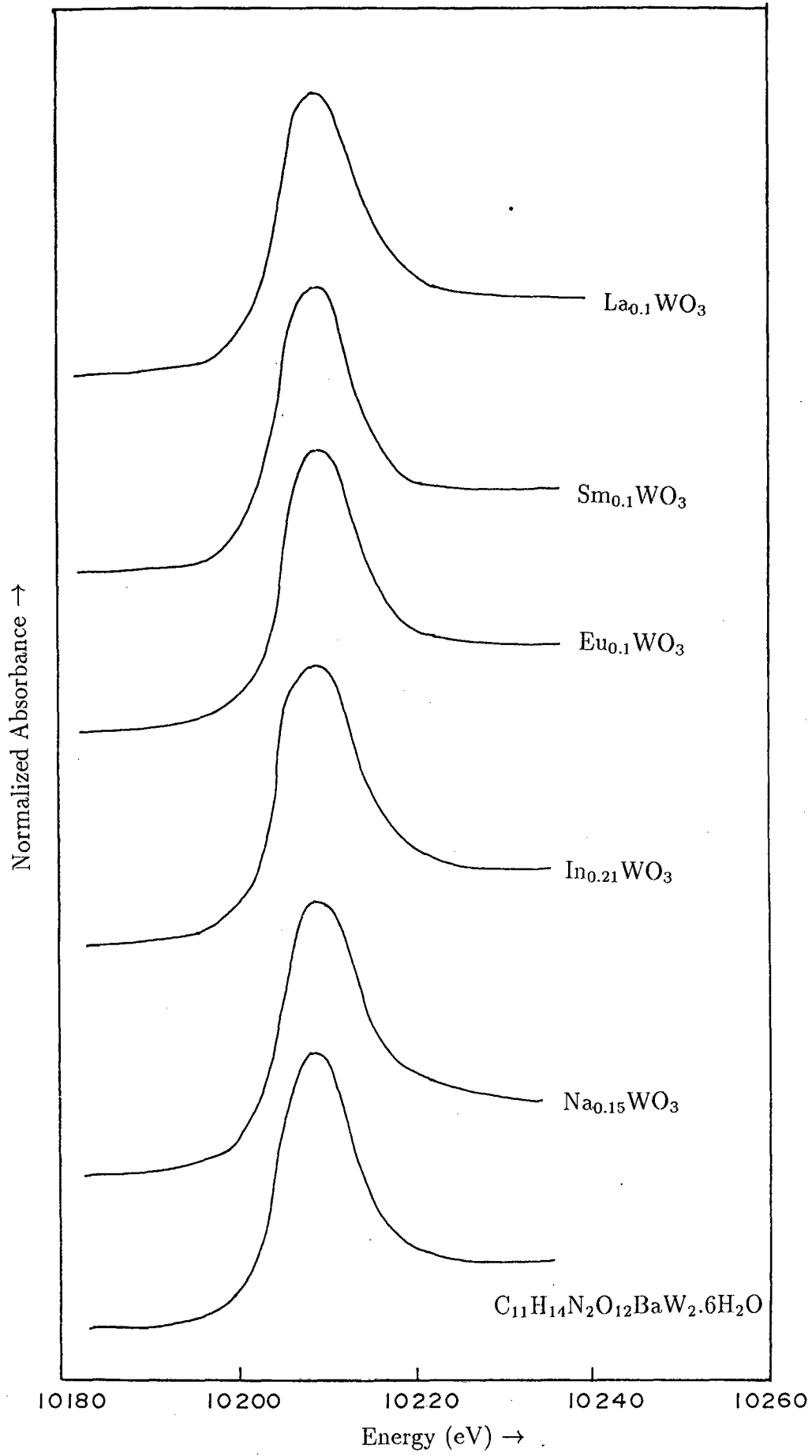
Figure 3.4: L$_{III}$-edge spectra in biocomplex and rare-earth tungsten oxide bronzes.
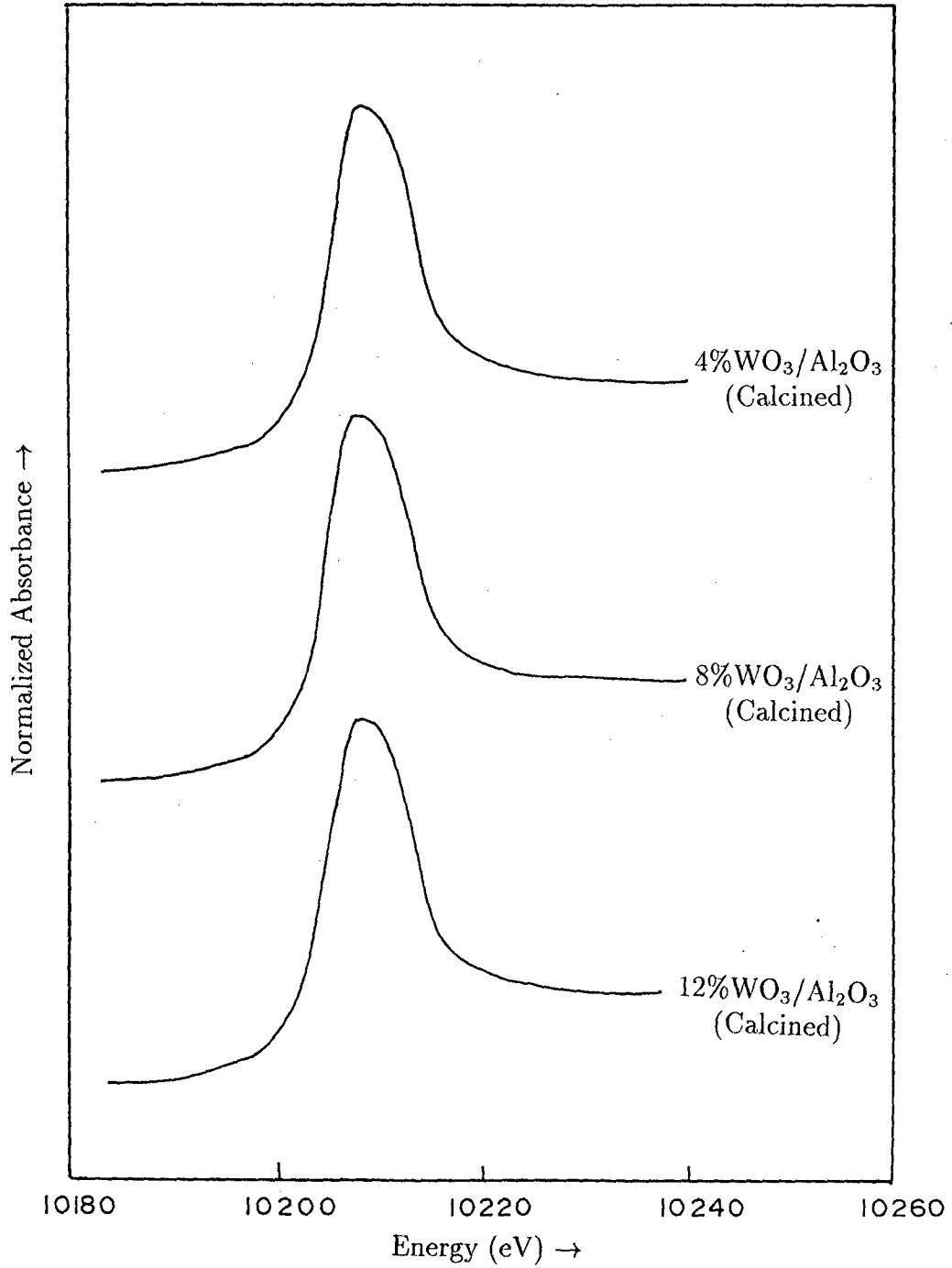
Figure 3.5: L_{III}-edge spectra in calcined WO_3/Al_2O_3 catalytic compounds of tungsten with 4, 8 and 12 % wt. loading of WO_3.
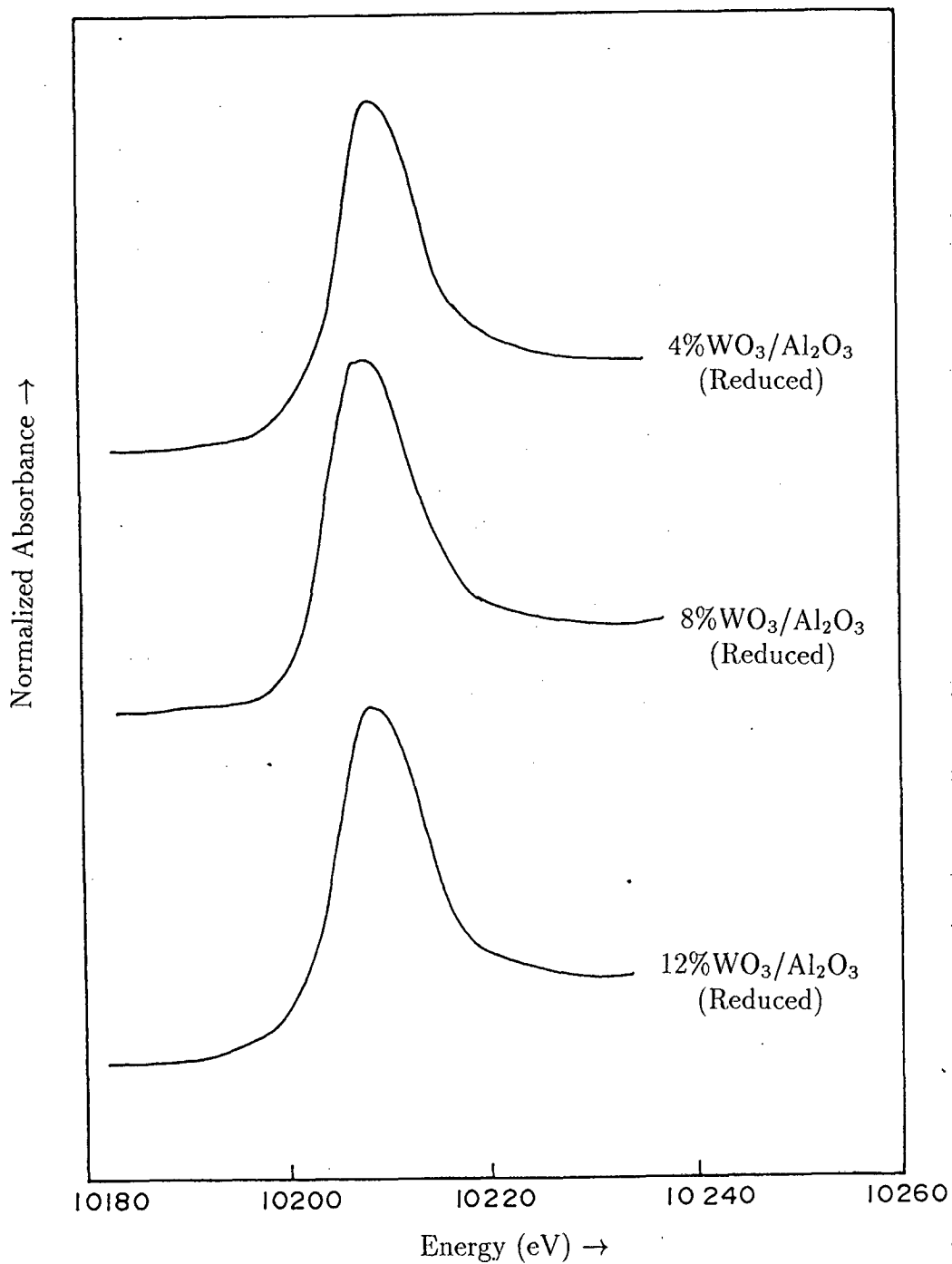
Figure 3.6: L_{III}-edge spectra in reduced WO_3/Al_2O_3 catalytic compounds of tungsten with 4, 8 and 12 % wt. loading of WO_3.
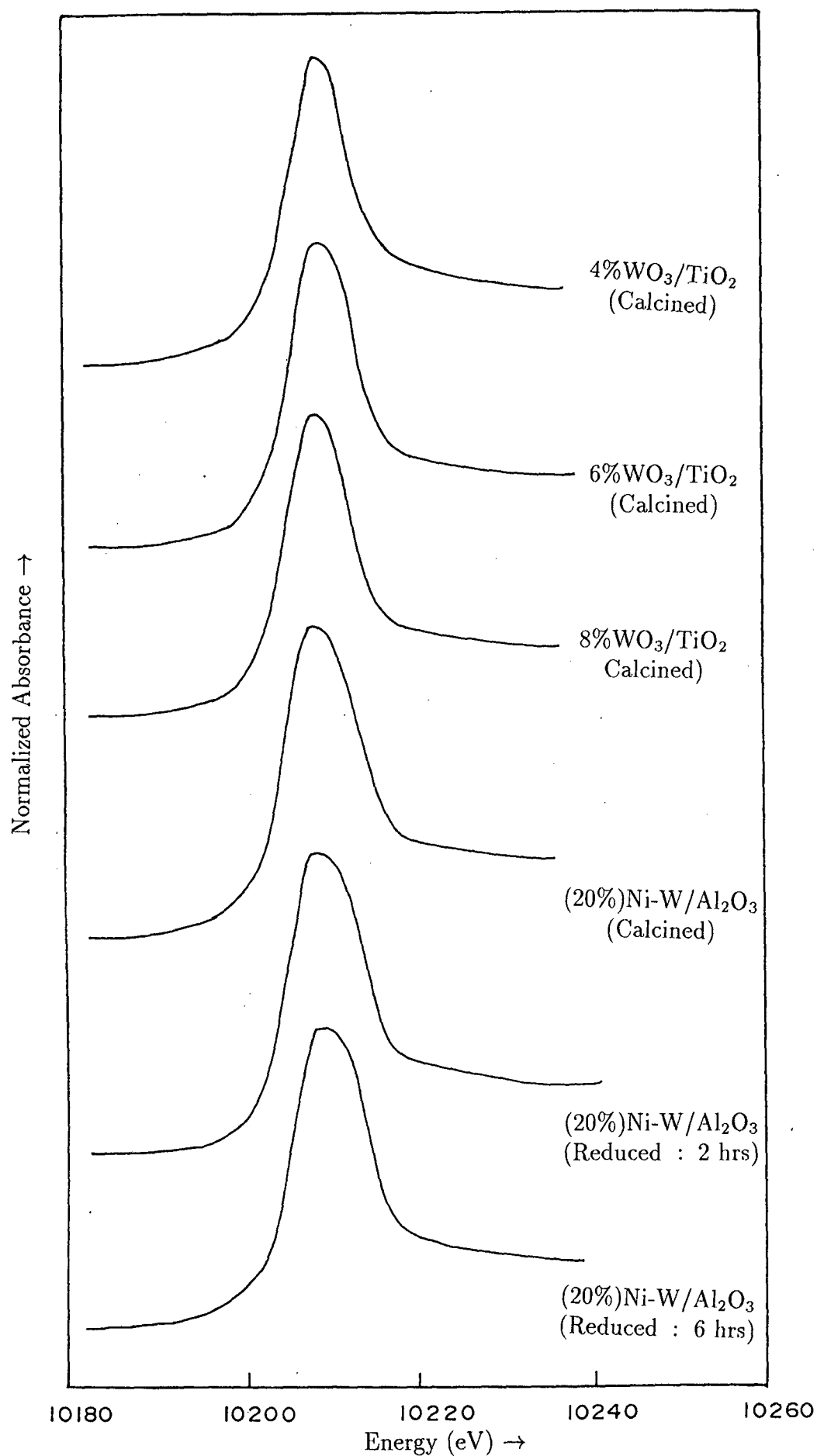
Figure 3.7: L_{III}-edge spectra in calcined WO_3/TiO_2 catalytic compounds of tungsten with 4, 6 and 8 % wt. loading of WO_3 and 20 % calcined and reduced $Ni - W/Al_2O_3$ catalyst.
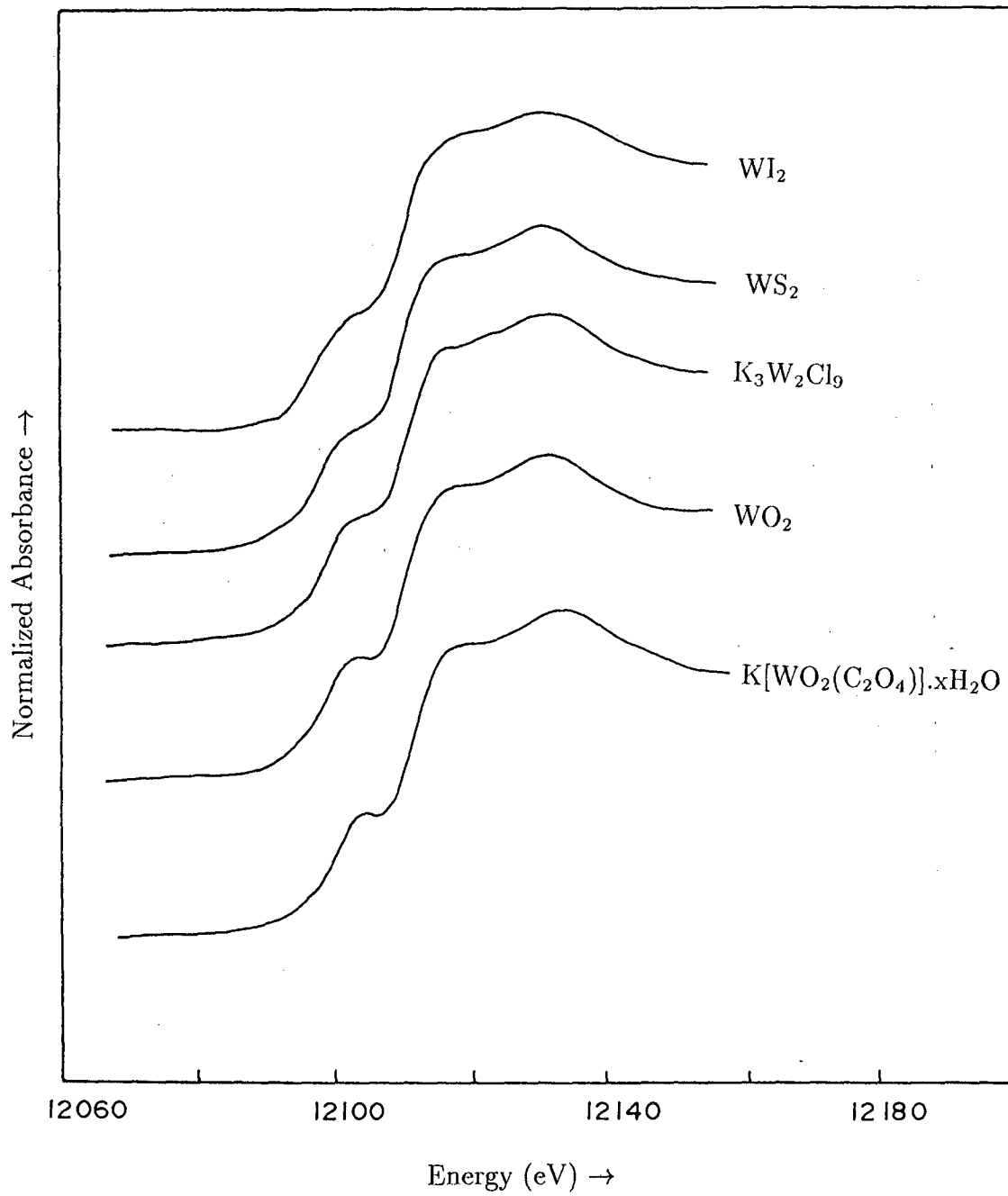
Figure 3.8: L_I-edge spectra in octahedral compounds of tungsten.
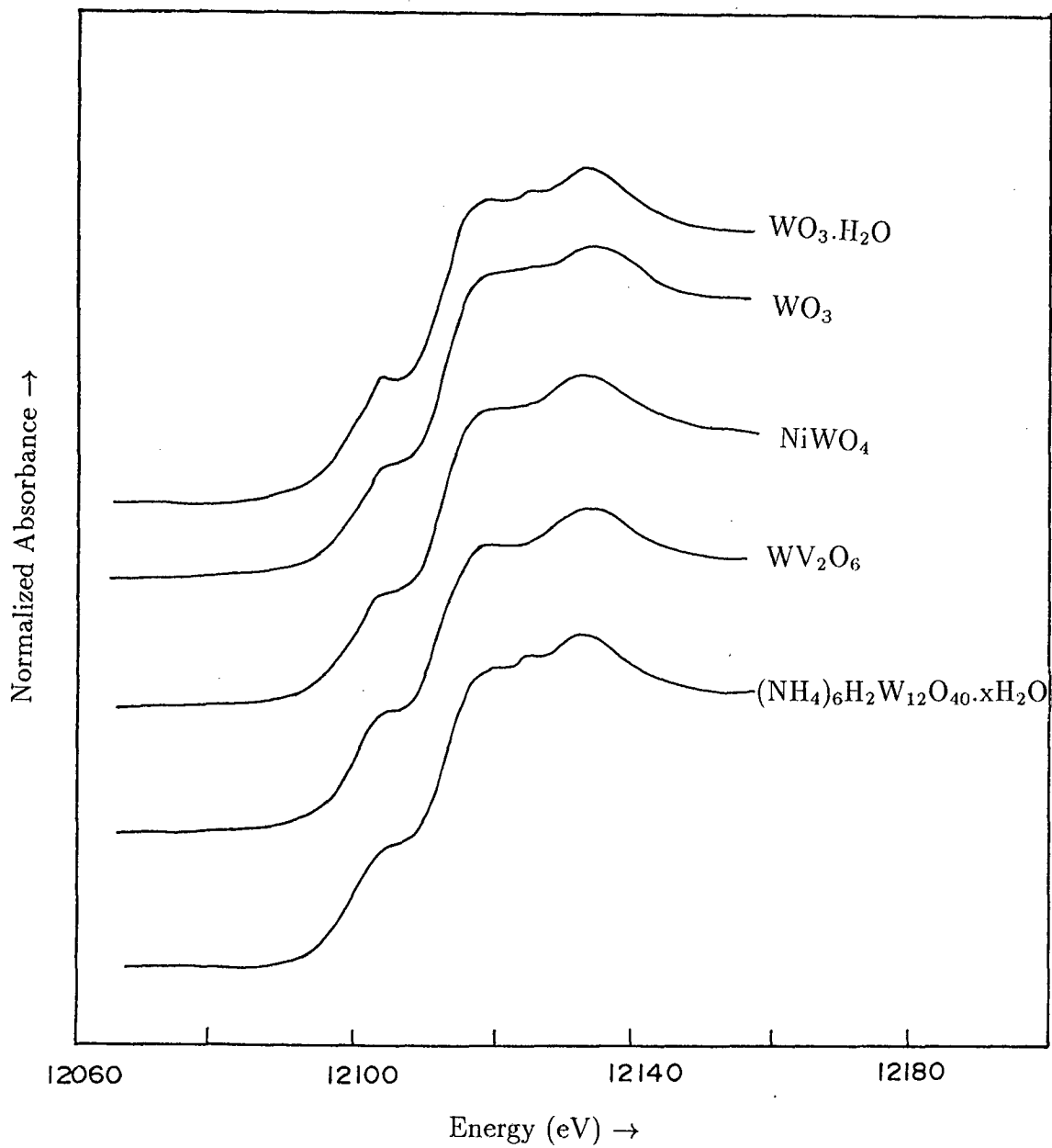
Figure 3.9: L_I-edge spectra in octahedral compounds of tungsten.
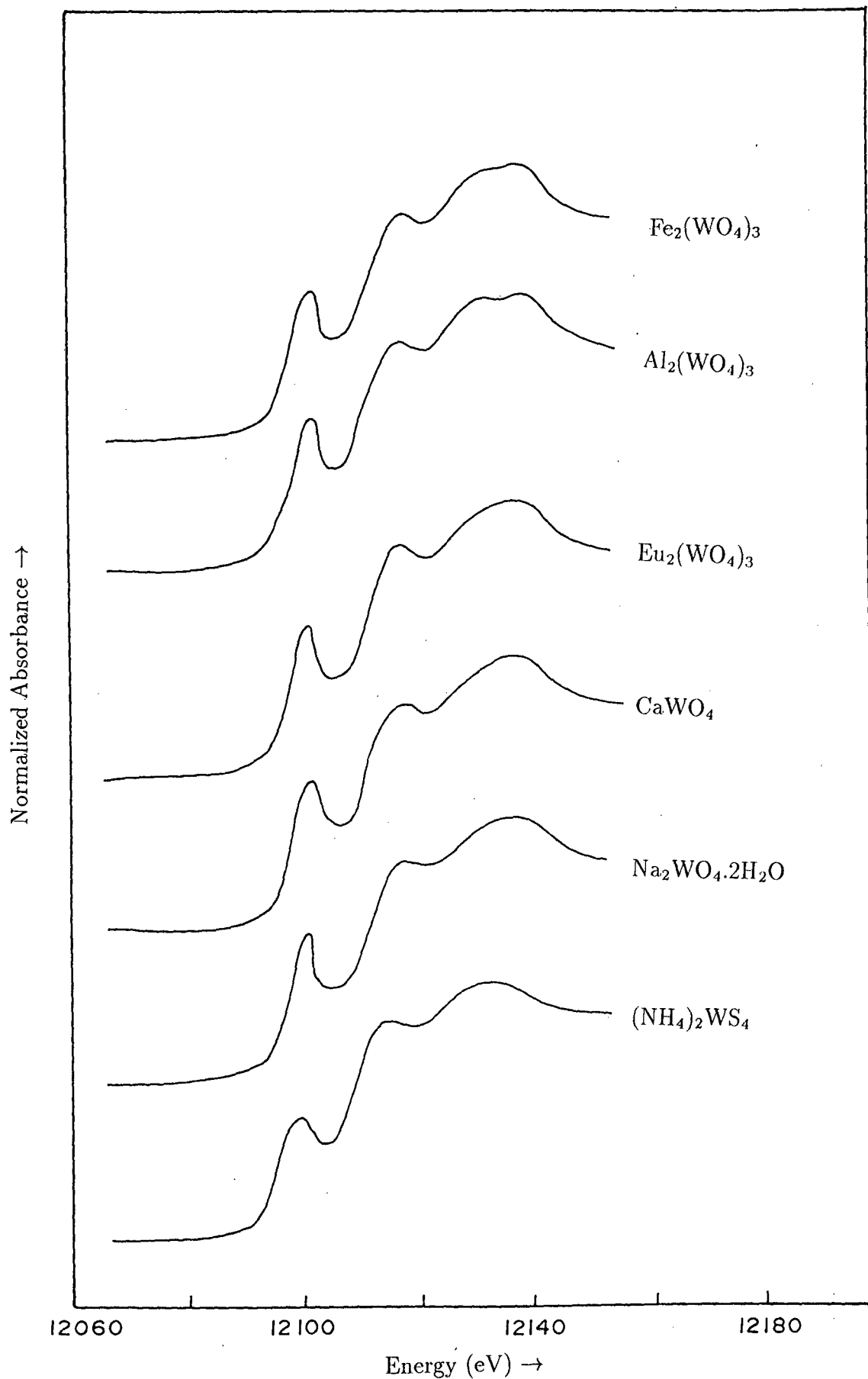
Figure 3.10: L$_I$-edge spectra in tetrahedral compounds of tungsten.
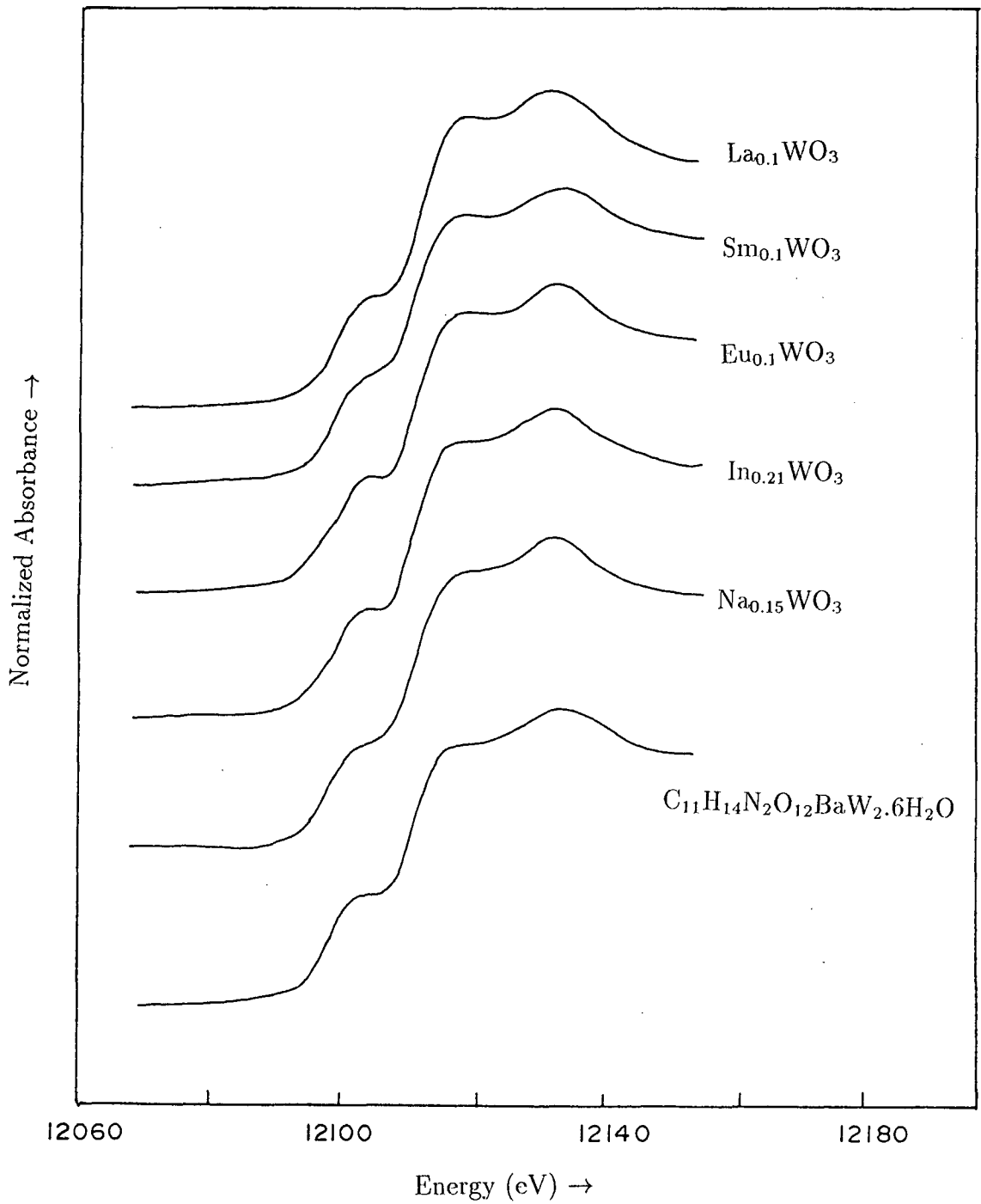
Figure 3.11: L_I-edge spectra in biocomplex and rare-earth tungsten oxide bronzes.
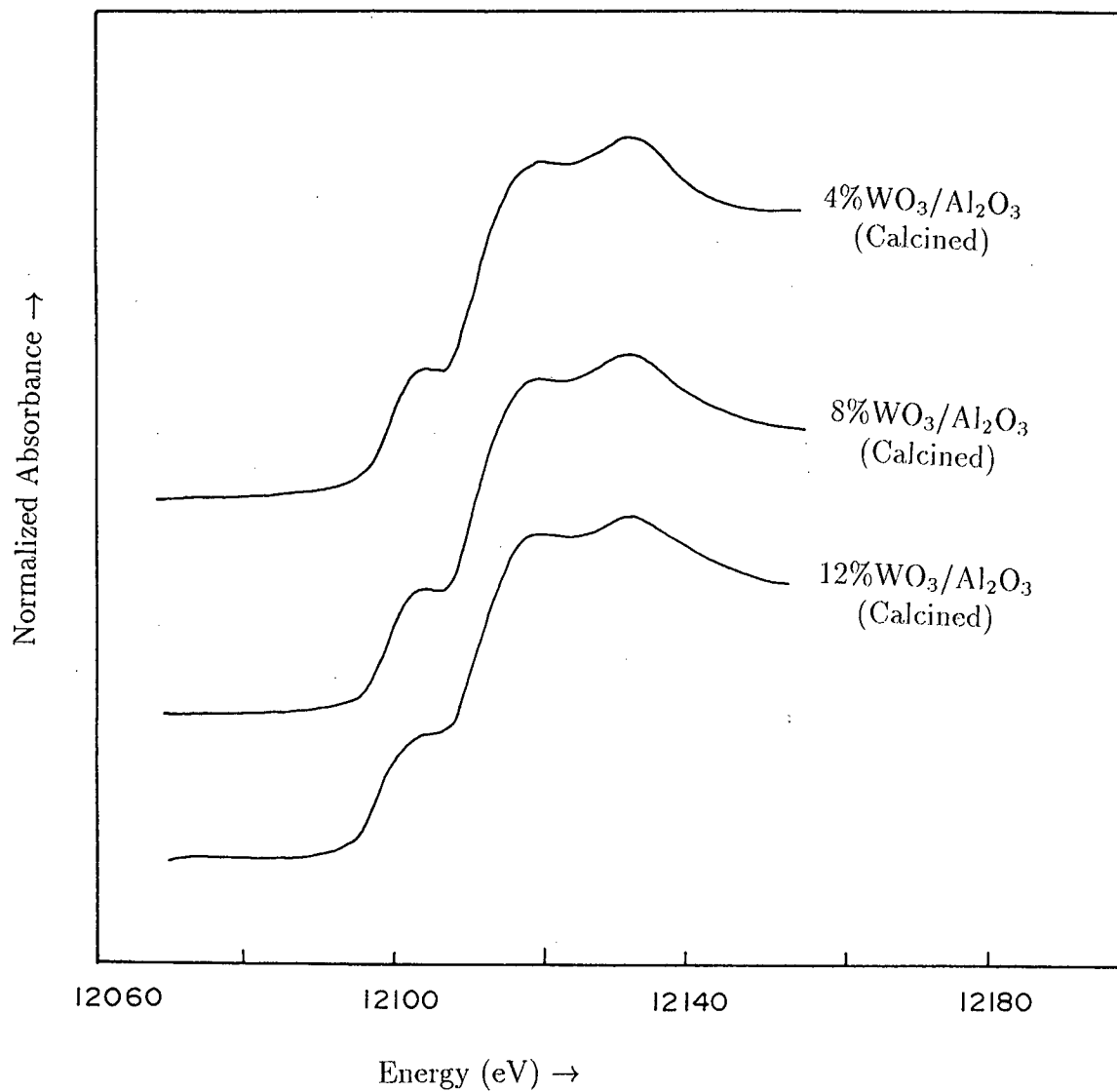
Figure 3.12: L_I-edge spectra in calcined WO_3/Al_2O_3 catalytic compounds of tungsten with 4, 8 and 12 % wt. loading of WO_3.
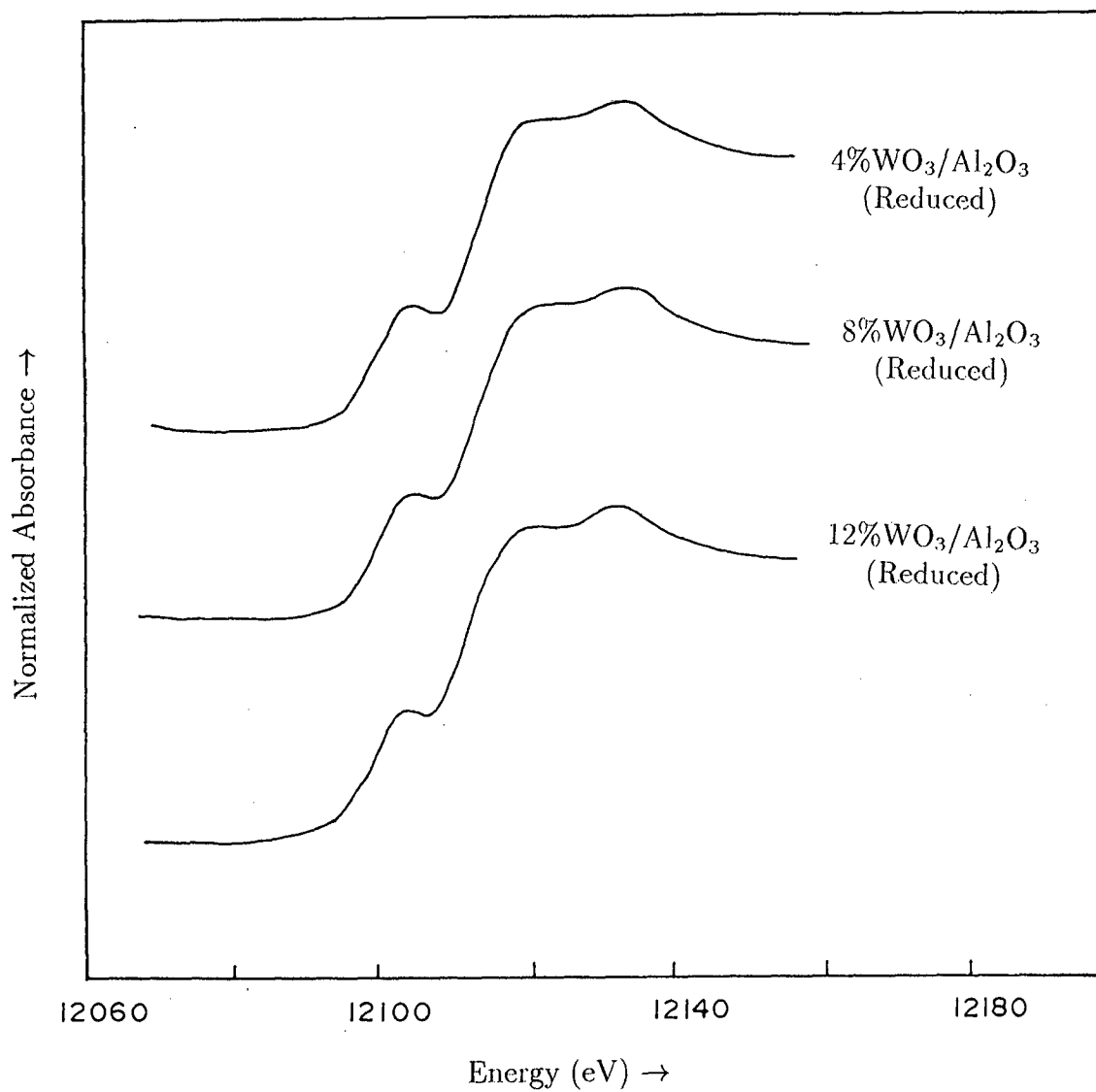
Figure 3.13: L_I-edge spectra in reduced WO_3/Al_2O_3 catalytic compounds of tungsten with 4, 8 and 12 % wt. loading of WO_3.
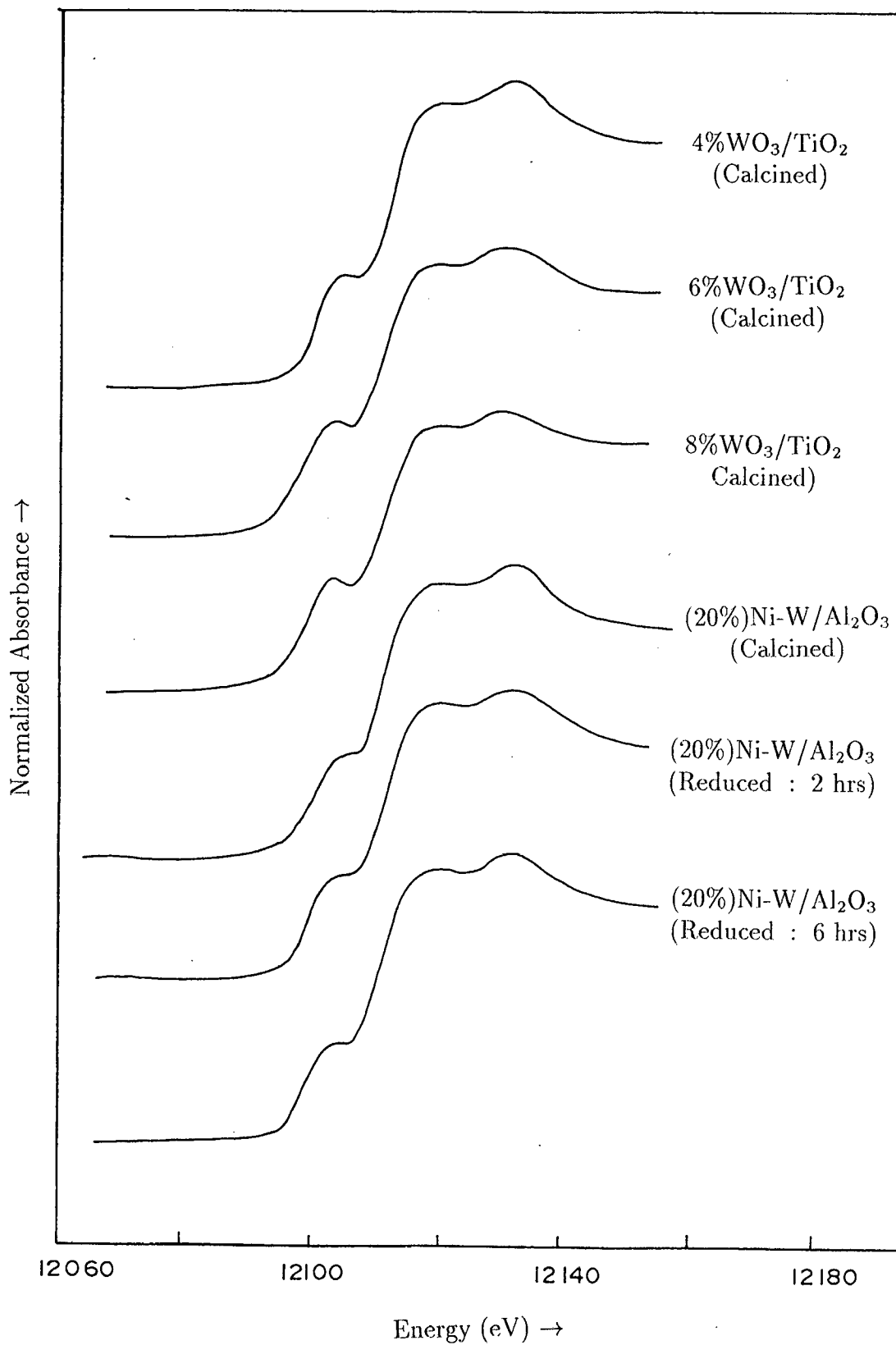
Figure 3.14: L_I-edge spectra in calcined WO_3/TiO_2 catalytic compounds of tungsten with 4, 6 and 8 % wt. loading of WO_3 and 20% calcined and reduced $Ni - W/Al_2O_3$ catalyst.

compounds are measured relative to this value. The energy calibration was also done by assigning the energy 12063.40 eV to the peak position of tungsten $L\gamma_4$ emission line. All these spectra were normalized by fitting a victoreen function to the pre-edge data and polynomial spline to the EXAFS region, extrapolating both functions to the zero of energy (E_o), subtracting the pre-edge data function from each point in the experimental spectrum, and dividing by the step height at E_o. This procedure thus results in a normalization of the data to unit step height.

These normalized X-ray absorption spectra suggest at once that the L_{III}-edges have far fewer features as compared to those of L_I-edges. We shall first discuss the tungsten L_{III}-edge spectra. It may be stated here that the L_{II}-edge spectra of tungsten are similar to L_{III}-edge spectra. Therefore, the profiles of L_{II}-edges are not given here. These profiles of absorption edges presented in the Figs.3.1-14 are obtained by averaging the results of a large number of spectra recorded in turn from each sample.

We see in from these figures that the L_I-absorption discontinuity of tungsten splits into three components whereas no splitting is observed in L_{III}-edges.

3.3 Tungsten L_{III}-edge spectra

Tungsten L_{III}-edge spectra in the representative octahedral tungsten compounds are shown in Figs.3.1 and 3.2. In Fig.3.3 are given the L_{III}-edge spectra in tetrahedral tungsten compounds of known crystal structure. The spectra, presented for octahedral compounds, show a pronounced absorption maximum, called white line, where for the tetrahedrally coordinated tungsten compounds, in addition to the intense narrow absorption maximum, a small peak around 15 eV is observed on the higher energy side of the absorption edge.

The outer electronic configuration of tungsten is $5d^4 6s^2 6p^0$ and for W^{2+}, W^{3+}, W^{4+}, W^{5+} and W^{6+} ions, the number of 5d electrons is 4, 3, 2, 1 and 0 respectively, i.e. the 5d band is partially filled in the case of divalent, trivalent, tetravalent and pentavalent compounds, while it is completely empty in the hexavalent compounds. The main absorption peak observed in all these compounds can be

assigned to the transition of $2p_{3/2}$ electron to the essentially empty or completely empty 5d band. The weak peak on higher energy side in tetrahedral compounds may arise due to the transition of $2p_{3/2}$ electron to empty high energy states of d or s symmetry.

The tungsten compounds like WO_2Cl_2, $WOCl_4$, WO_2Br_2, WCl_4Py_2 having mixed ligands also show single absorption peak similar to those given in Figs.3.1 and 3.2. We have not given their spectra as we have not used these spectra of them in the discussion.

We note two main differences between the L_{III}-edge spectra for octahedral and tetrahedral compounds :

1. The main absorption maximum (white line) in the octahedral compounds is broader (width $\sim$ 8.5 eV) and it is relatively sharp (width $\sim$ 5.5 eV) in the case of tetrahedrally coordinated compounds.

2. Appearence of weak peak on the high energy side of the main absorption maximum is a typical feature characterizing tetrahedral symmetry. Such spectral feature is absent in the octahedral compounds.

On the basis of the above spectral features associated with L_{III}-absorption spectra of tungsten compounds, one can distinguish between the tetrahedrally and octahedrally tungsten ions in the tungsten compounds wherein it is difficult to extract information on metal site symmetry in complex systems. In tungsten oxide bronzes and in the alumina and titania supported tungsten oxide catalysts, one can use these spectral features to extract structural information. Before doing this, it would be appropriate to first determine the coordination geometry of tungsten ion in well characterised biocomplex of tungsten namely, $Bis(\mu - oxo)(\mu - N, N' - (R) - propylenediaminetetraaceto)bis(oxotungstate(V))$. Its formula is $C_{11}H_{14}N_2O_{12}BaW_2.6H_2O$.

The L_{III}-absorption spectra of biocomplex is shown in Fig.3.4. The overall profile of the biocomplex is very similar to the L_{III} spectra of tungsten in their compounds like WO_3, $NiWO_4$, $K[WO_2(C_2O_4)].xH_2O$, and other octahedrally coordinated tungsten compounds, thereby suggesting octahedral environment of ligands around the central tungsten ions. From a more careful examination of

68

intensity and energy of the peak in the L_{III}-edge region, it is found that these two quantities are very close to those of $K[WO_2(C_2O_4)].xH_2O$. However, they are slightly different from those observed for octahedrally coordinated tungsten compounds. This seems to suggest that the octahedron of ligands around the tungsten ion is relatively distorted. This sort of distortion can be studied in detail if we analyze the EXAFS spectrum associated with the L_{III}-edge. These observations clearly indicate that the pentavalent tungsten ion in this biocomplex has distorted octahedral coordination. Our conclusion in this respect is in good agreement with that derived from X-ray crystallographic studies by Ikari et al [12].

After having confirmed the metal site symmetry in a well characterized biocomplex of tungsten, we are now in a position to determine the valence and site symmetry of tungsten ions in the rare-earth tungsten oxide bronzes. The X-ray L_{III}-edge absorption spectra for all the tungsten oxide bronzes namely, $La_{0.1}WO_3$, $Eu_{0.1}WO_3$, $Sm_{0.1}WO_3$, $Na_{0.15}WO_3$ and $In_{0.21}WO_3$ are shown in Fig.3.4. The absorption maxima in all these bronzes are slightly broadened. In these spectra, the white lines (or pronounced broadened absorption maxima) are very similar to that in the tungsten compounds having hexavalent tungsten ions in octahedral configuration as shown in Figs.3.1 and 3.2. This leads us to infer that octahedrally coordinated hexavalent tungsten ions are present in these oxide bronzes of tungsten.

Our findings that the tungsten ions are in 6^+ oxidation state in the bronzes are supported by the magnetic susceptibility measurements on rare-earth tungsten bronzes by Ostertag [13], by Shipunova et al [14] on their investigations on electrical properties of rare-earth tungstates and by Bialkowska et al [15] on their studies on ESR and Mössbauer spectroscopic investigation on cubic bronzes of the type Ln_xWO_3.

The L_{III}-absorption spectra for 4%, 8% and 12% WO_3/Al_2O_3 samples calcined at 500°C are shown in Fig.3.5. It can be seen that there is a slight decrease in the width of the white line as compared to the widths of WO_3, $WO_3.H_2O$ and other octahedral compounds but the width is larger than that observed for tetrahedral compounds and there is no change in the L_{III}-edge position also. Moreover for

all the samples, the spectra are almost identical. The slight change of width suggests that there may be formation of species containing a little proportion of groups other than WO_6, or perhaps WO_4-like groups. Although the X-ray edge energy measured for catalysts is close to the values measured for $Al_2(WO_4)_3$, $Fe_2(WO_4)_3$, $CaWO_4$, the occurence of this species cannot be based unambiguosly on edge energy alone. It is evident from the position of the edges, however, that the tungsten is present in the 6^+ oxidation state. Formation of $Al_2(WO_4)_3$ on catalyst surface is ruled out as the white lines are broader for catalysts than that for $Al_2(WO_4)_3$.

The degree of metal-support interaction present in supported heterogeneous catalysts can be effectively estimated by comparing the reduction properties of the supported species with the corresponding bulk metal oxides. The W L_{III}-edge spectra of catalysts containing 4-12% WO_3/Al_2O_3 are shown in Fig.3.6 after reduction for 12 hours at 500°C in flowing H_2 gas. It is apparent from the spectra shown that the tungsten species has not been reduced to any detectable extent in the composition range of catalysts studied. If at all there is any reduction, it may be occuring in the high concentration of WO_3 on the surface. We have not carried out such studies on high loading percentages of WO_3 on $\gamma - Al_2O_3$.

The L_{III}-edge absorption spectra for 4% to 8% WO_3/TiO_2 catalytic samples calcined at 500°C are shown in Fig.3.7. These spectra show similarity with the spectra of WO_3, $WO_3.H_2O$ and other such compounds. A very little change in intensity is observed. Intensity in this case is slightly higher than those observed for $WO_3.H_2O$, WO_3 and other octahedral compounds and width is slightly less. This indicates that the W^{6+} ions have mainly octahedral symmetry and very little tetrahedral symmetry. Even if WO_3 content increases no appreciable change is observed.

In the calcined $Ni/W/\gamma - Al_2O_3$ catalyst containing 20% W and 5% Ni, L_{III}-edge peak and the profile position are close to those observed in W^{6+} compounds having octahedral coordination. On reduction in H_2 at 500°C for 2 hrs and at 550°C for 6 hrs, there is no appreciable change in the profile. This suggests that the species formed on the surface may be a very stable interaction complex of tungsten.

70

3.4 Tungsten L_I-edge spectra

In Figs.3.8 and 9 are presented the normalized L_I-absorption spectra of model tungsten compounds.

In the L_I-absorption edge region of these compounds, one typically observes a series of discrete spectral peaks (due to transition of the 2s electron to unoccupied molecular orbitals of metal character) superimposed upon a steeply rising absorption trend (due to transitions of the 2s electron to the continuum levels) [11]. The *shape* of the edge which is determined by the relative intensities and width of these low-lying "bound-state" transitions, contains information about the geometry of the metal complex and nature of ligands present. Thus octahedral compounds of tungsten (Fig.3.8 and 3.9) have broad 2s → 6p, 2s → 6s and weak 2s → 5d transitions [16]. On the other hand, complexes with tetrahedral geometry (Fig.3.10) have strongly enhanced 2s → 5d transitions, because of mixing of 5d, 6s and 6p character in the excited state orbitals [16, 17].

Now in the foregoing discussion, we will restrict our attention to the hexavalent tungsten compounds having W-O bonds since the bronzes and catalytic compounds contain oxygen as bonding ligand of the hexavalent tungsten ion.

As mentioned above the intensity of the pre-edge feature is determined primarily by the site-symmetry of the metal ion[16-22]. According to Kutzler et al [23] when the ligand environment of the metal ion has octahedral symmetry, then the metal component of the upper state has d-character only. Since the initial state 2s has a gerade symmetry with respect to the centre of inversion of the octahedron, transition from 2s core level to 5d level is strictly dipole forbidden as it is in $NiWO_4$ and WI_2, which contain regular octahedral WO_6 and WI_6 units having a centre of inversion. At the most a very weak quadrupole-allowed transition may be observed in this case. However, when the symmetry of the ligands is lowered from O_h; inversion centre is broken. The pre-edge absorption becomes dipole allowed due to a combination of such stronger 5d → 6p mixing and overlap of the metal 5d orbital with the 2p orbital of the ligand. In our case a well-defined, fairly intense pre-edge feature is observed as in $CaWO_4$, $Eu_2(WO_4)_3$ and $Fe_2(WO_4)_3$, where the WO_4 groups have regular tetrahedral symmetry. Sharp

pre-edge features are also observed in the other tetrahedral tungsten compounds.

Bair and Goddard [24] have carried out *ab initio* self-consistent field calculations on the excited states of the $CuCl_2$ molecule involving excitations of the Cu 1s orbital into bound valence and unbound virtual orbitals. These authors have calculated both the absolute excitation energies and the transition strengths, and considered the presence of a fully relaxed core hole, in their theoretical method based on a multielectron model utilizing a Hartree-Focks configuration-interaction approach. They have found that the weak pre-edge peak is indeed due to a transition to a partially unoccupied orbital of a primarily metal 3d character, in agreement with the above discussion. The main absorption peak at 8993 eV is assigned as a transition to the orbitals that are primarily of a metal 4p character (1s → $4p_z$) again in agreement with some of the above studies. However, the shoulder (the lower energy feature at 8986 eV) is not assigned to any single-electron transition. The 1s → 4s monopole transition strength is found to be far too weak to be observed and appears at the wrong energy to fit the shoulder peak data. Rather, this feature is reassigned by these authors to a "shake down" satellite transition involving a Cu 1s → $4p_z$ transition simultaneous with ligand-to-metal charge transfer.

A similar interpretation has recently been proposed[22,24] for the polarised spectra of $CuCl_2.2H_2O$ and $(creat)_2CuCl_2$. Satellite peaks, which are pronounced in inner-shell XPS studies of many transition-metal complexes[27-31], are predicted to be significantly reduced in intensity in X-ray absorption edge studies due to the shielding of the valence electrons when the photoelectron is in the low-energy threshold region. A previous study [32] comparing the XPS and X-ray absorption spectra of $FeCl_2$, $MnCl_2$ and $CoCl_2$ found low intensity satellites to the high energy side of the principal absorption maxima at energies corresponding to those expected on the basis of the prominent satellites splittings found in XPS.

Any distortion of a regular octahedral environment will also remove the center of inversion and a pre-edge feature will be observed in this case as well, although it is usually broader and less intense than the pre-edge feature for compounds having metal ion in tetrahedral symmetry. As reported in literature, it is observed

in the case of K-edge spectra of vanadium compounds studied by Wong et al [33] in V_2O_3, V_2O_7 and V_2O_4 with distorted octahedra VO_6 groups and in V_2O_5 with distorted square-pyramidal VO_5 groups.

The pre-edge feature for WO_3 and the other compounds shown in Figs.3.7-3.8, where the WO_6 group has a distorted octahedral environment, is weak and is observed only as a shoulder on the rising absorption discontinuity. A similar explanation also does apply to the tungsten compounds having mixed ligands. For example, in WO_2Cl_2 (the spectrum is not given), wherein the metal ion is ligated to four oxygen and two chlorine atoms forming a distorted octahedral coordination.

Thus, we see that without going for the complicated methods of band structure calculations or other methods based on geometrical structure calculations, the fine structure of an absorption spectrum can be utilized as "fingerprint" for determining the changes in the local arrangement of the neighbouring atoms around the absorbing metal ion, in comparison with model compounds having well defined crystal structures.

In order to determine the metal-site symmetry in rare-earth tungsten oxide bronzes and the alumina and titania supported tungsten oxide catalysts, we have made comparison of the edge spectra of these materials with those of model compounds of tungsten as is done in the case of L_{III}-edge spectra above.

As a test of applicability of our method, we first determine the metal site symmetry of tungsten metal ion in $(NH_4)_6H_2W_{12}O_{40}.5H_2O$, wherein the crystal structure is well known [1]. The spectrum of this compound (Fig.3.8) compares very well with those of octahedrally coordinated tungsten compounds, thereby lending us confidence to our method of determining the metal site symmetry in tungsten compounds.

In Fig.3.11 are shown the L_I-edge spectra of $La_{0.1}WO_3$, $Sm_{0.1}WO_3$, $Eu_{0.1}WO_3$, $Na_{0.15}WO_3$, $In_{0.21}WO_3$ and in Fig.3.12 and 3.13, the spectra of calcined and reduced WO_3/TiO_2 and in Fig.3.14 the spectra of calcined WO_3/Al_2O_3 and calcined and reduced $Ni-W/Al_2O_3$ catalysts. We now compare the absorption features of these spectra with those of the model compounds for determining ligand coordination around tungsten ions in these complex oxides. The absorption-edge profiles

of L_I-edges in bronzes are similar to the profiles in the model compounds presented in Fig.3.8, indicating thereby the presence of WO_6 group. The pre-edge feature in the catalyst samples shows similarity with those of octahedral compounds. However, there is slight decrease in the width of the edge. This seems to suggest us that the surface species on catalytic samples may have WO_6-type species with small percentage of WO_4 groups. In case of reduced $Ni - W/Al_2O_3$ catalysts, no change of absorption profile or peak position is observed. This leads us to infer that there may be a formation of stable interaction complex on the surface of the catalyst.

In order to get a rough idea about the extent of WO_4 groups which are formed on the surface of the catalysts, a deconvolution of the tungsten L_I-edge spectrum into three Lorentzians and an arctangent function was carried out using a computer program developed in this laboratory on the basis of algoriothm proposed by Rosenbrock [34, 35]. In literature, such deconvolutions of absorption edges have been carried out by Breinig et al [36], Breinig [37], Cramer and Hodgson [38] and Chiu et al [39] in the transition metal compounds.

The results of such analysis of the edge spectra in two representative model compounds, $CaWO_4$ and $NiWO_4$, wherein the tungsten ions have tetrahedral and octahedral coordinations respectively are presented in Figs.3.15 and 3.16. The areas in these compounds corresponding to $2s\rightarrow5d$ (pre-edge) were computed by integration of the corresponding Lorentzians using Simpsons rule. The numerical values of these areas are found to be ~ 47.10 units for $CaWO_4$ and ~ 33.30 units for $NiWO_4$.

Similar analysis in one of the representative catalysts, 8% WO_3/TiO_2 was performed and the estimated area found is ~ 36.24 units (See Fig.3.17). This value, corresponding approximately to the integrated intensity of the pre-edge, although lies between those for $CaWO_4$ and $NiWO_4$, is very close to that of $NiWO_4$. This crude estimate also confirms our finding that the catalyst surface contains species having more WO_6 than WO_4 groups, the percentage of WO_4 groups being $\sim 10\%$.
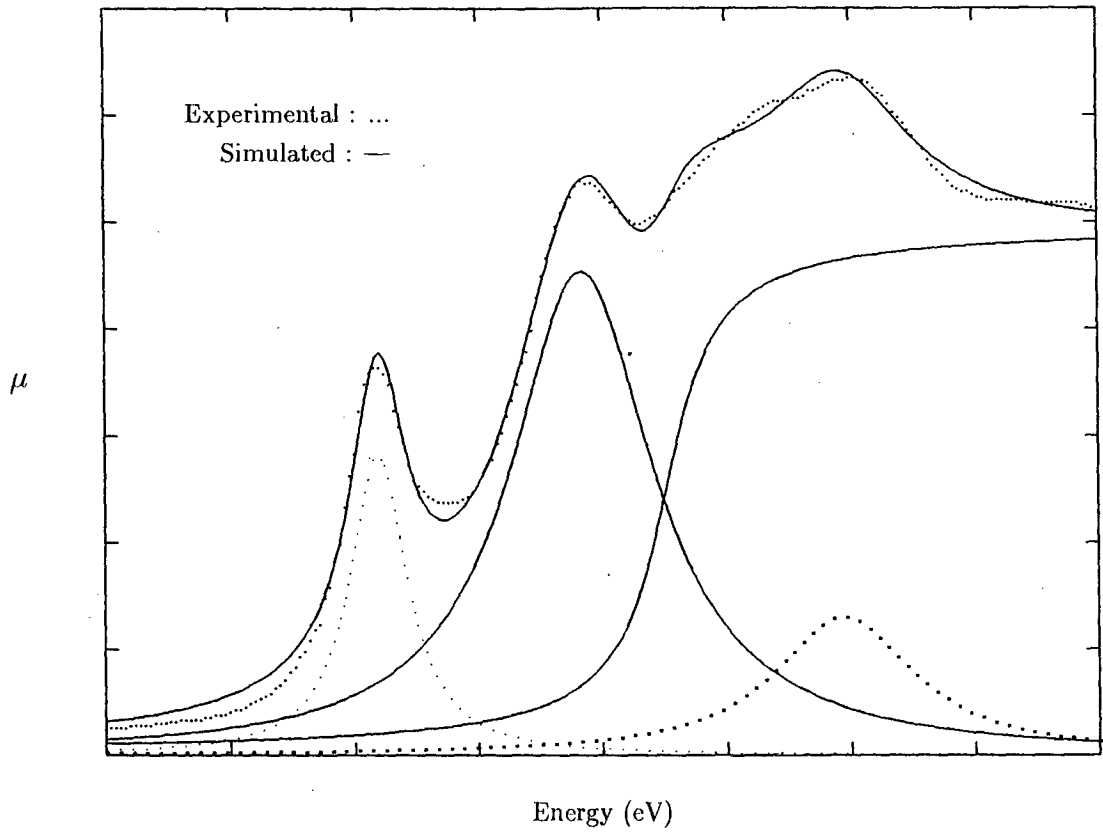
Fig. 3.15: L_I absorption edge of $CaWO_4$ showing deconvolution of the edge features by curve fitting with three Lorentzians and an arctangent function.
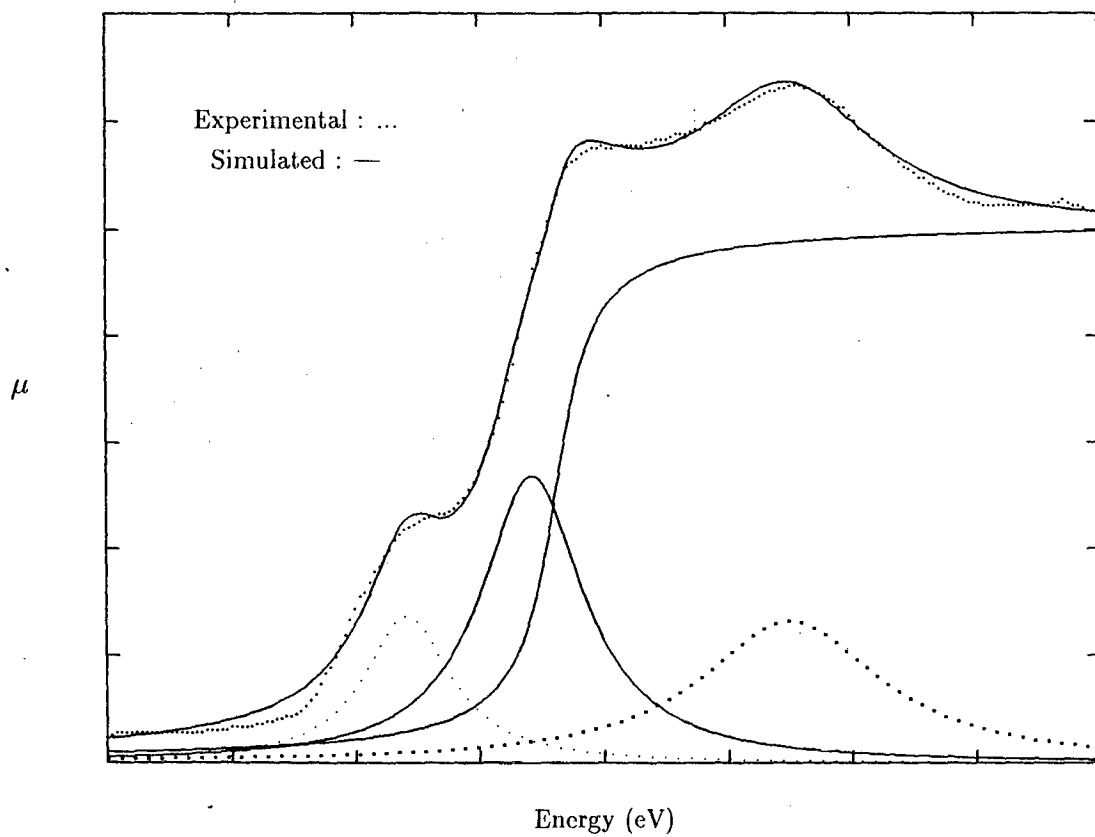
Fig. 3.16: L_I absorption edge of $NiWO_4$ showing deconvolution of the edge features by curve fitting with three Lorentzians and an arctangent function.
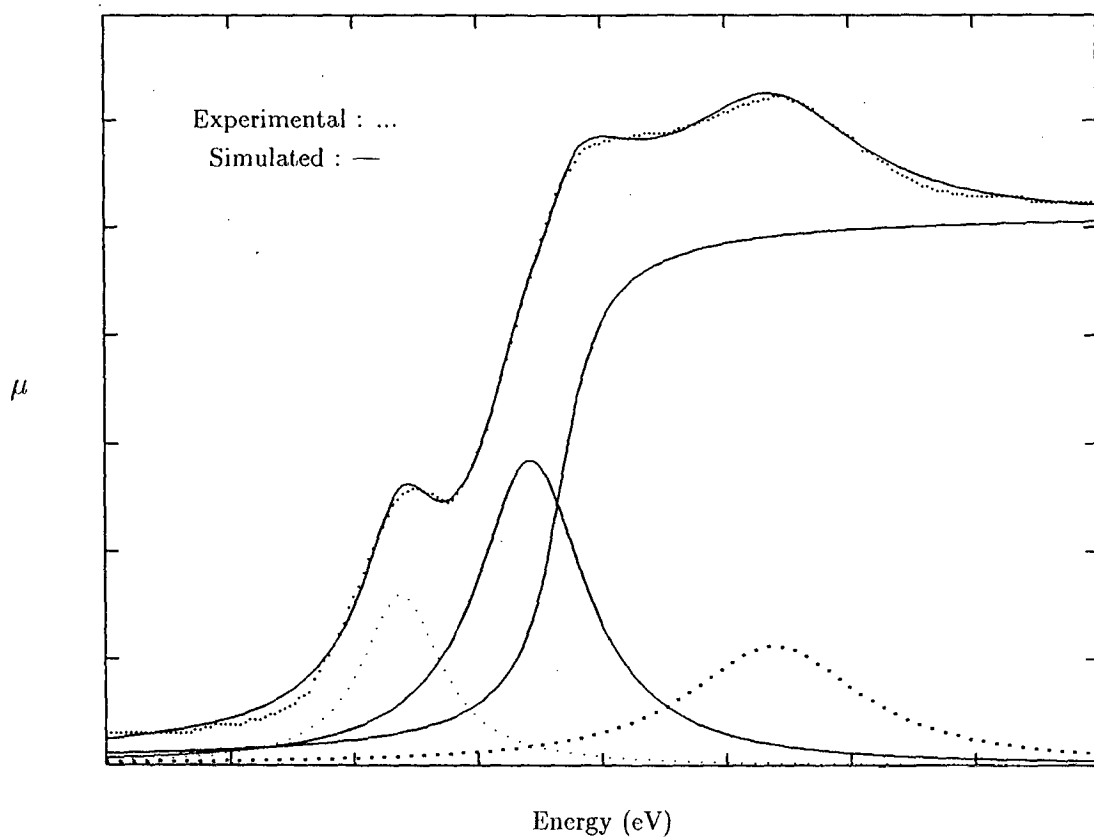
Fig. 3.17: L$_I$ absorption edge of 8% WO$_3$/TiO$_2$ showing deconvolution of the edge features by curve fitting with three Lorentzians and an arctangent function.

3.5 Molecular-orbital approach and W L-edge structure

The assignments 2s → 5d, 2s → 6s and 2p → 6p although useful in a qualitative sense, are unsatisfactory in one respect. They are based on an atomic model for the available orbitals that does not take into account the covalent bonding. Clearly, the final orbitals for the lower energy transitions cannot be of pure d or s character, since the angular momentum selection rules forbid 2s → nd or 2s → (n + 1)s transitions. In Ref. [16] Shulman et al have claimed that vibronic mixing of s, p and d character makes the low energy transitions allowed. However, in many complexes, covalent interactions between metal and ligands could also cause such mixing, in which case a molecular orbital (MO) description of the electronic transitions would be more desirable [40].

It is well known [22, 41] that the fine structure within about 20 to 25 eV of an absorption edge in a compound is characteristic of chemical bonding. Literature survey shows that the molecular orbital theory has been successfully employed by many workers to explain fine structure observed in the absorption edges of compounds. Fischer [42, 43], Sarode and Pendharkars [44], Pendharkar and Mande [45], Obashi [46, 47], Chetal and coworkers[48-50] and Rao et al [51] have assigned the fine structure peaks to the transition of core electron to the vacant molecular orbital levels of appropriate symmetry formed from interaction of ligands with central metal atoms. With the help of this model it will be possible for us to understand the variation in the intensities of the pre-edge feature by invoking electronic transitions to empty molecular orbitals formed from linear combination of atomic orbitals of tungsten and ligands.

A qualitative molecular orbital diagram for octahedral compounds like WO_3, $NiWO_4$, WO_2, $ZnWO_4$, etc., adapted from the book of Ballhausen and Gray [52] is shown Fig.3.18. This diagram takes into account the interactions of the metal 5d, 6s and 6p orbitals and the 2s and $2p(\sigma, \pi)$ orbitals of the liganding oxygen. In this figure, solid, half open, and fully open circles represent electron pairs, unpaired electrons and fully vacant states respectively. In the octahedral group, WO_6,

the tungsten atom contributes six electrons ($5d^4, 6s^2$) and six oxygen ligands contribute 36 electrons ($2s^2 2p^4$) to the formation of molecular orbitals. The $(WO_6)^{6-}$ ion has six more electrons because of its negative charge. Therefore the total number of electrons of WO_6 group contributed to the formation of the molecular orbitals is 48. After distributing all these electrons in the various molecular orbitals as shown in Fig.3.18, one finds that the orbitals below $2t_{2g}$ are completely filled. The higher energy orbitals $2t_{2g}$, $3e_g$, $3a_{1g}$ and $4t_{1u}$ are completely vacant. The antibonding orbitals $2t_{2g}$ and $3e_g$ have d symmetry, whereas the orbital $3a_{1g}$ has s symmetry and the outermost empty antibonding $4t_{1u}$ level has p symmetry.

In the 3d transition metal compounds (e.g. Na_2CrO_4) and 5d transition metal complexes like $Cs_2(ReCl_6)$, wherein transition metal ions are octahedrally coordinated to different ligands, the d orbital splitting is of the order of 4 eV [53, 54]. It is difficult to see two transitions from 2s core level to $3e_g$ and $2t_{2g}$ levels as the resolution of our spectrometer is ~ 4 eV and instrumental broadening is not subtracted from the reported spectra in Figs.3.1-7. Moreover, the initial core levels have finite widths. Therefore, the pre-edge peak in Fig.3.1 to 3.7 can now be attributed to the transitions of the 2s electrons of the L_I-shell to the vacant $(2t_{2g}, 3e_g)$ molecular orbital levels. The shoulder-like maximum and main absorption maxima can be assigned to the transitions 2s $\rightarrow$ $3a_{1g}$ and 2s $\rightarrow$ $4t_{1u}$ respectively.

It may be noted that the 2s $\rightarrow$ $(2t_{2g}, 3e_g)$ and 2s $\rightarrow$ $3a_{1g}$ transitions are dipole forbidden. However, as can be clearly seen from the molecular orbital picture shown in Fig.3.18, some amount of p character from oxygen orbitals mixes up with the metallic orbital to form these molecular orbitals, making these two electronic transitions allowed. If the liganding atom is nitrogen, chlorine or sulphur instead of oxygen, the same molecular orbital picture is valid only with a change in orbitals of ligands. Furthermore, in some compounds of tungsten having mixed ligands comprising halogen and oxygen atoms (for ex. WO_2Cl_2, WO_2Br_2, $WOCl_4$), the molecular orbital picture is quite complicated. No such MO level diagrams are available in literature for mixed ligands linked to the metal atoms. Therefore, it is difficult to interpret the edge structure in such compounds

79
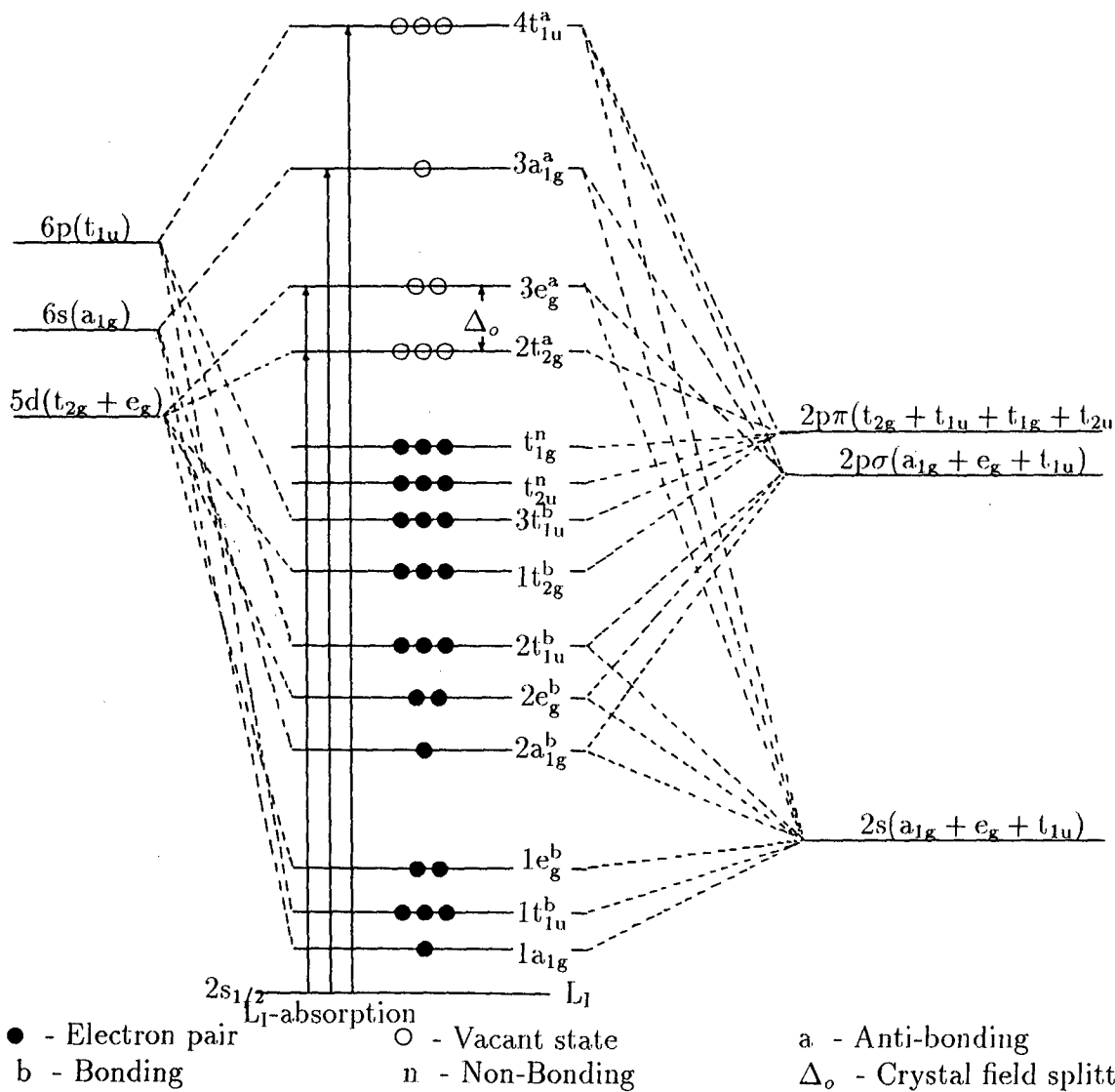
Fig. 3.18: Molecular orbital energy scheme for octahedral tungsten compounds.

on the basis of MO picture.

The L_{III}-edge structure in octahedrally coordinated tungsten compounds can be interpreted on the basis of MO theory in a manner similar to the L_I-edge structure discussed above. The only prominent maximum observed in Fig.3.1 - 3.7, can be assigned to dipole allowed transition of 2p electron to the vacant $(2t_{2g}, 3e_g)$ levels. We have not observed any pre-edge feature or shoulder on low energy side of this maximum and also any kink or peak-like structure within 25 eV on high energy side of the edge. Therefore, in L_{III}-edge structure, no electron transitions can be assigned to the empty antibonding orbitals $3a_{1g}$ and $4t_{1u}$.

For tungsten compounds like $CaWO_4$, $Eu_2(WO_4)_3$, $Fe_2(WO_4)_3$, wherein the tungsten ion is tetrahedrally bonded to the oxygen ligands, the molecular orbital picture is shown in Fig.3.19. This MO diagram is adopted from the Ref [52]. It takes into account the interaction of metal 5d, 6s and 6p orbitals and 2s and $2p(\sigma, \pi)$ orbitals of oxygen ligands. The tungsten atom contributes 6 electrons and four oxygen atoms contribute 24 electrons to the formation of molecular orbitals. Taking into consideration the charge on the $[WO_4]^{2-}$ ion, the total number of electrons is 32. After distributing these electrons in various molecular orbitals of WO_4 ion as shown in Fig.3.19, one finds that the orbitals below 2e are completely filled and the antibonding orbitals 2e, $4t_2$, $3a_1$ and $5t_2$ are completely vacant. The 2e molecular orbital is formed from 5d metal orbital and $2p(\pi)$ orbital of oxygen atom. The antibonding orbitals $4t_2$ have d+p admixture of metal character and $s + p(\sigma, \pi)$ admixture of ligand. The $3a_1$ orbital has s character of metal and s and $p(\pi)$ characters of ligand, whereas orbital $5t_2$ has d+p character of metal and $s + p(\sigma, \pi)$ of ligand. Hence the electrons from the L_{III} level can go, in the X-ray absorption process, to $(2e, 4t_2)$ level without violating the dipole selection rules. The pre-edge peak observed in L_I-edge can be interpreted as resulting from the electronic transition $2s \rightarrow (2e, 4t_2)$, since the 3d level splitting is very small as mentioned earlier. The shoulder peak and the main absorption peak in the L_I-edge spectra can be assigned to the transition of the 2s electron to the $3a_1$ and $5t_2$ molecular orbitals respectively.

It may be noted here that the relative intensity of pre-edge peak in L_I-edge

Tungsten Orbitals   Molecular Orbitals   Ligand Orbitals

$5t_2$

$6p(t_2)$ $3a_1$

$6s(a_1)$ $4t_2$ $2p\pi(t_1 + t_2 + e)$
                   Δ_o $2e$ $2p\sigma(t_2 + a_1)$
                   t_1
                   $3t_2$
$5d(t_2 + e)$ $2a_1$
                   $1e$
                   $2t_2$

                                    $2s(t_2 + a_1)$

                   $1t_2$
                   $1a_1$

$2s_{1/2}$ ——————————————— L_I
          L_I-Absorption

● = Electron pair   O = Vacant state Δ_o = Crystal field splitting
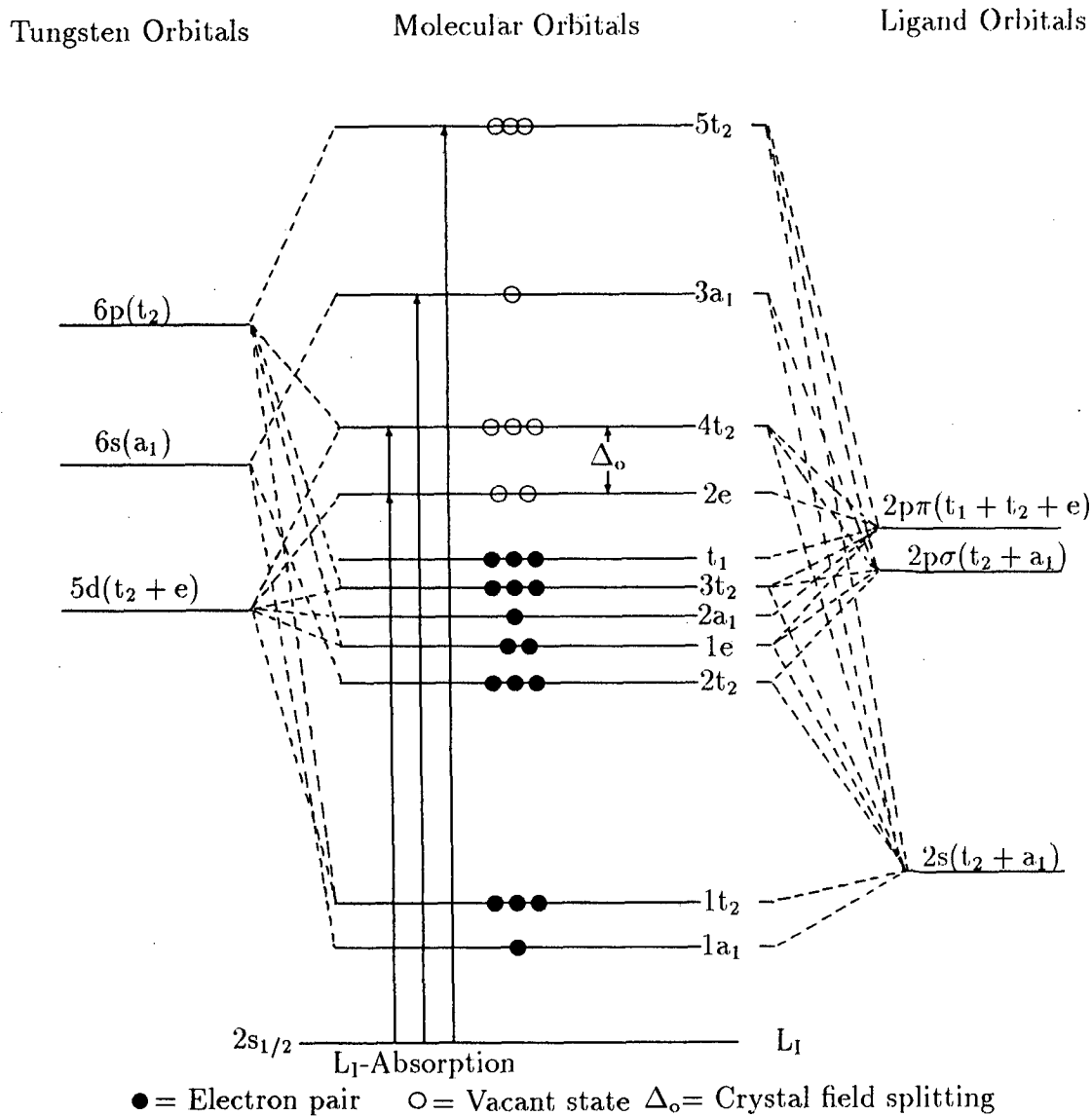
Fig. 3.19: Molecular orbital energy scheme for tetrahedral tungsten compounds.

spectra corresponding to 2s $\rightarrow$ 5d transition in tetrahedrally coordinated tungsten ions is relatively very large as compared to that of tungsten compounds wherein the tungsten ions are octahedrally coordinated. The reason is obvious, if we compare the transitions of 2s electron to $(2t_{2g}, 3e_g)$ and $(2e, 4t_2)$ levels in the octahedral and tetrahedral compounds respectively. The level $2t_{2g}$ or $3e_g$ has little p(σ, π) contribution from oxygen and hence the intensity of 2s $\rightarrow$ $(2t_{2g}, 3e_g)$ transition is very small in octahedral compounds. However, the level $(2e, 4t_2)$ has a relatively large amount of p contribution from metal as well as p(σ, π) contribution from ligand. It means that the $(2e, 4t_2)$ molecular orbital level has more p-contribution and the pre-edge peak corresponding to the transition 2s $\rightarrow$ $(2e, 4t_2)$ is more intense. This is the reason why many workers [9,19,23,33,55] have observed a very intense pre-edge transition in vanadium, chromium and manganese compounds.

It may be interesting to mention here that Walter and Butler [56] have studied the electronic structure of the vanadium and tungsten complexes by recording their absorption spectra derived from excitation spectra and emission spectra of unactivated yttrium vanadate and calcium tungstate. These authors have carried out a series of semiempirical LCAO-MO calculations on these compleses and have interpreted the absorption and emission spectra based on these calculations. In their results decomposition of absorption spectra into Gaussian components indicate the presence of an complex array of separate energy levels in these compounds. In the semiempirical MO calculations, these authors found the energy separations between $4t_2$ and $2e$, $4t_2$ and $5t_2$, and $5t_2$ and $3a_1$ to be 2.07, 14.8 and 7.23 eV respectively for $CaWO_4$.

In the compounds of tungsten studied by us, no splitting of pre-edge feature is observed. This may perhaps be due to the limited resolving power of our spectrometer and other factors mentioned above. However, since the differences in energies between pre-edge and shoulder and the shoulder and main absorption peak are more than 10 eV, we can safely compare the energy differences between these peaks corresponding to transitions of core electrons to $5t_2$ and $3a_1$ energy levels. In all tetrahedrally coordinated compounds, the differences in energy between pre-edge and shoulder peak is of the order of 14 eV. This difference in

energy is in good agreement with the value of 14.8 eV reported by Walter and Butler [56].

The energy difference between the shoulder peak and main absorption peak for tetrahedrally coordinated W compounds is ~ 20 eV. This difference seems to be very large as compared to the experimental value of 7 eV given by Walter and Butler. The reason for this discrepancy in the value of energy could be due either the widths of the core level, (which is of the order of few eV) or the broad main absorption peak believed to be consisting of two absorption maxima. In fact, if we carefully examine the L_I-spectrum of $CaWO_4$, we find there is indeed a peak between shoulder and main absorption peak. If we decompose this peak into Lorentzians, the separation is around 9 eV. Considering the uncertainties and other factors, this difference is close to the one reported by Walter and Butler [56].

We can interpret, in similar manner, the L_{III}-edge structure in the tetrahedrally coordinated tungsten compounds. The only prominent maximum observed in the tetrahedrally coordinated tungsten compounds in Fig.3.3, can be assigned to dipole allowed transition of 2p electron to the vacant $(2e, 4t_2)$ levels. The other absorption peak on the higher energy side of the main absorption is quite far from it and cannot be explained on the basis of molecular orbital diagram.

Vishnoi and Vishnoi et al [57, 58] have carried out work on L-absorption discontinuity in tungsten compounds and observed a strong white line accompanied by two weak peaks on the high energy side of the L_{II} and L_{III} discontinuities in tungstates of composition $M_2(WO_4)_3$, where M = La, Ce, Nd, Sm, Gd and Dy. In the L_{II} and L_{III}-absorption edge profiles (Figs.V.6 and V.7 of Ref. [57]) a weak feature on the high energy side of pronounced absorption maxima seen in WO_3 and $Sm_2(WO_4)_3$ is not observed by us. In the case of metal, no such weak feature is seen in L_{II}-spectra but in L_{III}-spectra reported by these authors clearly show a small kink after white line. In L_{III}-edge profile of tungsten in metal and tungstates (Fig.3.1-3.3) examined by us, no such weak features are observed. In some cases, a broad hump is noticed. It may be mentioned here that Bearden and Snyder [59] and Horsley et al [60] reported L_{III}-spectra similar to those given in Fig.3.1 - 3.3 recorded by us.

In the case of L_I-edge profiles reported by Vishnoi (Fig.V.4 in Ref. [57]), the

discontinuity splits into two components in W and WO_3 whereas in tungstates, in particular, $Sm_2(WO_4)_3$ there are three components observed. In our spectra, L_I-edge in W also show splitting into two components, however in WO_3 and other compounds, three distinct features are observed, intensity of which differ from compound to compound. The shoulder and main absorption peak (c and d in Vishnoi's case), have large intensity difference, whereas in Horsley et al [60] and in our case also, these features have almost the same intensities. It may be noted that we have recorded these spectra on computer controlled X-ray spectrometer with electronic counting technique, which gives fairly accurate spectra, comparable with those reported by Horsley et al [60] using two-crystal X-ray spectrometer and synchrotron radiation. It will also be recalled that the standard procedures for background subtraction, normalization and calibration have been used by us.

Full width at half maximum (FWHM) at L_{II} and L_{III}-edges have been determined by Vishnoi in tungsten metal, WO_3 and rare-earth tungstates to get information on chemical environment of tungsten ion and the density of states for 5d band. The author has used qualitative MO energy level diagram to account for the various spectral features observed in the spectra. The four peaks in L_{III}-edge spectra in $Gd_2(WO_4)_3$ [57] are attributed to the transition of $2p_{3/2}$ electron to the 2e, $4t_2$, $5t_2$ and $3a_1$ molecular orbitals and the crystal field splitting between 2e and $4t_2$ levels is determined. Its value is found to be 7.6 eV. It may be noted above that the 10Dq value obtained from the study of excitation and emission spectra as well as from semiempirical LCAO MO calculations by Walter and Butler [56] for $(WO_4)^{2-}$ is ~ 2.01 eV. So there is a large difference between the value of 10Dq determined by Vishnoi et al and that obtained by Walter and Butler. The 2.01 eV separation between 2e and $4t_2$, being small, cannot be obtained from a spectra for which resolution is of the order of 8 eV in the region of L_{III}-edge. Moreover, by taking into account the widths of L_{II} and L_{III} as well as broadening due to finite window of the spectrometer and experimental conditions, it is very difficult to get 2 eV separation between two spectral features in the L_{II} and L_{III} spectra. So the electronic transitions assigned by these authors could have been similar to those assigned by us.

We feel that one cannot attribute a peak lying at 40 eV from the inflection

85

point to the transition of core electrons to vacant MO level because, if we scan the literature [9, 10, 51, 55] on MO approach and XANES, the fine structure of the edge, is generally believed to be due to the vacant MO levels within 20 eV from the ground state level (2e in the case of tetrahedral complexes).

Finally it may be interesting to mention here the results of work done on these catalysts using different experimental techniques. Salvati et al [61] have carried out the detailed investigation on tungsten-alumina catalysts using X-ray photoelectron spectroscopy. These authors have studied the catalysts having the wt% of WO_3 in the range 1 to 48. From their ESCA spectra, it is observed that the binding energy position of W $4f_{7/2}$ line remains almost constant for all catalysts, the value of binding energy position being ~ 36.0 eV. This value is close to that measured for $Al_2(WO_4)_3$, indicating thereby the presence of hexavalent tungsten species on the surface of the catalysts. However, these authors commented that the surface species formed is different from $Al_2(WO_4)_3$.

These authors have also investigated the full width at half-maximum (FWHM) of the tungsten 4f doublet and found that the fwhm decreases as WO_3 loading increases. From the plot of Al 2p fwhm vs. the WO_3 metal loading, they ruled out the possibility of formation of multiple species or the existence of a charge transfer between the metal and the support as the origin of this broadening.

These authors plotted experimentally determined W 4f / Al 2p intensity ratio as a function of the bulk atomic W/Al ratio. In this plot a break in the curve occurs at a bulk atomic ratio of ~ 0.069 - 0.094 (24 - 30 % WO_3). According to them, this point is particularly significant as it is consistent with the maximum theoretical coverage of $\gamma - Al_2O_3$ by WO_3. It may be noted that in the case of MoO_3/Al_2O_3 catalysts studied by Zingg et al [62], their plot is linear for the entire range of bulk atomic Mo/Al ratios. This can be explained by the fact that in MoO_3/Al_2O_3 catalysts, $Al_2(MoO_4)_3$ is formed at metal loadings near monolayer coverage (15 - 20 % MoO_3), whereas no $Al_2(WO_4)_3$ formation occurred in WO_3/Al_2O_3 catalysts.

In the reduced WO_3/Al_2O_3 catalysts, for 4 % and 12 % samples, it is observed from the W4f spectra that the tungsten species has not been reduced to any detectable extent. In their spectra, the first evidence of reduction is apparent

from the formation of a small shoulder on the low-binding energy side of W 4f spectra and for metal loading above 30%. The shoulder at $\sim$ 31.0 eV found in the spectra closely matches with the 4f binding energy of metallic tungsten. XPS spectra of 20, 40 and 48 % samples show that the intensity of this W° like species increases almost linearly as the metal loading is raised.

Detailed investigations on WO_3/Al_2O_3 catalysts have been carried out by these authors [61] using Raman Spectroscopy. The authors have given Raman spectra of representative catalysts, namely 10, 15, 24 and 32 wt % of WO_3 loading. Below 15 % loading, two major bands at 973 and 333 cm^{-1} are observed. By comparing these features with those of model tungsten oxides, it is suggested that the surface consists of a tetrahedrally coordinated WO_4^{2-} species. According to the scheme suggested by Thomas et al [63], these catalysts bands can be assigned respectively as W=O stretching mode (973 cm^{-1}) and a W=O bending mode (333 cm^{-1}). In the spectra of catalysts, both these modes are shifted proportionally ($\sim$ 4%) to a higher frequency which can be attributed to the presence of a strong metal-support interaction.

At loading of $\sim$ 15% WO_3, several additional bands begins to appear in the Raman spectra. These bands become better defined with increasing tungsten concentrations. The frequencies of these new bands were found comparable with the major Raman bands of WO_3. However, a close comparison to the catalyst spectra with that of WO_3 indicated that there are also some major differences in these spectra. The differences were mainly in the lattice band region (100 - 400 cm^{-1}) which reflects the crystallinity of the sample. Differences in this region of the spectra suggest that the supported tungsten species are present in a dispersed state and show little crystallinity. It has also been shown that the degree of WO_3 crystallinity increases as the catalyst loading is raised. This is evident from the increased intensity and structure of the lattice bands for catalyst having 32 wt % loading relative to that with 24 wt % loading. Catalyst with 48 wt % loading exhibits even more structure in the lattice band region. These authors also have not observed presence of a band at 1046 cm^{-1} in any of the spectra for catalysts indicating thereby the absence of formation of $Al_2(WO_4)_3$ on the surface of the catalyst to any measurable extent. Thus considering the

87

results of these investigations and the results of our work, we conclude that the species formed on the surface of WO_3/Al_2O_3 caalysts is not $Al_2(WO_4)_3$ but it may be some interaction complex of WO_3 and Al_2O_3.

References

[1] C. L. Rollinson, in Comprehensive Inorganic Chemistry, Edited J. C. Bailar Jr., H. J. Emeleus, R. Nyholm and A. F. Trotman-Dickenson, Vol. 3, pp.623-769, Pergamon press, Oxford (1973).

[2] G. D. Rieck, Tungsten and Its Compounds, Pergamon press, Oxford (1967).

[3] E. N. Simons, "Tungsten", in Guide to Uncommon Metals, Hart, New York (1967).

[4] J. E. Fergusson, "Halide Chemistry of Chromium, Molybdenum Tungsten", in Halogen Chemistry, Vol. 3, p.249, Academic Press, New York (1967).

[5] R. V. Parish, "The Inorganic Chemistry of Tungsten", in Advances in Inorganic Chemistry and Radiochemistry, Vol. 9, p.320, Academic press, New York (1966).

[6] D. L. Kepert, "Isopolytungstates", in Progress in Inorganic Chemistry, Vol.4, Interscience, New York (1967).

[7] S. Siegel and D. A. Northrop, Inorganic Chemistry, 5, 2187 (1966).

[8] D. J. Nagel, Advan. X-ray Anal., 13, 182 (1976).

[9] W. Seka and H. P. Hanson, J. Chem. Phys., 50, 344 (1969).

[10] P. E. Best, J. Chem. Phys., 44, 3248 (1966).

[11] U. C. Srivastava and H. L. Nigam, Coordination Chem. Rev., 9, 275 (1973).

[12] S. Ikari, Y. Sasaki and T. Ito, Inorg. Chem., 29, 53 (1990).

[13] W. Ostertag, Inorganic Chem., $\underline{5}$, 758 (1968).

[14] M. T. Shipunova, V. V. Kozik and V. V. Serebrenikov, Zh. Neorg. Khim., $\underline{33}$, 2732 (1988).

[15] E. Bialkowska, E. Polaczkowa, A. Polaczek and A. Gesci, Bull. Acad. Pol. Sci. Ser. Sci. Chim., $\underline{21-2}$, 137 (1973).

[16] R. G. Shulman, Y. Yaffet, P.Eisenberger and W. E. Blumberg, Proc. Natl. Acad. Sci., U.S.A., $\underline{73}$, 1384 (1976).

[17] V. W. Hu, S. I. Chan and G. S. Brown, Proc. Natl. Acad. Sci., U.S.A., $\underline{74}$, 3921 (1977).

[18] T. A. Smith, J. E. Penner-Hahn, M. A. Berding, S. Doniach and K. O. Hodgson, J. Amer. Chem. Soc., $\underline{107}$, 5945 (1985).

[19] L. S. Kau, D. J. Spira-Solomon, J. E. Penner-Hahn, K. O. Hodgson and E. I. Solomon, J. Amer. Chem. Soc., $\underline{109}$, 6433 (1987).

[20] A. L. Roe, D. J. Schneider, R. J. Mayer, J. W. Pyrz, J. Widom and I. Que Jr., J. Amer. Chem. Soc., $\underline{106}$, 1676 (1984).

[21] F. Babonneau, S. Doeuff, A. Leaustic, C. Sanchez, C. Cartier and M. Verdaguer, Inorg. Chem., $\underline{27}$, 3166 (1988).

[22] L. A. Grunes, Phys. Rev., B$\underline{27}$, 2111 (1983).

[23] F. W. Kutzler, C. R. Natoli, D. K. Misemer, S. Doniach and K. O. Hodgson, J. Chem. Phys., $\underline{73}$, 3274 (1980).

[24] R. A. Bair and W. A. Goddard, Phys. Rev., B$\underline{22}$, 2267 (1980).

[25] N. J. Kosugi, T. Yokoyama, K. Asakuna and H. Kuroda, Chem. Phys., $\underline{91}$, 249 (1984).

[26] N. J. Kosugi, T. Yokoyama, K. Asakuna and H. Kuroda, Springer Proc. Phys., $\underline{2}$, 55 (1984).

[27] T. A. Carlson, J. C. Carver, I. J. Saethre, F. G. Santibanez and G. A. Vernon, J. Electron Spectrosc. Relat. Phonom., 5, 247 (1974).

[28] Rosenawaring, G. K. Wertheim and H. J. Guggenheim, Phys. Rev. Lett., 27, 479 (1971).

[29] T. A. Carlson, J. C. Carver, and G. A. Vernon, J. Chem. Phys., 62, 932 (1975).

[30] G. A. Vernon, G. Stucky and T. A. Carlson, Inorg. Chem., 15, 278 (1976).

[31] D. C. Frost, A. Jshitani and C. A. McDowell, Mol. Phys., 24, 861 (1972).

[32] E. A. Stern, Phys. Rev., B10, 3027 (1974).

[33] J. Wong, F. W. Lytle, R. P. Messmer and D. H. Maylotte, Phys. Rev., 30, 5596 (1984).

[34] H. H. Rosenbrock, Computer J., 3, 175 (1960).

[35] S. S. Rao, Optimization, Wiley Eastern Ltd., Third Reprint, New Delhi (1987).

[36] M. Breinig, M. H. Chen, G. E. Ice, F. Parente, B. Crasemann and G. S. Brown, Phys. Rev., A22, 520 (1980).

[37] M. Breinig, Ph.D. Thesis, University of Oregon, (1979) (unpublished).

[38] S. P. Cramer and K. O. Hodgson, in Progress in Inorganic Chemistry, edited by S. J. Lippard, Wiley, New York, Vol.25, p.1 (1979).

[39] N. S. Chiu, S. H. Bauer and M. F. L. Johnson, Journal of Catalysis, 89, 226 (1984).

[40] S. P. Cramer, Ph.D. Thesis, Stanford University, Stanford, U.S.A. (1975).

[41] H. C. Yes and L. V. Azaroff, J. Appl. Phys., 38, 4034 (1964).

[42] D. W. Fischer, J. Appl. Phys., 41, 3561 (1970).

[43] D. W. Fischer, Band Structure Spectroscopy of Metals and Alloys, eds. D. J. Fabian and L. M. Watson, p.669, Academic Press, London (1971).

[44] P. R. Sarode and A. V. Pendharkar, Chem. Phys., 28, 455 (1978).

[45] A. V. Pendharkar and C. Mande, Chem. Phys., 7, 244 (1975).

[46] M. Obashi, Jap. J. Appl. Phys., 16, 167 (1977).

[47] M. Obashi, Physica Fennica, 9, 148 (1974).

[48] H. Hemachandran and A. R. Chetal, Phys. Stat. Solidi (b)132, 503 (1985).

[49] P. Bhattacharya and A. R. Chetal, Phys. Stat. Solidi (b)119, 179 (1983).

[50] T. Chattopadhyay and A. R. Chetal, J. Phys. C : Solid State Phys., 18, 5373 (1985).

[51] K. J. Rao, B. G. Rao and J. Wong, J. Chem. Soc., Faraday Trans. I, 84, 1779 (1988).

[52] C. J. Ballhausen and H. B. Gray, Molecular Orbital Theory, Benjamin, New York (1965).

[53] B. M. Figgis, "Introduction to Ligand Fields", Interscience, New York, (1967).

[54] C. K. Jorgensson, Adv. Chem. Phys., 5, 33 (1963).

[55] D. W. Fischer, J. Phys. Chem. Solids, 32, 2455 (1971).

[56] W. Walter and K. H. Butler, J. Electrochem. Soc., 116, 1245 (19).

[57] A. D. Vishnoi, Ph. D. Thesis, Nagpur University, Nagpur (1990).

[58] A. D. Vishnoi, V. B. Sapre and C. Mande, X-ray Spectrom., 17, 213 (1988).

[59] J. A. Bearden and T. H. Snyder, Phys. Rev., 59, 162 (1941).

[60] J. A. Horsley, I. E. Wachs, J. M. Brown, G. H. Via, and F. D. Hardcastle, J. Phys. Chem., 91, 4014, (1987).

[61] L. Salvati, Jr., L. E. Makovsky, J. M. Stencel, F. R. Brown and D. M. Hercules, J. Phys. Chem., 85, 3700, (1981).

[62] D. S. Zingg, L. E. Makovsky, R. E. Tischer, F. R. Brown and M. Hercules, J. Phys. Chem., 84, 2898 (1980).

[63] R. Thomas, J. A. Moulijn and F. P. J. M. Kerkhof, Recl. Trav. Chim. Pays-Bas, 96, M134 (1977).

Chapter 4

Chemical Shift of the L_{III} Absorption Discontinuity of Tungsten

4.1 Results and Discussion

In Figs.3.1 to 3.2 are shown the X-ray L_{III}-absorption edge profiles of tungsten in some of its typical compounds. In Fig.3.3 are given the W L_{III}-edge spectra in lanthanum, samarium, europium, sodium and indium tungsten oxide bronzes and a biocomplex of tungsten and in Figs.3.4 to 3.6 are shown the L_{III} spectra of tungsten in alumina and titania supported tungsten oxide catalysts and $Ni - W/\gamma - Al_2O_3$. These spectra have been recorded at room temperature on a Rigaku X-ray spectrometer equipped with Si (220) monochromator.

The energy of an X-ray absorption edge is generally measured [1] at its inflection point. The shape of the L_{III}-absorption discontinuity of tungsten is found to be fairly simple in pure tungsten metal as well as in all the compounds studied. No splitting of the edge has been observed. The results of the measurement of energies of tungsten L_{III} discontinuity in the pure tungsten metal, in the compounds, bronzes and oxide catalysts are presented in Table 4.1. In all the cases, the inflection point, which corresponds to the electronic transition $2p \rightarrow 5d$ has been used to determine the energy position of the discontinuity in order to maintain uniformity in the measurements. Because of the small values of the chemical shifts observed in some compounds (e.g. WI_2, WS_2, WSe_2, $K_3W_2Cl_9$, etc.), to obtain reliable results, the measurements are made on a large number of profiles obtained from several spectra recorded for each absorber. Our value of energy of the L_{III}-edge of pure tungsten metal agrees fairly well with that given by Cauchois and Senemaud, Vaughan and also with that adopted by Bearden[2-4] within experimental error. The slight differences may be probably be ascribed to the different reference lines used and other experimental conditions. It is presumed that the values of chemical shifts obtained by us will not be affected by the choice of reference lines, since for the energy measurements of the L_{III} edges in the compounds studied the same reference lines were used.

The results of tungsten L_{III}-absorption edge measurements given in Table 4.1 show that the L_{III}-absorption discontinuity of tungsten shifts towards the high energy side relative to the position of the discontinuity in the pure tungsten metal in all the compounds investigated. It also shows that the magnitude of

95

the chemical shift lies in the range 0.30 - 6.40 eV. It is found to be maximum in the case of hexavalent tungsten compounds and minimum for WSe_2. The uncertainties in the measurements were found to be within ± 0.5 eV. Since similar results are obtained on L_{II}-absorption edge measurements, the values of chemical shifts in the compounds are not included in Table 4.1.

Since the profiles of L_I-edge of tungsten in all these compounds are quite complicated (see Figs.3.7 to 3.12), the measurements on chemical shifts were not carried out.

4.2   Chemical Shift and Valence of Metal Ion

Chemical shift in X-ray absorption spectra is defined as the energy shift of the inflection point position on the absorption edge of a metal ion in a compound, complex, or catalysts relative to the edge position in pure metal, i.e.

$$\Delta E = E_{(compound)} - E_{(metal)} \qquad (4.1)$$

where E refers to the energy of the inflection point on the X-ray absorption edge. It arises due to the change in the local potential set up by the differences in charge distribution among the atoms in a molecule [5, 6]. This local potential around the absorbing atom is the aggregate (superposition) of the atomic and molecular potentials - the former, the dominant one, being proportional to the charge on the atom and the later, the perturbing one, being set up by the charge distribution in the rest of the molecule. Normally an atom in a metal, when transformed into a positive ion in a compound, shows a positive shift due to : (i) the displacement of electronic charge from the cation towards the anion, thus increasing the electrostatic potential felt by the inner electrons of the cations which increases the core electron binding energy and (ii) the screening by polarization of the neighbouring anions in ionic compounds.

The shift of the X-ray absorption edge due to chemical combination was first observed by Bergengren [7] and later by several others [8, 9]. In these investigations, it is found that the chemical shift depends primarily on the valence of the element in question. Kunzl [10] made a critical examination of the experimental

work concerning the displacements of the K - absorption discontinuities of atoms in different valence states. On the basis of his results, he proposed an empirical law, known as Kunzl's law, for the chemical shifts. This law states that the X-ray absorption edge shifts are proportional to the valence of the absorbing ion. It has later been shown [11, 12] that this law holds good only qualitatively for cationic shifts in compounds. One observes either a positive or a negative shift depending upon whether the absorbing ion is a cation or a anion. A critical examination of Table 4.1 shows that chemical shift does depend on the valence. Thus for $K_3W_2Cl_9$ and WCl_6, tungsten ions which are in +3 and +6 oxidation states respectively and have chlorine as ligating atom, show different chemical shifts. A similar trend is observed in WO_2, $K[WO_2(C_2O_4)].xH_2O$ and WO_3, wherein tungsten ions have +4, +5 and +6 valence states and are bonded to oxygen neighbours. Sarode et al [13, 14] have studied the K-absorption edge-shifts in the first and second row transition metal compounds and have shown such variations. Wong et al [15] and Hodgson et al [16] have also observed such variations in the case of vanadium and molybdenum compounds. Recently Bhagatsingh [17] and others [18] have studied a similar variation of chemical shifts with oxidation states in the case of vanadium compounds.

It is interesting to note that in some of the tungsten compounds, eg. WCl_6, $WOCl_4$, $CaWO_4$, etc., though the tungsten ion is present in the same oxidation state and is bonded to different ligands, the magnitudes of the observed shifts are not the same. Similar trend is also seen in the other compounds of tungsten (Table 4.1). It seems in such cases, nature of chemical bonding plays an important role. However, on the basis of our X-ray chemical shift data on tungsten compounds, it is possible to modify the statement of Kunzl's law : "For chemically similar compounds wherein variation in the valence of metal ion varies widely, the chemical shifts of absorption edges are governed by the valence of the absorbing ion under consideration".

In order to establish the relation in a mathematical form, between the chemical shift and the formal oxidation state, we have plotted ΔE values versus Q in Fig.4.1. In this plot, we have also taken the data on WTe_2 and $Tl_3W_2Cl_9$ from ref. [19]. The detailed regression analysis of the data show that instead of a linear
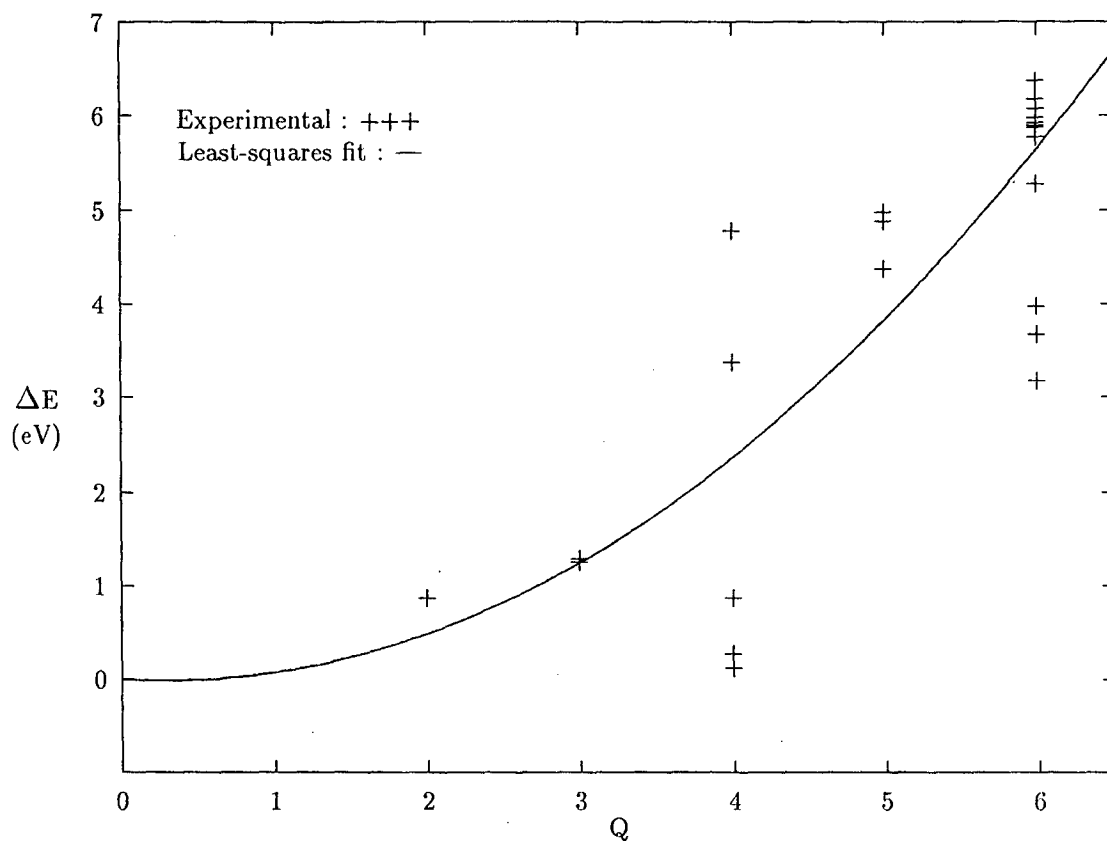
Fig. 4.1: Plot of chemical shift, ΔE (in eV) of L_{III}-absorption edge against the oxidation state of tungsten ion, Q.

correlation suggested by Kunzl himself and presumed by others, a quadratic relation of the type, $\Delta E = A_1 Q + A_2 Q^2$, where A_1 and A_2 are least-squares constants, is more probable, the standard error of estimates and correlation coefficient being 1.140 and 0.833 respectively.

Critical examination of these plots reveals that for the same oxidation state, there is a substantial variation in chemical shifts, wherein the data points lie on either side of the regression lines. This could perhaps, as mentioned earlier, be due to the nature of chemical bonding in the tungsten compounds. To elucidate this, the data points for tungsten compounds having oxygen as ligand have been plotted. The least-squares analysis of this data again suggests quadratic relation to be the most probable, although the linear and cubic relations also give equally good fits. However, based on the values of the correlation coefficients and the standard error of estimates, the linear and cubic fittings have been discarded and plot corresponding to quadratic equation for tungsten compounds having oxygen as the ligand is shown in Fig.4.2.

It may be noted here that the ΔE versus Q curve (linear, quadratic or cubic) is assumed to pass through the origin and that is why the relation suggested does not contain the constant term. This is because the energy values for the absorption edges in compounds are measured with reference to the energy position of the L_{III}-absorption discontinuity in the tungsten metal wherein there is no effective charge transfer from one atom to another.

Having obtained the probable functional relationship for the Kunzl's law, it is possible to apply this law to the tungsten compounds, viz. bronzes and catalysts to ascertain the valence states of tungsten. However, before applying the present results to complex systems like bronzes and catalysts, it is necessary to test the applicability of this relationship for the model compounds wherein the formal oxidation states are well established. Two such test compounds from present work have been chosen e.g., $C_{11}H_{14}O_{12}N_2BaW_2.6H_2O$ and $H_3PW_{12}O_{40}.5H_2O$ on which structural information is available [20, 21]

The L_{III}-edge energy of biochemical complex, $C_{11}H_{14}O_{12}N_2BaW_2.6H_2O$ is comparable with the edge energy of $K[WO_2(C_2O_4)].xH_2O$ wherein the tungsten ion is in pentavalent state. This confirms the observation that the tungsten ions
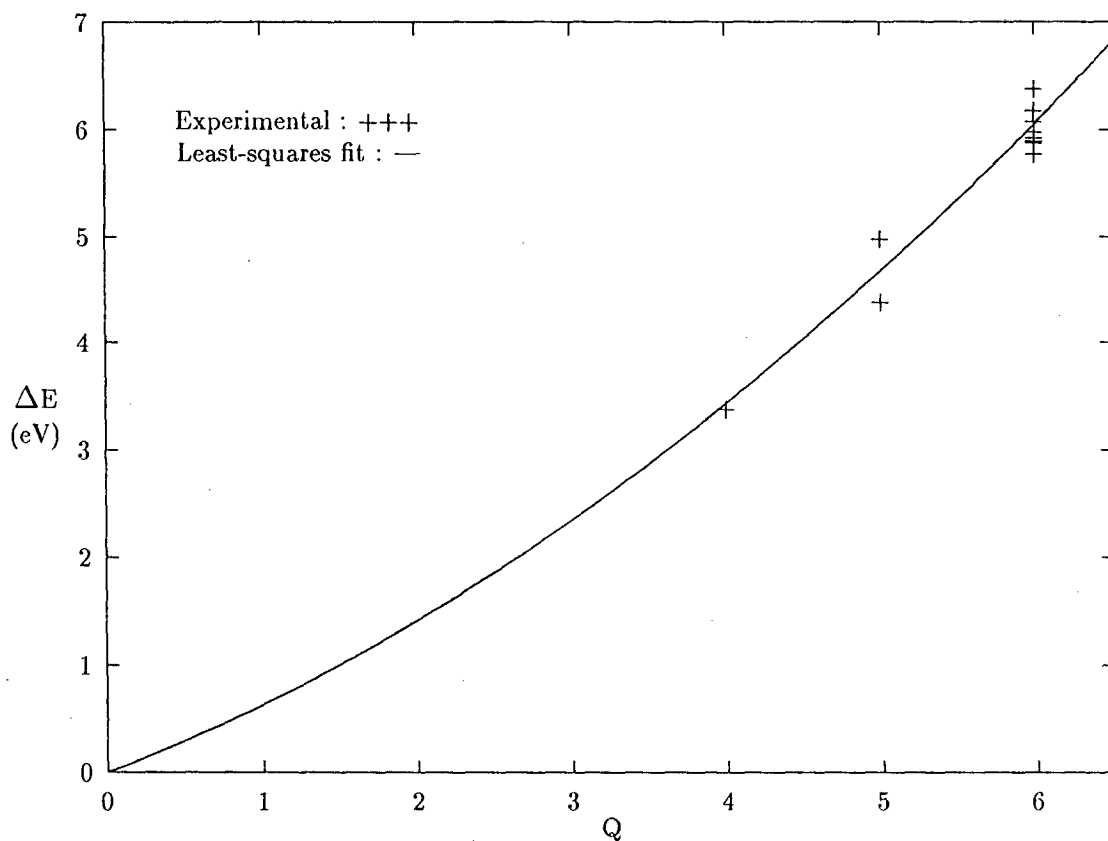
Fig. 4.2: Plot of chemical shift, ΔE (in eV) of tungsten compounds wherein tungsten ion is bonded to oxygen, against the oxidation state of tungsten ion, Q.

in above biochemical complex are in a pentavalent state. The chemical shift of the W L_{III}-edge in $H_3PW_{12}O_{40}.5H_2O$ is found to be very close to that in tungsten compounds in which tungsten ion is in hexavalent state. Hence it is observed that the predicted valence states from X-ray absorption spectroscopy agrees with those calculated using standard techniques [20, 21]. This lends confidence to our ability to predict valence states in those tungsten compounds where it is not known.

The chemical shifts of the W L_{III}-edges in the tungsten oxide bronzes namely, $La_{0.1}WO_3$, $Eu_{0.1}WO_3$, $Sm_{0.1}WO_3$, $Na_{0.15}WO_3$ and $In_{0.2}WO_3$ are close to the model hexavalent tungsten compounds (refer Table 4.1). The calculated valence from the quadratic relation is close to six. This suggests the presence of W^{6+} ion in all these complex oxides. Our findings that the tungsten ion is in hexavalent state in the tungsten bronzes studied by us have some support from the results of Bialkowska et al [22] on ESR and Mössbauer spectroscopic study of cubic rare-earth tugsten oxide bronzes.

W L_{III}-edge inflection point energies in the calcined and reduced alumina and calcined titania supported tungsten oxide catalytic samples and in calcined and reduced $Ni/W/\gamma - Al_2O_3$ samples, are near to those observed in model hexavalent compounds of tungsten and the estimated value of valence is nearly six, thereby indicating the presence of hexavalent tungsten ion in the species formed on surfaces of alumina and titania. The conclusion that the tungsten ions are present in hexavalent state in all these catalysts is in good agreement with those obtained by Hilbrig et al [23], Horsley et al [24], Salvati et al [25] and Ng et al [26].

On the basis of results presented in this work and the results of Sarode et al, Wong et al and Hodgson et al[13-16], it can be inferred that for the determination of valence state in unknown materials from X-ray absorption chemical shifts, model compounds of various valence states must be used. A very recent work in this laboratory by Bhagatsingh [17] and others [18] supports this view. These authors have determined the valence states of copper and vanadium in their biocomplexes and superconducting oxides by examining the copper and vanadium K - absorption shifts in model Cu and V compounds, where the valence of the

metal ion varies widely. It may be noted here that earlier workers [11, 12] have studied chemical shifts in compounds having metal ion in the same oxidation state and concluded that Kunzl law has limited applicability.

4.3 Chemical Shift and Electronegativity Difference

Table 4.1 gives the values of chemical shifts of the L_{III}-absorption discontinuity of tungsten in its compounds along with the values of electronegativities given at the bottom of this table. These values are taken from Ref. ([27]). Since no electronegativity (χ) data is available in literature on different oxidation states of tungsten and since it is difficult to calculate electronegativities for different oxidation states of tungsten because of unavailability of related data, the value given by Pauling [27] is used. It is observed from this table that the chemical shift of the L_{III}-edge decreases with decrease of electronegativity difference between the absorbing atom and its nearest neighbouring ligand. Kondawar [28] has earlier observed that in the transition metal compounds, there is decrease in the magnitude of the chemical shift with increasing electronegativity of the atoms surrounding the absorbing atom. Singh and Agarwal [29] have also correlated the chemical shifts in the X-ray absorption spectra with the electronegativities in some transition metal compounds. Recently, in this laboratory, Sonaye [17] has observed similar trends in the case of copper compounds.

It is well known [27] that greater the difference in electronegativities of the constituent atoms in compound, the greater is the ionic character of the chemical bond between them. Thus chemical shift gives an idea of nature of the bond.

It is to be noted in case of WO_2, $K[WO_2(C_2O_4)].xH_2O$ and WO_3 that although the valence of tungsten is different, we have used the same value of electronegativity of tungsten, this may lead to a wrong picture of chemical bonding. If the values of the electronegativities for different oxidations states of tungsten were available, it would have given a correct picture of chemical bonding. According to Sanderson [30] and Gordy and Thomas [31], one expect higher electronegativity values

102

for higher oxidation state. In that case the electronegativity difference between W and O will be least in WO_2, slightly greater for that in $K[WO_2(C_2O_4)].xH_2O$ and greatest for WO_3; This is what one expects on the basis of chemical bonding prevalent in these compounds.

In the tetravalent tungsten compounds; viz., WO_2, WS_2 and WSe_2, the electronegativity difference between tungsten and oxygen is large for WO_2 and therefore in this compound, the magnitude of chemical shift is large (3.4 eV) indicating a large ionic character of W-O bond. In WSe_2, the electronegativity difference between W and Se is small, and accordingly chemical shift is small (0.30 eV) implying less ionic character of W-Se bonds. The electronegativity difference for W-S bond lies in between those of W-O and W-Se and the observed chemical shift also lies between those for WO_2 and WSe_3. Similar trends can be seen in the hexavalent compounds of tungsten. For example, in $Na_2WO_4.2H_2O$ and $(NH_4)_2WS_4$, wherein the $W^{6+} - O$ bonds are more ionic than $W^{6+} - S$ bonds, the chemical shift is higher in oxide compound (6.40 eV) as compared to that in sulfide (3.20 eV).

The chemical shifts of W L_{III}-edges in $La_{0.1}WO_3$, $Sm_{0.1}WO_3$, $Eu_{0.1}WO_3$, $Na_{0.15}WO_3$ and $In_{0.2}WO_3$ are close to those in WO_3 and other hexavalent compounds oftungsten suggesting thereby that the nature of W-O chemical bonding in these rare-earth tungsten oxide bronzes is similar to that in WO_3 and other model hexavalent tungsten compounds.

The magnitudes of chemical shifts in WO_3/Al_2O_3 and WO_3/TiO_2 catalysts, with variable WO_3 loading between 2 - 12% and 20% $Ni - W - Al_2O_3$ are more or less of the same order of magnitude as compared to those in WO_3 and other hexavalent oxides of tungsten. These findings suggests that the nature of chemical bonds in these catalytic materials is similar to that in hexavalent oxides of tungsten.

4.4   Chemical Shift and Coordination Charge

Agarwal and Verma [32] has given a qualitative rule which states that "In general, the chemical shift is towards the high energy side of the metal X-ray absorption

edge and it increases progressively with the increase in the valency of the cation, unless the shift is either suppressed by the covalent character of the bond or enhanced by the formation of the metal-metal bonding". Sapre and Mande [11, 12] have shown that in a compound the absorption edge of an atom shifts towards the high or low energy side relative to its position in the pure element, depending upon whether the absorbing ion is a cation or anion. In the tungsten compounds studied by us, the observed positive shift of the L_{III} discontinuity of tungsten indicates that the tungsten ions behave as cations in these compounds as one would normally expect on the basis of Pauling's electronegativity criterion.

The X-ray absorption spectra determine the difference between the energies of the initial and final states. Therefore, in one-electron picture [33] the shifts of both the core level and outer level are involved. The initial state involved in the absorption process of the tungsten compounds studied in this work is the $L_{III}(2p_{3/2})$ level having p-symmetry, while the final state is of d (or s or d+s) symmetry. The X-ray photoelectron spectroscopic data on $2p_{3/2}$ level shifts in all these compounds studied is unavailable, hence it is difficult to make estimates of the shifts in our compounds from XPS data. However, since several researchers [34, 35, 36] have in fact observed appreciable core level shifts in the transition metal compounds, it is perhaps appropriate to begin with the assumption that the core level shifts of these ions, although small, are finite and that the chemical shifts are due to the shifts of both inner and outer levels.

In section 4.2, we have seen that the energy shifts of absorption edges are related to the formal valence of the central tungsten atom as per modified Kunzl's law, which is applicable for systems having the same ligand. Generally, the chemical shifts in the X-ray absorption spectra are due to a combination of valence, electronegativity, type of ligands, coordination number and other structural features. These factors are approximately accounted for in the concept of charge.

The calculation of the charge distribution is difficult since it is not easy to conceive what is meant by charge distribution, and more so, to evaluate it quantitatively in terms of charge per atom. An appropriate solution to this problem can be approached by a study of the electronic adjustments that occur with the formation of chemical bonds. This approach, although far from rigorous, leads to

atomic charges in the reasonable accord with other approaches, e. g. dipole moments. Various other theoretical and experimental methods have been developed to determine charges in compounds[37-42]. However, the charges calculated by these different methods cannot always be compared due to the different physical arguments inherent in them. Batsanov [43] has proposed a method for evaluation of effective coordination charges in compounds. Its calculation is based on a combination of bond character, valence and coordination number. This method of charge calculation is relatively simple and straight forward and permits the calculation of the coordination charges in all types of compounds, and has been successfully used in X-ray spectroscopic work [44].

The effective coordination charge, q is defined as

$$q = Z - cN \qquad (4.2)$$

where Z is the formal valence of the atom in a given compound, N is the coordination number and c is the degree of covalence of the chemical bond. The coordination charge, q represents the charge that appears at the periphery of the atom as a result of participation in the chemical bonding of its electron (Z) and the electrons received from the neighbouring atoms (cN). When the number of neighbouring atoms is more so that the chemical bond is more covalent and the positive charge, q is thus compensated. In qualitative terms, the coordination charge concept simply states that as the valence electrons are pulled away from the metal atoms by the electronegativity χ_B of the coordinating ligands, all of the other electrons of the central atom become more tightly bound in order to shield the unchanging nuclear charge. In the limiting case of fully ionic bonds, q=Z, (c=0); while in the other limiting case of fully covalent bonds, q=0.

Wong et al [45] adopted a relatively simpler way to arrive at the expression for effective coordination charge. These authors have used the Pauling's formula [27] for calculating the ionicity. The multiple-bond ionicity (i), according to Pauling is given by

$$i = 1 - \frac{Z}{N} \exp\left[-\frac{1}{4}\left(\chi_A - \chi_B\right)^2\right] \qquad (4.3)$$

while the single bond ionicity (I) by

$$I = 1 - \exp\left[-\frac{1}{4}(\chi_A - \chi_B)^2\right] \qquad (4.4)$$

where χ_A and χ_B are electronegativities of metal atom and ligand respectively.

Combining equations (4.2 - 4.4), we obtain

$$q = ZI \qquad (4.5)$$

The values of coordination charges calculated using equation (4.5) are given in Table 4.1. In this table, the calculated charges on tungsten ions in compounds having mixed ligands are determined by averaging the charges on tungsten ions in different bonds. For example, in WCl_2Pyr_2, there are 4 W-Cl and 2 W-N bonds; the estimated charge on W, is the weighted average of charges on W in W-Cl and W-N bonds.

It is observed from this table that the energy shift of the L_{III}-absorption edge of tungsten in various compounds and complexes does depend on the magnitude of the coordination charge on the absorbing atom. The chemical shift decreases with decrease of magnitude of charge on the W ions indicating a decrease of ionic character or an increase of covalent character of the W-X (where X is ligand) bond. In order to find out a functional relationship between the chemical shift and coordination charge, we have plotted in Fig.4.3 chemical shift of the L_{III}-absorption discontinuity against the coordination charge q, calculated using Batsanov's aproach. However, before attempting to find any such correlation, it would be in order here to briefly mention the work of various researchers who proposed different empirical relationships between these two physicochemical parameters.

Kondawar and Mande [46], Rao and Chetal [47] and Sarode [48] have shown that the chemical shift ΔE is directly proportional to the effective charge q on the absorbing atom, their relationship being given as

$$\Delta E = aq \qquad (4.6)$$

Sarode et al [13, 14] have examined several first and second row transition metal compounds and derived a quadratic relation between ΔE and q on the basis of theoretical model. This relation is of the form
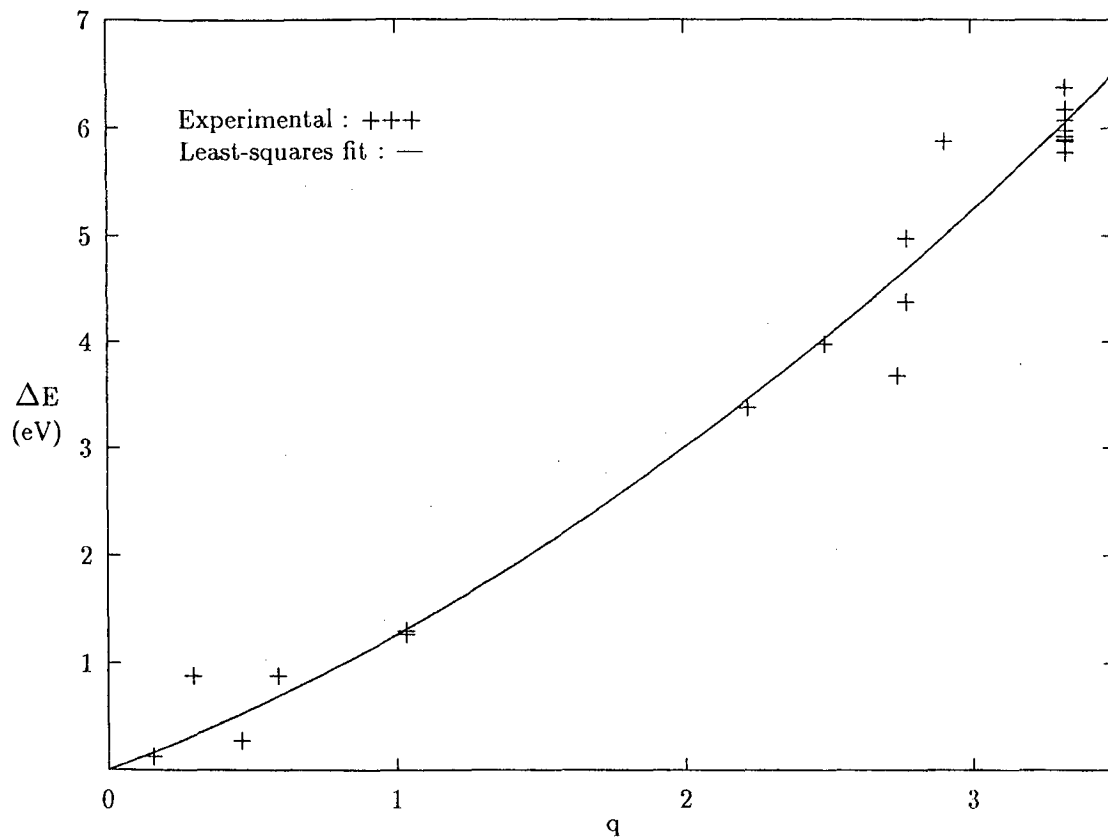
$$\Delta E = aq + bq^2 \qquad (4.7)$$

Fig. 4.3: Plot of chemical shift, ΔE (in eV) of tungsten compounds against effective coordination charge, q.

Suchet [49] has analysed the results of Sapre and Mande [11, 12] and has shown empirically that ΔE is related to q by the relation

$$\Delta E = aq + bq^3 \qquad (4.8)$$

where a and b are constants which depend on the bonding prevalent in compounds. Apte et al [50] have modified the above equation by adding a constant to explain the dependence of ΔE on q in terms of number of 3d electrons in the case of manganese compounds. The modified relation given by them is

$$\Delta E = aq + bq^3 + c \qquad (4.9)$$

Pandey et al [51] have studied the dependence of ΔE on q in copper compounds including cuprate superconductors and fitted a fourth order polynomial to their data on copper K-edge chemical shifts of the form

$$\Delta E = aq + bq^2 + cq^3 + dq^4 \qquad (4.10)$$

In this work, the five relations mentioned above were examined to find out the most appropriate relationship between ΔE and q for the compounds studied.

To determine which one of these equations provides a significantly better fit to the data (Table 4.1), a least-squares analysis of the data was carried out on a PC-486 using a general purpose computer program developed in this laboratory. In this analysis we have also taken data on WTe_2 and $Tl_3W_2Cl_9$ from literature [19].

On critical examination of the data points, it is found that some data points show large deviation from the least-squares line. These data points correspond to WCl_6, $(NH_4)_2WS_4$, WCl_4Pyr_2 and $[WCl_4L_2]Cl$. Excluding the data points for these compounds, if the regression analysis is again performed, it is found that out of five relations, the fittings for quadratic and cubic equations (4.7) and (4.8), give better values of standard error of estimates and correlation coefficient. For quadratic curve, the values of standard error of estimates and correlation coefficient are 0.332 and 0.989 respectively and for the cubic curve, 0.330 and 0.989 respectively. However, if a comparison is made between the least-squares coefficients A_1 and A_2, one finds that the A_2 coefficient for cubic curve (0.0475) is much smaller than the A_2 value for quadratic (0.238) equation, indicating thereby

that the second term in equation (4.8) contributes very little to the chemical shift as compared to the relatively higher value for quadratic curve. In this work, we have used a quadratic equation for estimating the charges since there is a theoretical justification [13] for quadratic curve and other relations are only of emipirical nature. The plot of ΔE versus q using a quadratic relation is shown in Fig.4.3.

Although it is difficult to give any satisfactory explaination for the large deviation in the chemical shifts observed in the case of compounds mentioned above, the nature of bonding seems to have some role to play in their large chemical shifts. For example, W-S and W-N bonds are relatively more covalent in nature as compared to other compounds wherein there are strong ionic W-O bonds

Thus it is concluded that irrespective of the fitting equation, there seems to be a good correlation between chemical shift (ΔE) and coordination charge (q).

Having found a relationship between ΔE and q, it is possible to estimate charges in compounds where Batsanov's method cannot be directly applied due to the unknown nature of chemical bonding. It is however to be noted that such estimates of coordination charge, q are subject to uncertainty of the order (*ca* 0.2). From these estimates (given in parenthesis in Table 4.1), it is seen that the charge on tungsten ion in all the tungsten bronzes under investigation is in the range 3.0 - 3.3, implying thereby that the nature of chemical bonding in these systems is similar to that in hexavalent tungsten compounds having W-O bonds.

In the case of calcined alumina supported tungsten oxide catalysts, the magnitudes of charges are more or less similar to those in hexavalent tungsten compounds having W-O bonds, the estimated charge on tungsten ion being in the range 3.0 - 3.4. The estimated charge in the case of reduced alumina supported tungsten oxide catalysts also is of the same order as that in the hexavalent tungsten compounds.

In the calcined titania supported tungsten oxide catalysts, the estimated value of charge is in the range 3.0 - 3.3. These values are close to those obtained in the case of model hexavalent compounds of tungsten. This suggests the presence of hexavalent tungsten ions in these catalytic samples.

In the calcined and reduced $Ni - W/\gamma - Al_2O_3$ catalysts studied in the present

investigation, the calculated value of charge is very close to that in WO_3, $ZnWO_4$ and $CaWO_4$, which indicates a similar nature of chemical bonding in these catalysts wherein the valence of tungsten ion is six.

4.5 Chemical Shift and Hardness of ligands

The intrinsic properties of distinct isolated chemical species (atoms, ions or molecules) are significant input for the determination of the properties of combined systems (molecules, molecular ions), though they are in no simple sense completely sufficient. Any chemical system (atom, molecule, ion, radical) is characterized [52, 53] by its electronic chemical potential μ, and absolute hardness, η. The exact definition of these quantities are

$$\mu = \left(\frac{\delta E}{\delta N}\right)_v \quad and \quad \eta = (1/2)\left(\frac{\delta \mu}{\delta N}\right)_v \qquad (4.11)$$

where N is the number of electrons and v is the potential due to nuclei, plus any external potential. However, the operational and approximate definitions of the chemical potential and the absolute hardness given by Pearson [54] are

$$\mu = -(I + A)/2 = \chi \quad and \quad \eta = (I - A)/2 \qquad (4.12)$$

where I is the ionization potential and A is the electron affinity. Since the ionization potential is always greater than or equal to the electron affinity, the minimum value of hardness is zero. Zero hardness constitutes maximum softness. A bulk metal has I=A and η=0 and maximum softness.

As can be seen from the above equations, the hardest atoms and ions are those with high ionization energies and low electron affinities. If the ionization energy is much larger than the electron affinity, as is often the case, hardness is correlated with high ionization energy. Hence, the hardest atoms and ions are the small atoms and ions near fluorine. The softest atoms and ions are the ones with low ionization energies and low electron affinities. These are the atoms and ions of the heavier alkali metals and the heavier halogens. The light atoms of a group are generally hard and the heavier atoms soft. The hardness of an atom is

generally complementory to the electronegativity in determining the outcome of reactions, and it is important to acquire a sense of when one influence is likely

Thus hardness is a state independent global parameter which implies the molecular property. The nonchemical meaning of the word "hardness" is resistance to deformation or change. It is resistance of the chemical potential to change in the number of electrons.

Parr and Pearson [53] have calculated absolute hardness for a number of atoms, and in some special circumstances for ions, using the appropriate experimental values of ionization potentials and the electron affinities from the literature. As claimed by these authors their values are highly satisfactory when compared with the known chemical behaviour of the selected systems. The hardness values given by them for N, O, S, Se, Cl, Br and I are shown in Table 4.2 along with the values of ionization potentials and electron affinities.

Since hardness is an important chemical parameter related to some aspects of the chemical bonding, it was thought worthwhile to investigate a functional relationship between the features of X-ray absorption spectra which also depend on the nature of chemical bonding, and this physicochemical parameter. For this purpose, a graph between chemical shift, ΔE and hardness, η is plotted and regression analysis of these data points was carried out. In compounds having mixed ligands, values of hardness were calculated by taking the averages of the values for individual bonds. This plot (shown in Fig.4.4) if extrapolated, is found to intersect the hardness axis at $\eta = 3.23 \pm 0.4$. This value of η is very close to the reported value of hardness for tungsten atom (3.58) corresponding to zero chemical shift i.e. in tungsten metal wherein the ligand is also a tungsten atom. It can be observed from this plot that a large scatter of data points is present in this graph. Such a large scatter could perhaps be thought to be due to the same value of hardness used, even when the valence of metal ion in the compounds used is different. For example, in WO_2 and WO_3, although the liganding atom is oxygen and valence of W ion in both these compounds are different, the same value of η (=6.08) is used for both these compounds. A relation between chemical shift and the product of hardness and oxidation state therefore seems to be more appropriate. The values of ηQ are given in Table 4.1 and the plot of ΔE versus
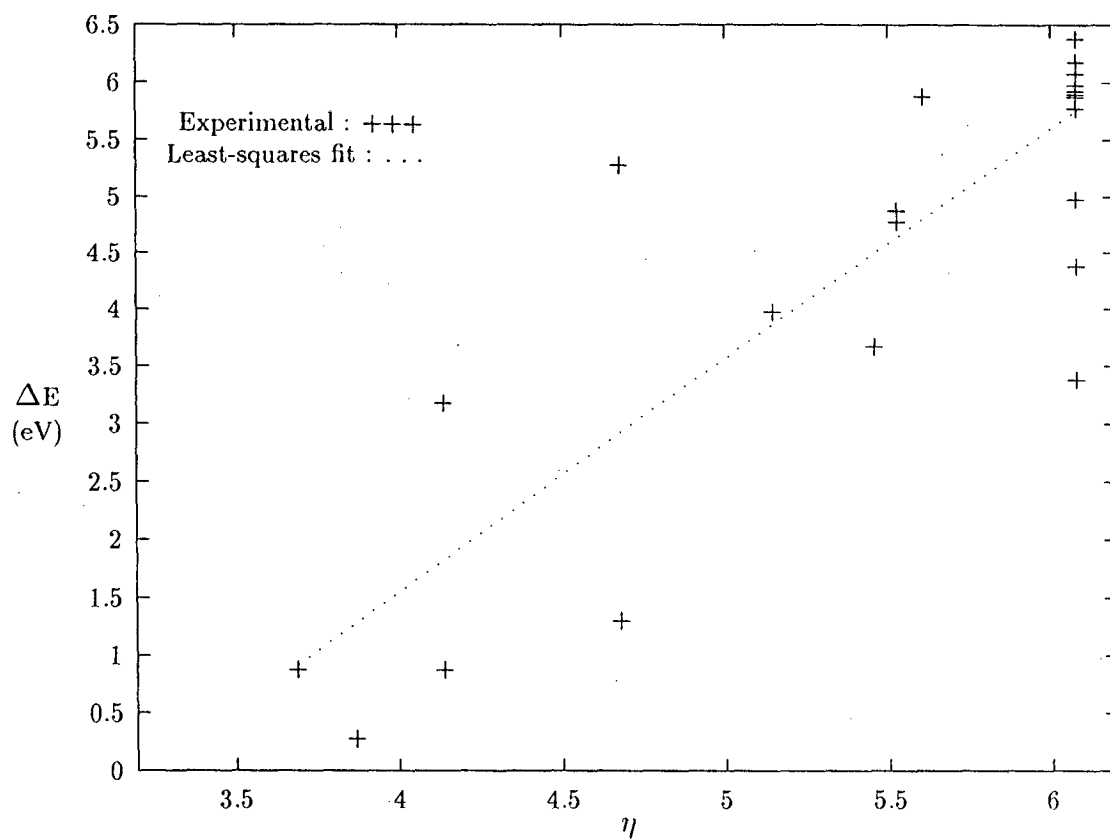
111

Fig. 4.4: Plot of chemical shift ΔE (in eV) of tungsten compounds versus the hardness, η of the ligating atom.

ηQ is shown in Fig.4.5. In this graph it is observed that the scatter is reduced and indeed there is a good correlation between these two quantities.

In order to obtain exact mathematical relation between the chemical shift and ηQ; polynomial equations upto the third degree were fitted and regression analysis was carried out. This analysis suggest that the quadratic equation of the type $\Delta E = A_1(\eta Q) + A_2(\eta Q)^2$ gives better values of standard error of estimates (0.702) and correlation coefficient (0.926) as compared to that obtained for linear and cubic fits. This fit is shown in Fig.4.5.

Using the parabolic correlation between the ΔE and (ηQ), we can, in principle, compute (ηQ) in the case of tungsten oxide bronzes, alumina and titania supported reduced and calcined tungsten oxide catalysts and the $Ni - W/\gamma - Al_2O_3$ catalysts. Estimates of (ηQ) for these complex systems can be used to calculate hardness, η and therefrom it is possible to get idea of the nature of ligands surrounding the tungsten metal ion in these complex systems. Here, the oxidation state Q of the tungsten ion in these complex systems estimated from ΔE versus q plot (see Section 4.2) was used.

The values of (ηQ) for all the tungsten oxide bronzes studied in the present investigation is in the range 33.78 - 36.18. By using the oxidation state Q calculated from the parabolic correlation fit of the ΔE versus Q curve, the values of the hardness for the ligands in the bronzes obtained were in the range 5.74 - 5.85. This range is very close to the value, 6.08 for oxygen atom. Hence it can be concluded that the neighbouring ligand of the tungsten ion in these bronzes is oxygen.

In case of the calcined and reduced alumina and titania supported tungsten oxide catalysts, the (ηQ) product is within a range 36.96 - 35.74. The calculated value of hardness in these catalyst systems us very close to the hardness value of oxygen atom. This implies that oxygen atoms surround the tungsten ion in these catalytic systems.

In both calcined as well as reduced $Ni - W/\gamma - Al_2O_3$ catalyst samples studied, results similar to the above are obtained and it is therefore concluded that in these systems also the oxygen ligands surround the tungsten ion.

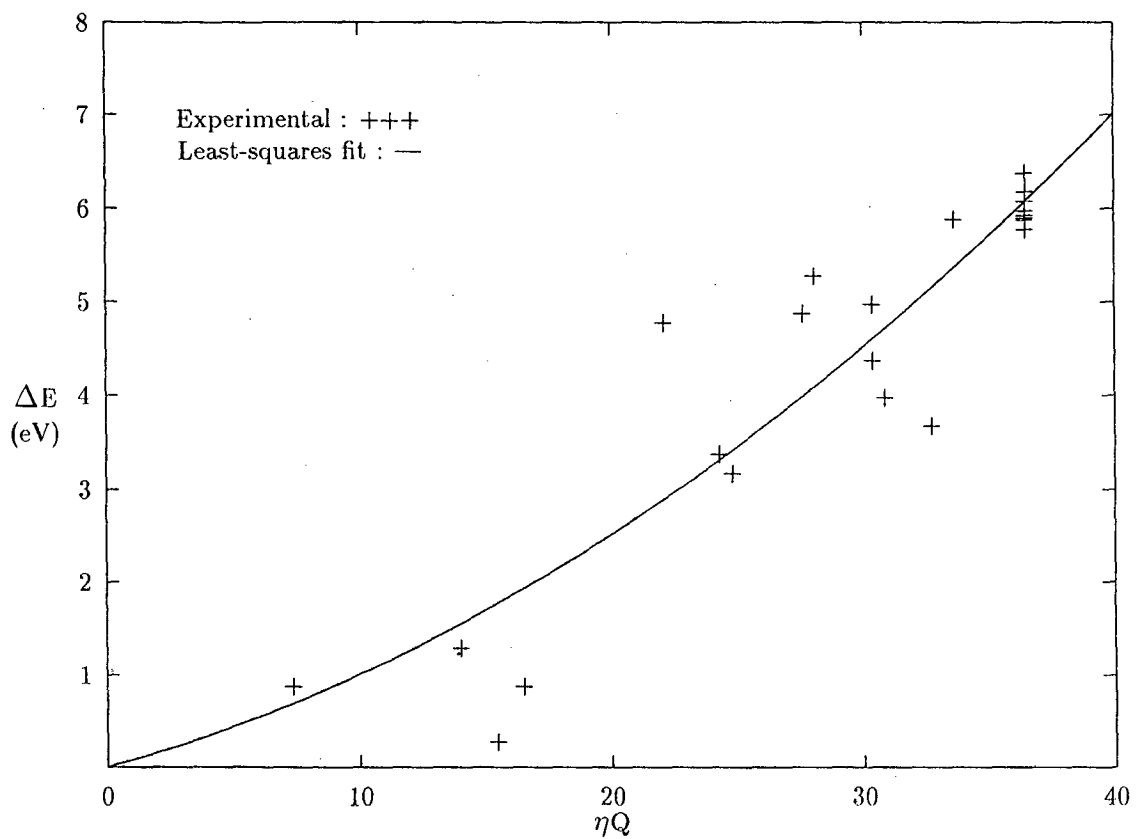Thus from the simple correlation between chemical shift and hardness, one

Fig. 4.5: Plot of chemical shift of tungsten compounds versus the product of hardness and oxidation state.

can determine the nature of ligands in complex systems.

4.6   Physical Basis of Chemical shifts

The process of X-ray absorption involves an inner level, i.e. the K level, from which the electron is ejected and outer level of appropriate symmetry in which the ejected photoelectron may be trapped. Essentially, the problem of interpreting the shape of the main absorption edge and the near edge structure is to know what happens to the ejected photoelectron when the atom absorbs a quantum of energy from the incident X-ray beam. As mentioned earlier, the inflection point on the main absorption edge in the case of a metal represents the transition of the ejected photoelectron to the Fermi limit. In a compound the corresponding final level could be a level of appropriate symmetry and -type in the valence/conduction band.

It can be assumed that in a compound the deep-lying orbitals (e.g., the 1s or 2p orbitals) of the absorbing atom are much less affected by external influences as compared to the outer orbitals which participate directly in the formation of the chemical bonds, since the inner levels are comparatively closer to the nuclei and the overlap of wavefunctions of the ligand atoms is significant on the outer levels only. Hence, the character of the chemical bond should have a considerably smaller effect on the position of the inner level. One may therefore assume that the observed chemical shift is due to the shift of the outer final level to the higher or the lower energy side depending upon the magnitude and nature of the charge on the absorbing ion.

Several researchers [34, 35, 36, 55] have studied theoretically and experimentally the chemical shift in the core levels and have shown that the effect of chemical combination on the core levels especially in the case of heavy elements is very small. It has therefore been the usual practice [46, 56] in X-ray spectroscopic studies to ignore the effect of chemical combination on the inner levels for the physical interpretation of chemical shifts. Hence for this purpose it can be safely assumed that the L_{III} level in tungsten remain unaffected in its compounds and also that the final levels (valence or conduction levels) are mainly responsible for

the observed shifts. In Fig.4.6 are shown the transitions responsible for the L_{III} discontinuity in pure metal and in the compounds of tungsten. In this figure (not to the scale), the final level of the tungsten metal is shown to be at zero energy for the purpose of normalization. This figure clearly shows that the final level (above the Fermi level) shifts its position with respect to that in the pure metal depending upon the coordination charge on the absorbing atom. This picture is rather approximate and qualitative and has been put forth simply to interpret the results of the present work.
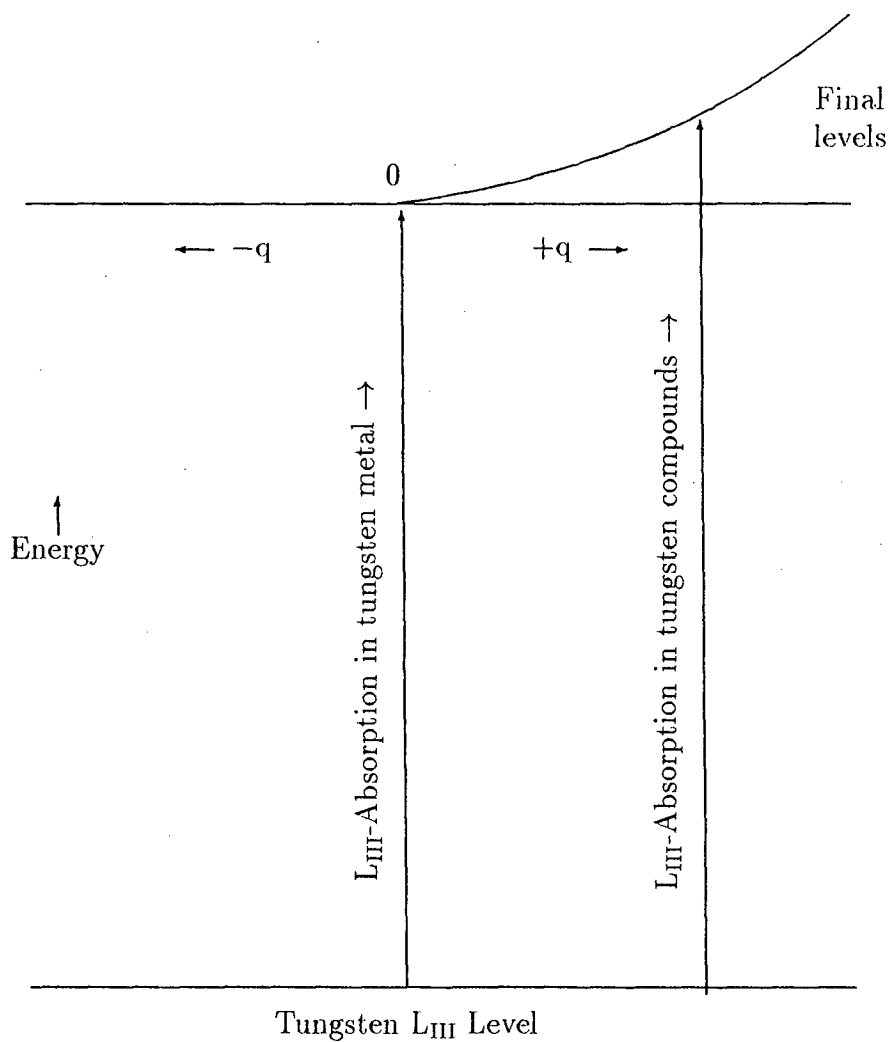
Fig. 4.6: Schematic representation of chemical shifts in X-ray absorption spectra.

References

[1] A. E. Sandström, Encyclopaedia of Physics, Vol XXX ed. S. Flügge, Springer Verlag, Berlin p. 309 (1957).

[2] Y. Cauchois and C. Senemaud, Wavelengths of X-ray Emission Lines and Absorption Edges, International Tables of Selected Constants, Vol. 8, Pergamon Press, Oxford (1978).

[3] D. Vaughan, ed. Center for X-ray Optics : X-ray Data Booklet, U.S. Department of Energy Publication No.490, U.S. G.P.O., Washington DC (1985).

[4] J. A. Bearden, X-ray Wavelengths, Atomic Energy Commission U.S.A. Rept. No.AT (30-1) 2543 (1964).

[5] K. Siegbahn, Phil. Trans. Royal Soc. London, A 268, 33 (1970).

[6] K. Siegbahn, J. Electron Spectrosc. and Relat. Phenom., 5, 3 (1974).

[7] J. Bergengren, Z. Phys., 3, 247 (1920).

[8] A. E. Lindh, Z. Phys., 6, 303 (1921).

[9] D. Stelling, Z. Phys. Chem., B7, 210 (1932).

[10] V. Kunzl, Collections Czech. Commun., 4, 213 (1932).

[11] V. B. Sapre and C. Mande, J. Phys., C5, 793 (1972).

[12] V. B. Sapre and C. Mande, J. Phys. Chem. Solids, 34, 1351 (1975).

[13] P. R. Sarode, S. Ramasesha, W. H. Madhusudan and C. N. R. Rao, J. Phys. C : Solid State Phys., 12, 2439 (1979).

[14] A. Manthiram, P. R. Sarode, W. H. Madhusudan, J. Gopalkrishnan and C. N. R. Rao, J. Phys. Chem., 84, 2200 (1980).

[15] J. Wong, F. W. Lytle, R. P. Messmer and D. H. Maylotte, Phys. Rev., B30, 5596 (1989).

[16] S. P. Cramer, K. O. Hodgson, W. O. Gillum and L. E. Mortenson, J. Amer. Chem Soc., 100, 3398 (1978).

[17] Bhagatsingh Sonaye, Ph.D. Thesis, Goa University, Goa (1994).

[18] Anjli Chhikara, Ph.D. Thesis, Goa University, Goa (1996).

[19] Shantanu Gauns, M. Phil. Dissertation, Goa University, Goa (1991).

[20] S. Ikari, Y. Sasaki and T. Ito, Inorg. Chem., 29, 53 (1990).

[21] D. L. Kepert, "Isopolytungstates", in Progress in Inorganic Chemistry, 4, Interscience, New York (1967).

[22] E. Bialkowska, E. Polaczkowa, A. Polaczek and A. Gesci, Bull. Acad. Pol. Sci. Ser. Sci. Chim., 21-2, 137 (1973).

[23] F. Hilbrig, H. E. Göbel, H. Knözinger, H. Schmelz and B. Lengeler, J. Phys. Chem., 95, 6973 (1991).

[24] J. A. Horsley, I. E. Wachs, J. M. Brown, G. H. Via and F. D. Hadcastle, J. Phys. Chem., 91, 4014 (1987).

[25] L. Salvati Jr., L. E. Makovsky, J. M. Stencel, F. R. Brown and D. M. Hercules, J. Phys. Chem., 85, 3700 (1981).

[26] K. T. Ng and D. M. Hercules, J. Phys. Chem., 80, 2094 (1976).

[27] L. Pauling, The Nature of Chemical Bond, 3rd edn., Cornell University Press, Ithaca, New York 1960.

[28] V. K. Kondawar, Ph.D. Thesis, Nagpur University, Nagpur (1976).

[29] V. B. Singh and B. K. Agarwal, J. Phys. Chem. Solids, 35, 485 (1974).

[30] R. T. Sanderson, Inorganic Chemistry, Affiliated East-West Press Pvt. Ltd., New Delhi (1971).

[31] W. Gordy and W. J. O. Thomas, J. Chem. Phys., 24, 439 (1956).

[32] B. K. Agarwal and L. P. Verma, J. Phys. C : Solid State Phys., 3, 535 (1970).

[33] D. J. Fabian, L. M. Watson and C. A. W. Marshall, Reports Prog. Phys., 34, 601 (1972).

[34] J. C. Carver, G. K. Schweitzer and T. A. Carver, J. Chem. Phys., 67, 973 (1972).

[35] L. Ramquist, B. Ekstig, R. Kallne, E. Noreland and R. Manne, J. Phys. Chem. Solids, 30 , 1849 (1969).

[36] K. Siegbahn et al., ESCA - Atomic Molecular and Solid State Structure Studies by means of Electron Spectroscopy, (North-Holland Publishing Co., Amsterdam, (1967).

[37] C. A. Coulson, L. B. Redei and D. Stocker, Prac. Ray. Soc., London, 270, 357 (1962).

[38] B. F. Levine, Phys. Rev., B7, 2591 (1973).

[39] J. C. Phillips, Rev. Mod. Phys., 42, 317, (1970).

[40] J. P. Suchet, Chemical Physics of Semiconductors, D. Van Nostrand Company, London (1965).

[41] W. Cochran, Nature, 191, 60, (1961).

[42] G. Leonhardt and A. Meisel, J. Chem. Phys., 52, 6189 (1970).

[43] S. S. Batsanov, Electronegativity of Elements and Chemical Bonds, Novosibirsk (1962).

[44] I. A. Ovsyannikova, S. S. Batsanov, L. I. Nasonova, L. R. Batsanova and E. A. Nekrasova, Bull. Acad. Sci. USSR, Phys. Ser., $\underline{31}$, 936 (1967).

[45] J. Wong, F. W. Lytle, R. P. Messmer and D. H. Maylotte, Phys. Rev., B$\underline{30}$, 5596 (1984).

[46] V. K. Kondawar and C. Mande, J. Phys. C : Solid State Phys., 9, 1351 (1976).

[47] B. J. Rao and A. R. Chetal, Phys. Stat. Solidi, (b)$\underline{122}$, 193 (1984).

[48] P. R. Sarode, Z. Naturforsch, $\underline{33}$a), 946 (1978).

[49] J. P. Suchet, C. R. Acad. Sci. Paris, $\underline{281}$, 87 (1975).

[50] M. Y. Apte, C. Mande and J. P. Suchet, J. Chem. Phys., $\underline{79}$, 325 (1982).

[51] S. K. Pandey , A. R. Chetal and P. R. Sarode, J. Phys. Soc. of Japan, $\underline{59}$, 1848 (1990).

[52] R. G. Parr, R. A. Donnelly, M. Levy and W. E. Palke, J. Chem. Phys., $\underline{68}$, 3801 (1978).

[53] R. G. Parr and R. G. Pearson, J. Am. Chem. Soc., $\underline{105}$, 1503 (1983).

[54] R. G. Pearson, Inorg. Chem., $\underline{27}$, 734 (1988).

[55] J. R. Cuthill, A. J. McAlister, N. E. Frickson and R. E. Watson, AIP Conference Proceedings No.18, p.1039 (1974).

[56] C. Mande and V. B. Sapre, in X-ray spectra and Electronic Structure of Matter, ed. A. Faessler and G. Wiech, München, Vol I, p.237 (1973).

Table 4.1: (a) X-ray absorption and crystal structure data on tungsten compounds.

Sr. No.	Absorber	Q	Bond Type	q	$\eta \times Q$	ΔE ± 0.5 eV
1.	W	—	W-W	—	—	0.00^+
2.	WI_2	2^+	W-I	0.296	7.40	0.90
3.	$K_3W_2Cl_9$	3^+	W-Cl	1.034	14.10	1.32
4.	WO_2	4^+	W-O	2.221	24.32	3.40
5.	WS_2	4^+	W-S	0.591	16.48	0.90
6.	WSe_2	4^+	W-Se	0.461	15.44	0.30
7.	WCl_4Pyr_2	4^+	W-Cl/Pyr	1.378	22.24	4.80
8.	$C_{11}H_{14}N_2O_{12}BaW_2.6H_2O$	5^+	W-O	2.776	30.40	4.40
9.	$[WCl_4L_2]Cl$	5^+	W-Cl/N	1.723	27.80	4.90
10.	$K[WO_2(C_2O_4)].xH_2O$	5^+	W-O	2.776	30.40	5.00
11.	$(NH_4)_2WS_4$	6^+	W-S	0.887	24.72	3.20
12.	$Fe_2(WO_4)_3$	6^+	W-O	3.331	36.48	5.90
13.	$Al_2(WO_4)_3$	6^+	W-O	3.331	36.48	6.00
14.	$CaWO_4$	6^+	W-O	3.331	36.48	6.10
15.	$Eu_2(WO_4)_3$	6^+	W-O	3.331	36.48	6.40
16.	$Na_2WO_4.2H_2O$	6^+	W-O	3.331	36.48	6.40
17.	WO_2Br_2	6^+	W-O/Br	2.742	32.82	3.70
18.	$WOCl_4$	6^+	W-O/Cl	2.489	30.96	4.00
19.	WCl_6	6^+	W-Cl	2.068	28.20	5.30
20.	WO_2Cl_2	6^+	W-O/Cl	2.910	33.72	5.90
21.	$NiWO_4$	6^+	W-O	3.331	36.48	5.92
22.	$ZnWO_4$	6^+	W-O	3.331	36.48	6.00
23.	$H_3PW_{12}O_{40}.5H_2O$	6^+	W-O	3.331	36.48	5.95
24.	$(NH_4)_6H_2W_2O_{40}.xH_2O$	6^+	W-O	3.331	36.48	5.80
25.	WO_3	6^+	W-O	3.331	36.48	6.00
26.	$WO_3.H_2O$	-6^+	W-O	3.331	36.48	6.00
27.	WV_2O_6	6^+	W-O	3.331	36.48	6.20

Q = Formal valence   q = Coordination charge η = Hardness
ΔE = Chemical shift   L = 2,4,6 trimethylpyridine

+: X-ray L_{III}-edge energy in tungsten metal = 10199.50 eV
The values of electronegativities χ of W, O, S, Se, Cl, N, Br and I are 1.7, 3.5, 2.5, 2.4, 3.0, 3.0, 2.8 and 2.5 respectively.

Table 4.1: (b) X-ray absorption and crystal structure data on tungsten oxide bronzes, alumina and titania supported tungsten oxide catalysts and $20\%Ni - W/Al_2O_3$ catalysts

Sr. No.	Absorber	Q	Bond Type	q	η	ΔE ± 0.5 eV
1.	$Eu_{0.1}WO_3$	(6^+)	(W-O)	(3.072)	(5.75)	5.40
2.	$La_{0.1}WO_3$	(6^+)	(W-O)	(3.152)	(5.78)	5.60
3.	$Sm_{0.1}WO_3$	(6^+)	(W-O)	(3.191)	(5.80)	5.70
4.	$Na_{0.15}WO_3$	(6^+)	(W-O)	(3.269)	(5.84)	5.90
5.	$In_{0.2}WO_3$	(6^+)	(W-O)	(3.308)	(5.85)	6.00
6.	$4\%WO_3/Al_2O_3$ (calcined)	(6^+)	(W-O)	(3.308)	(5.85)	6.00
7.	$6\%WO_3/Al_2O_3$ (calcined)	(6^+)	(W-O)	(3.384)	(5.89)	6.20
8.	$8\%WO_3/Al_2O_3$ (calcined)	(6^+)	(W-O)	(3.384)	(5.89)	6.20
9.	$10\%WO_3/Al_2O_3$(calcined)	(6^+)	(W-O)	(3.384)	(5.89)	6.20
10.	$12\%WO_3/Al_2O_3$(calcined)	(6^+)	(W-O)	(3.421)	(5.90)	6.30
11.	$4\%WO_3/Al_2O_3$ (reduced)	(6^+)	(W-O)	(3.269)	(5.84)	5.90
12.	$6\%WO_3/Al_2O_3$ (reduced)	(6^+)	(W-O)	(3.346)	(5.87)	6.10
13.	$8\%WO_3/Al_2O_3$ (reduced)	(6^+)	(W-O)	(3.346)	(5.87)	6.10
14.	$10\%WO_3/Al_2O_3$(reduced)	(6^+)	(W-O)	(3.384)	(5.89)	6.20
15.	$12\%WO_3/Al_2O_3$(reduced)	(6^+)	(W-O)	(3.384)	(5.89)	6.20
16.	$4\%WO_3/TiO_2$ (calcined)	(6^+)	(W-O)	(3.384)	(5.89)	6.20
17.	$6\%WO_3/TiO_2$ (calcined)	(6^+)	(W-O)	(3.269)	(5.84)	5.90
18.	$8\%WO_3/TiO_2$ (calcined)	(6^+)	(W-O)	(3.308)	(5.85)	6.00
19.	$20\%Ni/W/\gamma - Al_2O_3$(calcined)	(6^+)	(W-O)	(3.346)	(5.87)	6.10
20.	$20\%Ni/W/\gamma - Al_2O_3$(reduced)	(6^+)	(W-O)	(3.308)	(5.85)	6.00

Table 4.2: Values of Ionization potential, Electron affinity and Hardness

Atom	Ionization potential, I	Electron Affinity, A	Absolute hardness, η
N	14.53	0.00	7.27
O	13.61	7.53	6.08
S	10.36	6.22	4.12
Se	9.75	5.89	3.86
Cl	13.01	7.31	4.70
Br	11.84	7.60	4.24
I	10.45	6.76	3.70

These values are taken from Ref.[53]

Chapter 5

EXAFS

5.1 Introduction

Catalysts consisting of small metal clusters dispersed on the surface of a carrier are technologically very important. The carrier is commonly a refractory oxide such as alumina or silica in a high surface area form. The metal dispersion, defined as the ratio of surface atoms to the total atoms in the metal clusters, approaches unity in some catalysts when the metal concentration is low. A good example of such a high dispersion is provided by the alumina supported nickel-tungsten catalysts which have been widely used in the hydrogenation processes [1]. The most common method of obtaining information on the degree of metal dispersion involves measurement of the extent of chemisorption of a gas such as hydrogen or carbon monoxide on the metal. More direct information on metal cluster sizes and shapes can be obtained by high resolution electron microscopy.

After the development of high intensity X-ray sources, it has been found that extended X-ray absorption fine structure (EXAFS) to be very promising for investigating the structure and properties of catalytic materials [2-4]. From EXAFS measurements one can obtain information on the environment about a particular type of atom in a material, i.e., the number and kind of neighbouring atoms and their distances from the absorbing atom. Information on the vibrational motions and the extent of static disorder of the atoms can also be obtained. Prior to EXAFS measurements, it has been difficult to obtain such data on supported catalysts with dispersions approaching unity. In this Chapter, the application of EXAFS to alumina and titania supported tungsten oxide catalysts is discussed.

The data analyzed in this thesis were collected in the In-House EXAFS laboratory. Details about the source of X-rays as well as the experimental equipment and setup are given in Chapter II. Briefly, X-rays emitted from the rotating anode X-ray generator or a conventional X-ray tube are monochromated by a Johnsson type bent-crystal or a flat silicon crystal. The monochromated beam passes through the first detector and then through the sample. The transmitted X-rays are then detected by another detector. Even one detector can be used by moving the sample in and out of the X-ray beam. The voltage pulses produced are fed into a digital scalar and counted for a given length of time, the number of counts

per unit time being directly proportional to the number of photons entering into the detector. With the sample between the two detectors, the ratio of counts from the first and the second detector gives I_0/I. The logarithm of this value is proportional to the absorption coefficient, μ. As a spectrum is measured, (I_0/I) is recorded as a function of monochromator crystal position. The crystal is mounted on a goniometer driven by a stepping motor, so that monochromator steps are proportional to the incident angle of the X-ray beam on the crystal face. The data to be analysed, is originally in the form of monochromator steps versus I_0/I.

The EXAFS measurements were made on model tungsten oxides, sulphide and catalysts at room temperature.

5.2   Results and Discussion

Before discussing the results on the EXAFS, it would be appropriate here to briefly discuss the method of EXAFS data analysis.

To extract the extended X-ray absorption fine structure information from the above raw data, the data was processed. The processing steps involve a background subtraction which is done by a method due to Lytle et al [5]. In this method, a Victoreen function is fitted to the pre-edge portion of the raw data upto 100 eV below the absorption edge and extrapolated it over the whole range of absorption data and subtracting it from the data range.

After this pre-edge subtraction, a third degree polynomial is fitted through the center of the EXAFS oscillations. This curve is assumed to be the μ_0 versus energy curve, μ_0 being the absorption coefficient in the absence of neighbouring atoms. It is subtracted from the data and the difference is then divided by it in order to get $(\mu - \mu_0)/\mu_0$. This procedure gives the normalized absorption coefficient, χ as a function of X-ray photon energy.

For performing Fourier transform analysis, the above data were transformed from energy to wavevector k using the relation

$$k = \sqrt{\frac{2m}{\hbar}(E - E_0)} \tag{5.1}$$

where E is the energy of the photoelectron measured from the inflection point on

127

the edge, and E_0 is the effective average potential felt by an excited electron and represents the potential "zero" above which the kinetic energy must be added to determine the total energy E. Since E_0 is difficult to determine experimentally, in the begining of the data analysis an arbitrary value is given to E_0 and then the value of E_0 is floated in the analysis and that value of E_0 is taken for which the imaginary part and the absolute value of the Fourier transform peak at the same distance [6].

The data thus obtained were multiplied by the Hanning window function in order to minimize the termination ripples. Subsequently, it was multiplied by a weighting function, k^3 to compensate for amplitude reduction as a function of k. Fourier transforms, for both the real and imaginary components were done by using Simpson's rule to numerically integrate the EXAFS region of interest within the integration limits k = 4 to k =14 $A^{\circ^{-1}}$. The modulus of the Fourier transform was obtained as a square root of the sum of the squares of real and imaginary parts.

For the excitation of a s level (K or L_I edge) the absorption coefficient normalized to a smooth background μ_0 can be described [2, 5] by

$$\chi(k) = \frac{1}{k} \sum_j \frac{N_j}{R_j^2} F_j(k) \exp\left(-\sigma_j^2 k^2\right) \exp\left(-2R_j/\lambda\right) \sin\left[2kR_j + \phi_j(k)\right] \qquad (5.2)$$

where k is the electron wave vector, N_j is the number of atoms in the jth coordination sphere, R_j is the average radial distance to the jth atoms, $F_j(k)$ is the electron back-scattering amplitude, λ is the mean free path of the electron, the exponential term containing σ_j^2 is a Debye-Waller-type term where σ_j is the rms fluctuations of the atom about R_j, and $\phi_j(k)$ is the total phase shift experienced by the photoelectron.

The form of this equation is a sinelike scattering from each shell of atoms at R_j with the EXAFS signal proportional to the number of atoms surrounding the absorbing atom and inversely proportional to R_j^2. A decrease in temperature has the effect of sharpening the EXAFS. Each coordination sphere contributes a sinelike term of period $2kR_j$. The total result is a summation over all the coordination spheres within range of the effect. For all practical purposes the $L_{I,II}$ edge can be analyzed in the same way as K or L_I-edges with the use of $l = 2$

128

phase shifts [7].

The object of the data analysis procedure is therefore to decompose the observed EXAFS spectrum into its component waves and determine the phase and amplitude of each component. This in turn gives information about the distance in the coordination shells and disorder in the distance as well as the number of atoms in the shells.

For curve-fitting analysis the data have been processed by a Fourier filtering procedure. The data (actually $k^2\chi(k)$ versus k), were Fourier transformed as mentioned above to R (frequency) space, then the region of interest in the Fourier transform spectrum was retransformed back to k space in order to isolate the first coordination shell.

Seven parameter fits were performed on the Fourier filtered data using a parametrized form of EXAFS equation (eqn.5.2)

$$\chi_{param} = \frac{C_1}{k^{C_3}} \exp\left(-C_2 k^2\right) \sin\left(C_4 + C_5 k + C_6 k^2 + \frac{C_7}{k^3}\right) \qquad (5.3)$$

Fits were done by least-squares adjustment of parameters C_1 to C_7 using a general optimization program written by Sarode [8] based on algorithm of Rosenbrock [9]. In this program, the function minimized[10] in the fitting procedure is given by

$$F = \left[\frac{\sum k^6 (\chi_{expt} - \chi_{param})^2}{N}\right]^{1/2} \qquad (5.4)$$

where χ_{param} is the parametrized EXAFS function, χ_{expt} is Fourier filtered EXAFS function, N is the number of data points in the fit and the sum is over the number of data points. F is a measure of the goodness of the fit and is lower for a better fit.

The curve fitting procedure for determining the distance R to a shell of atoms in an unknown compound is as follows. EXAFS data from a model compound whose crystal structure is known is fitted with equation (5.3) by adjusting all the seven parameters. The standard parameters C_3, C_4, C_6 and C_7 are then used as fixed constants in fitting equation (5.3) to data from the unknown compound by adjusting C_1, C_2 and C_5. If the phase shift $\phi(k)$ is assumed to have the form

$$\phi(k) = C_4 + C_5 k + C_6 k^2 + C_7/k^3 \qquad (5.5)$$

129

then comparison of the theoretical equation (5.2) with the parametrized equation (5.3) shows that $C_5 = 2R + A$. The linear phase term parameter A is determined from the standard fit since R is known, and then A is used to calculate R from the fit of the unknown. The number of atoms in the unknown, N can be estimated by

$$N_u = N_m \cdot \frac{C_{1u}}{C_{1m}} \cdot \frac{R_m^2}{R_u^2} \qquad (5.6)$$

where R_u and C_{1u} refer to the unknown and C_{1m} and R_m refer to the model compound, whose crystal structure is known. From the value of C_2 for the unknown, σ^2 can be determined. By taking difference between the values of σ^2 for reference and unknown, the relative disorder can be calculated.

5.2.1 Fourier Transforms of Model Compounds

Fourier transforms of the EXAFS, $k^2(\chi)$ at the tungsten L_{III}-edge of $CaWO_4$, $(NH_4)_2WS_4$ and WO_3 are shown in Fig.5.1. The peaks in the modulus of FT correspond to the different coordination shells. The two peaks indicated by the arrows in $CaWO_4$ in Fig. 5.1 at 1.78 and 2.91 Å are due to the nearest neighbour oxygen atoms. The single peak in the Fourier transforms of $(NH_4)_2WS_4$ at 2.18 Å is due to W-S distance. In WO_3 the three observed peaks in the range 1 - 2.5 Å are due to W-O and the fourth peak at 3.73 Å is due to W-W interaction.

The position of the peak in Fourier transforms of catalyst can be used to estimate the bond length by using model compounds like those mentioned in Fig.5.1 having known R_j so that a ΔR_j correction can be made due to the effect of $\phi_j(k)$ [11]. The height and width of the peak according to equation (5.3) are related to N_j and σ_j but precise determination of N_j and σ_j is difficult due to convolution effects of the Fourier transforms of $F_j(k)$ and the other $\chi(k)$ terms in R space [12].

A more reliable method to determine N_j and σ_j is by isolating a given peak in a radial structure function and performing an inverse Fourier transform. This procedure decouples, as mentioned above, the contribution of adjacent coordination shells so that the effect of only the coordination shells of interest is preserved.
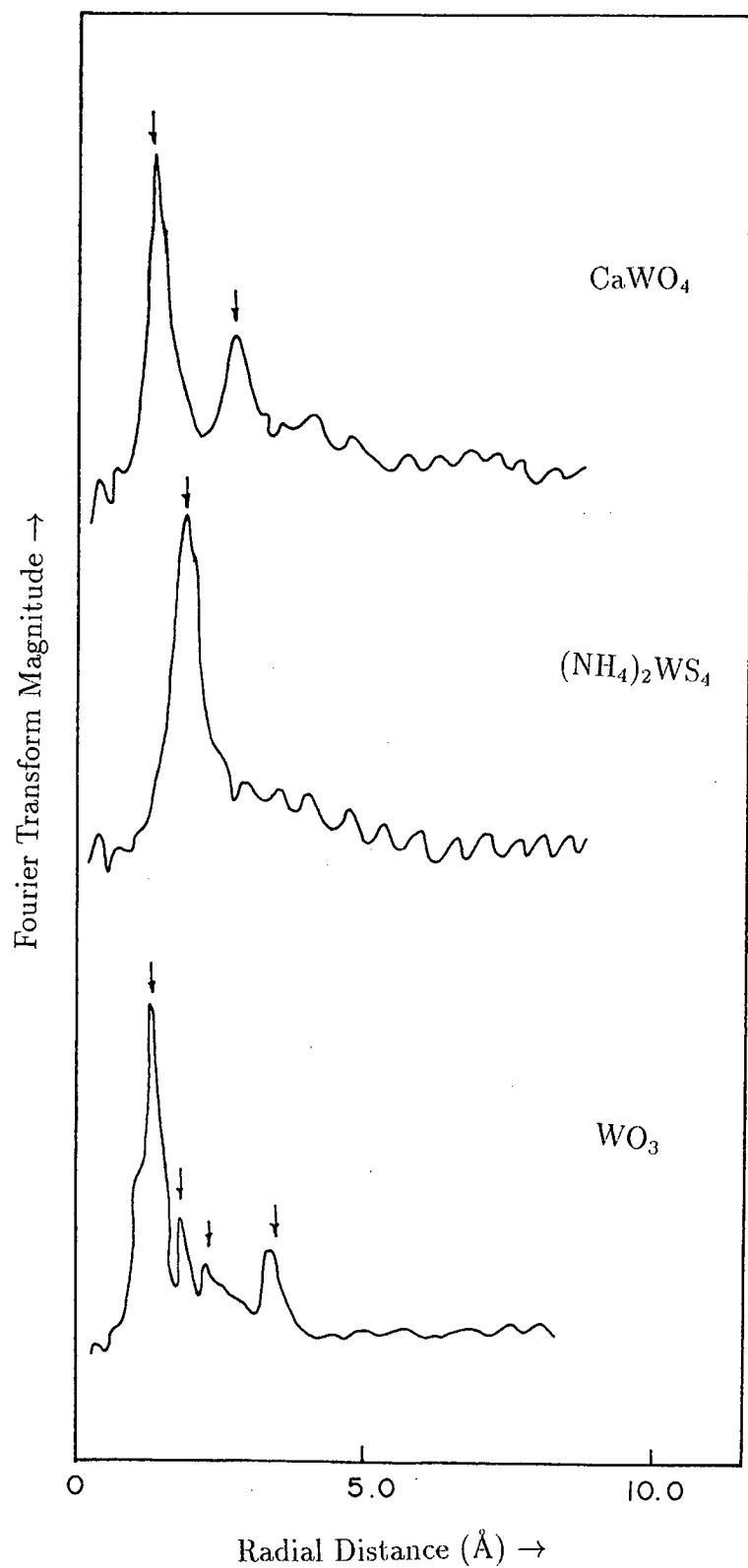
130

Figure 5.1: Fourier transforms of the L_{III}-edge EXAFS data from $CaWO_4$, $(NH_4)_2WS_4$ and WO_3.

The resultant χ for one shell or two shells can be used in a least-squares fitting routine to determine R, N and σ.

To obtain empirical parameter for the pairwise phase shift and amplitude functions, we have used $CaWO_4$, $(NH_4)_2WS_4$ and WO_3 as model compounds for obtaining parameters for W-O, W-S and W-W interactions. The first peaks in $CaWO_4$ and $(NH_4)_2WS_4$ and fourth peak in WO_3 were isolated using a suitable window function by retransforming them to the k-space and then fitting with equation (5.3) adjusting all the seven parameters. Table 5.1 summarizes the results of fits of these model compounds including the values of the fitting functions, values of the parameters, C_1, C_2, C_3, C_4, C_5, C_6 and C_7 as well as E_0 values. In Fig. 5.2 we have shown the fitted and experimentally observed Fourier filtered EXAFS data of these compounds. The simulated spectra obtained from the parametrized form of EXAFS equation match very well with the Fourier filtered spectra. From the values of fitting function (which indicates the level of goodness of fit), it can be seen that the equation (5.3) is suitable for the analysis of tungsten L_{III}-edge EXAFS.

The value of the constant C_7 in all the three cases is very small suggesting thereby that the equation of the type,

$$\chi_{param} = (C_1/k^{C_3}) \exp\left(-C_2 k^2\right) \sin\left(C_4 + C_5 k + C_6 k^2\right)$$

will also give a good fit. However for high Z elements the equation (5.3) has been successfully employed [13] for structure determination. We have therefore used eqn. (5.3) for the EXAFS analysis.

One important feature of these Fourier filtered spectra is the different amplitude envelopes observed for different type of scattering atoms (see dotted curves Fig 5.2). As expected [7], the amplitude for oxygen atom dies out monotonically, while the sulphur amplitude peaks at relatively low k value and then dies away. The amplitude for W-W wave clearly shows the EXAFS peaking at higher k value as atomic number of scatterer increases. Here all points of fine structure have been multiplied by k^2 to make the higher k EXAFS visible. The physical basis for this variation in EXAFS amplitude behaviour is related to trends in the electron-atom backscattering amplitudes, which peak at higher k-value as Z
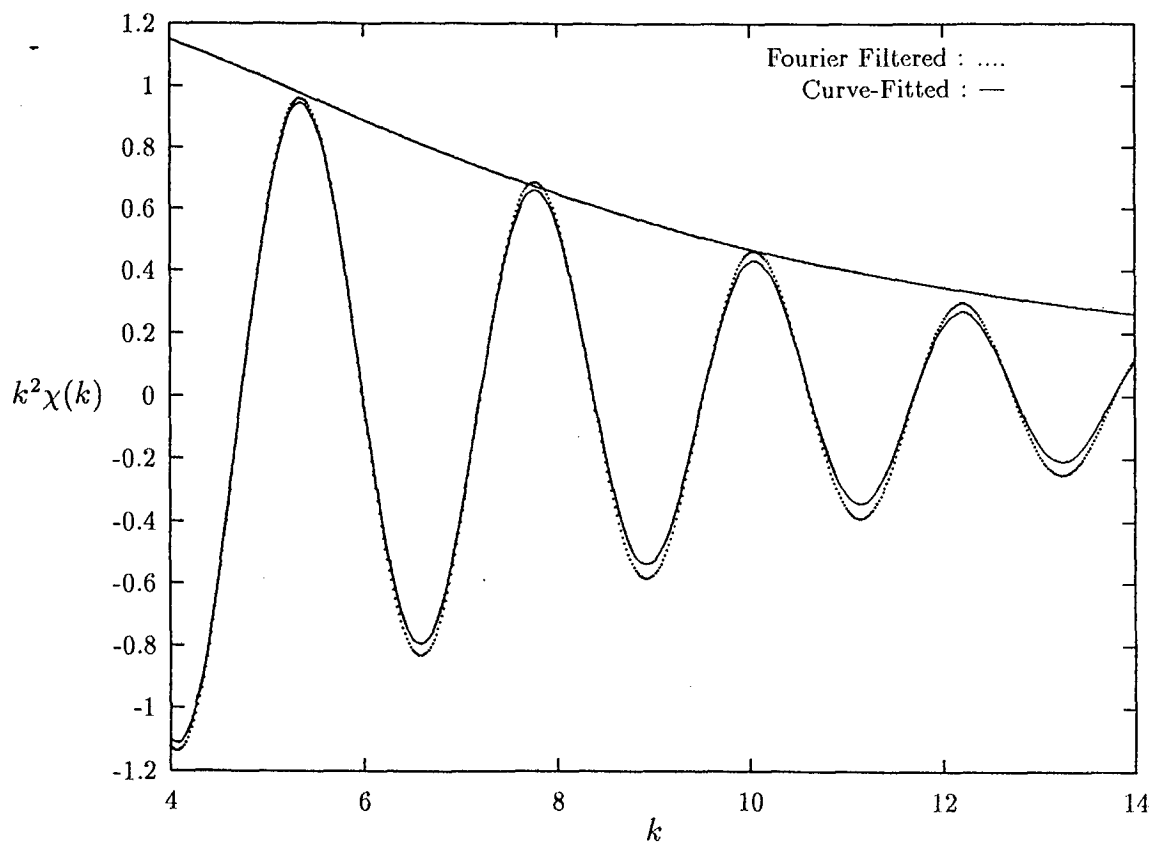
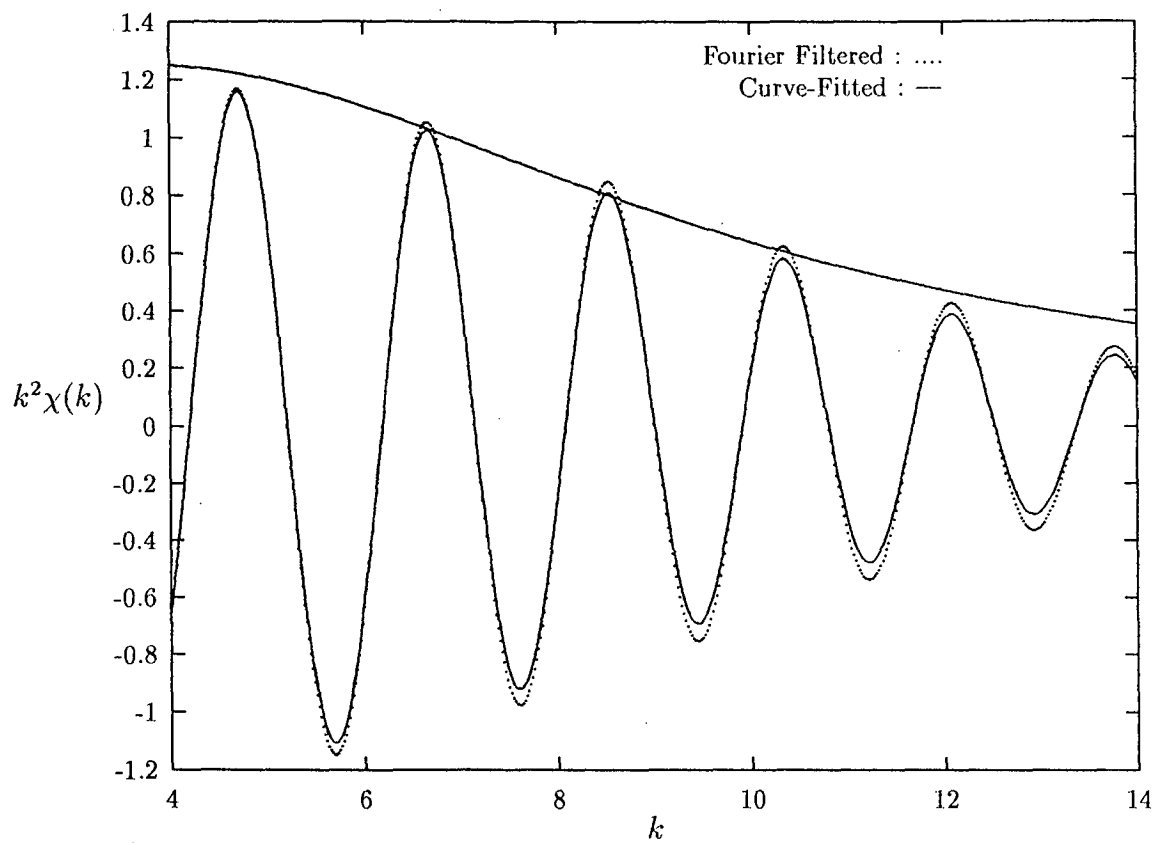Fig. 5.2: (a) Fourier filtered EXAFS spectra and single-shell fit for $CaWO_4$.

Fig. 5.2: (b) Fourier filtered EXAFS spectra and single-shell fit for $(NH_4)_2WS_4$.
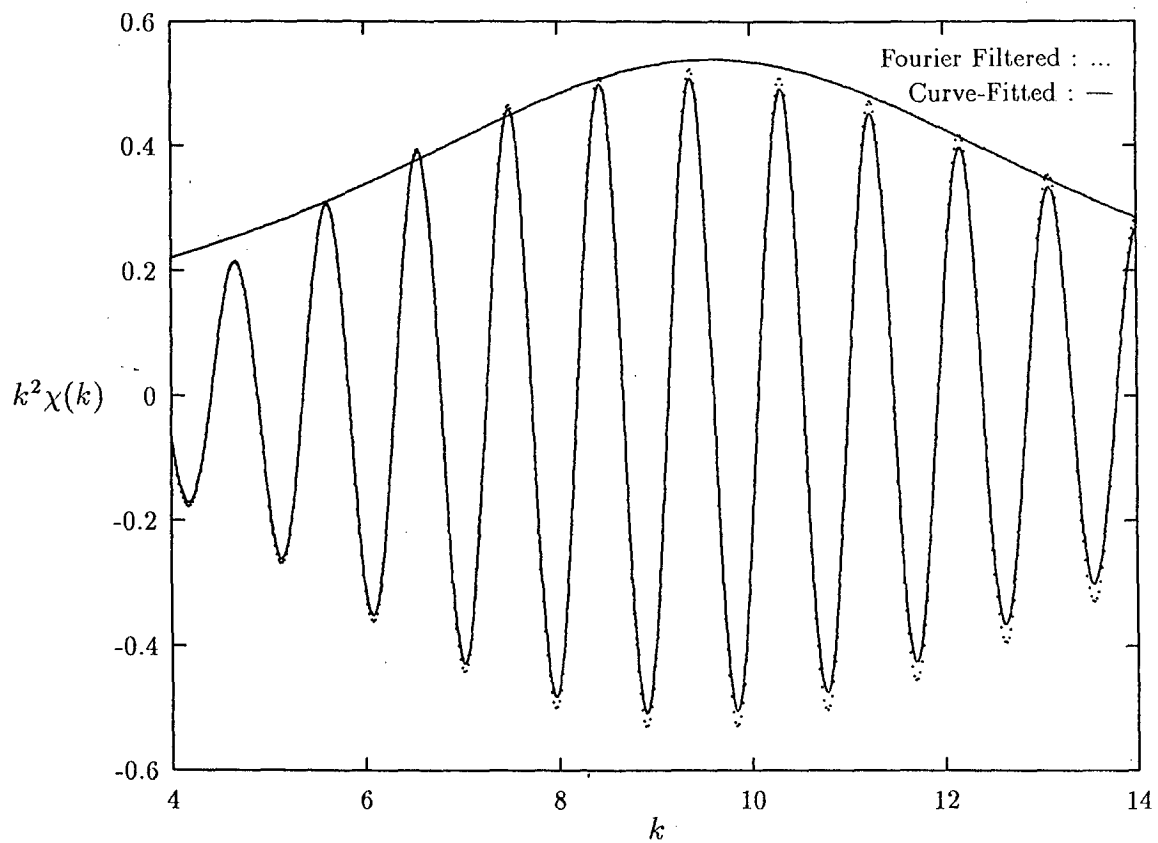
Fig. 5.2: (c) Fourier filtered EXAFS spectra and single-shell fit for WO_3.

(atomic number) increases [7, 14].

The total phase shift was obtained by subtracting $2Rk$ from $C_4 + C_5k + C_6k^2 + C_7/k^3$) for each of three model compounds. These empirical phase shifts are plotted in Fig.5.3(a) and in Fig.5.3(b) theoretically determined phase shifts from the Tables of Teo and Lee [7] are plotted for comparison. It can be seen that W-O, W-S and W-W shifts are all very similar to those in Fig.5.3(b). The phase shifts for W-S differs from those of W-O by an average of about 2.3 radians. This difference is closer to π than to zero, which means that the best fit of W-S standard parameters to W-O data and vice versa should yield a negative amplitude. In the present investigation, the nature of near neighbour is known, e.g., in all the catalysts studied, the oxygen atoms are coordinated to the absorbing tungsten atom. If the near neighbours are unknown, the phase shift versus k curves for different atom-pairs from model compounds are compared with the curves from unknown ones and then the curve lying close to the curve obtained from the standard will determine the nature of the liganding atoms.

According to Citrin et al [15], Lengeler et al [16] and Chetal et al [17], all the phase (C_4, C_5, C_6, C_7) and amplitude (C_1, C_2, C_3) parameters obtained from the inverse FT of the model compound can now be transferred to the catalytic systems in which the absorbing atoms have the similar chemical environment to predict the structural parameters. This is done in the next section.

5.2.2   Fourier Transforms of Catalytic Samples

Before discussing the results on EXAFS analysis of catalytic samples, we will first examine the FT spectrum of WO_3.

The Fourier transforms of the L_{III}-edge EXAFS ($k^2\chi$) WO_3 is shown in Fig.5.1. As is known [11], this spectrum gives the radial structure function of the neighbouring coordination shells around tungsten atom with noncorrected distances R_j. From this spectrum, we see four peaks above background, the first three peaks in the range 1 - 2.5 Å and the fourth one at 3.73 Å. The disorder in the first two peaks is ~ 0.0075 Å. On the basis of crystal structure of WO_3 [18], as mentioned earlier the first three peaks can be attributed to three W-O distances
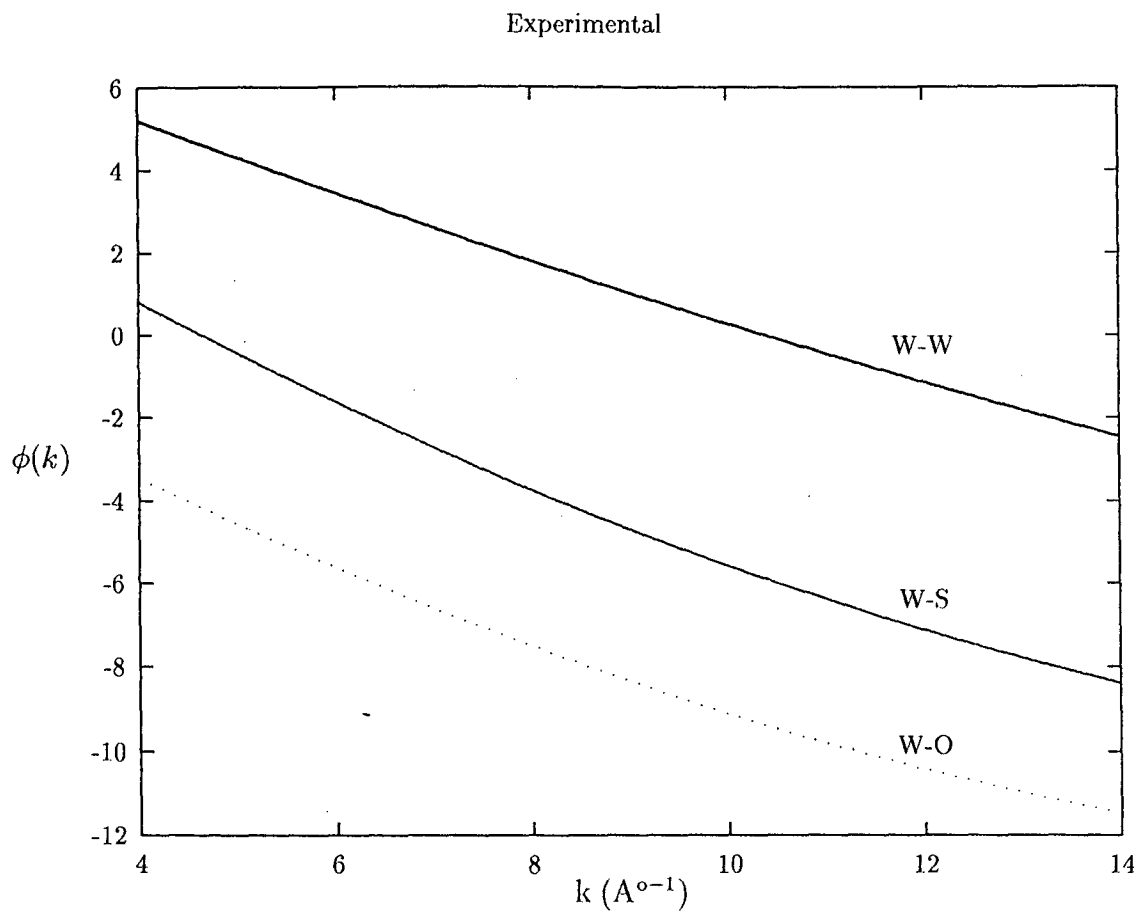
Fig. 5.3: (a) Plot of phase shift function, $\phi(k)$ (in radians) versus photoelectron wave vector k ($\Lambda^{\circ-1}$) (Experimental)
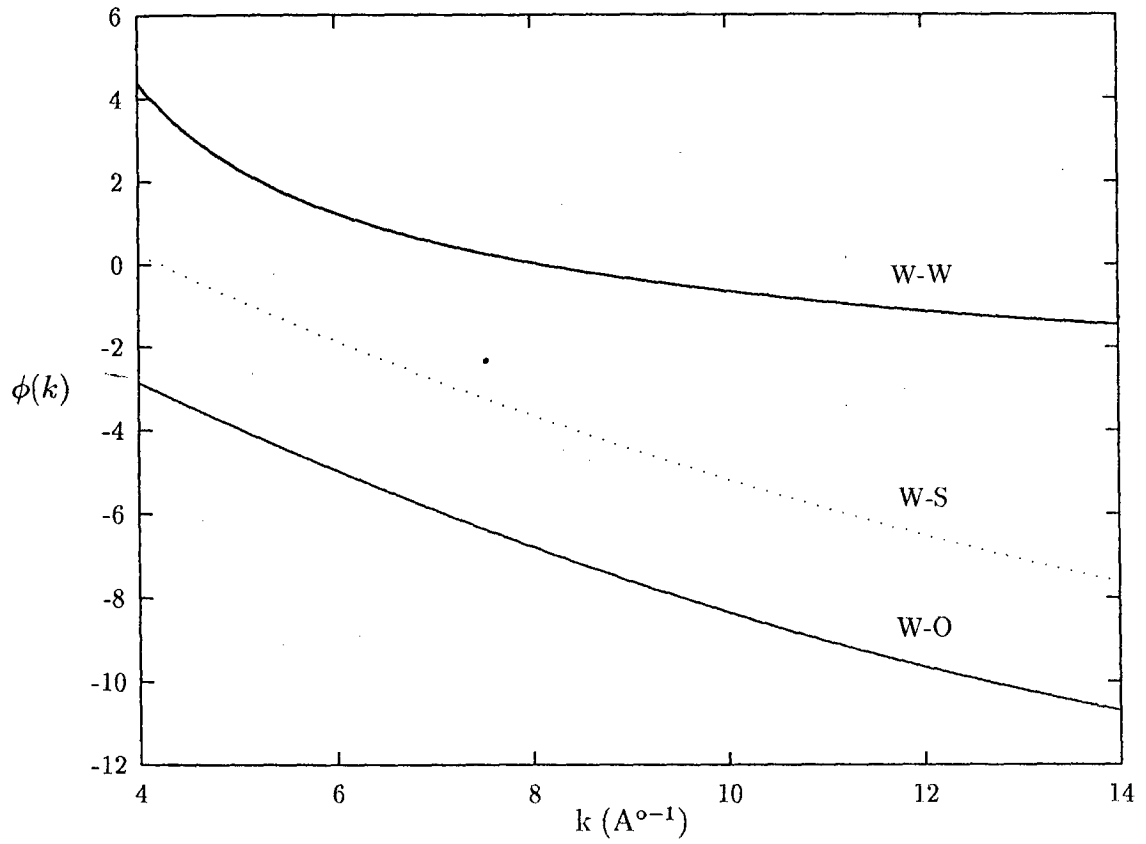
Theoretical

Fig. 5.3: (b) Plot of phase shift function, $\phi(k)$ (in radians) versus photoelectron wave vector k ($A^{\circ-1}$) (Theoretical)

138

within 1 - 2.5 Å and the fourth peak at 3.73 Å to W-W distance. Our FT spectrum for WO_3 matches fairly well with that obtained by taking FT of the EXAFS spectra recorded using synchrotron radiation [19].

Fig 5.4 shows the Fourier transforms of calcined catalysts, WO_3/Al_2O_3 with varying WO_3 content along with the FT spectrum of WO_3 for comparison. The W-O distances and structural disorders as well as coordination numbers of tungsten obtained from the curve-fitted spectra are given in Table 5.2. The bond distances of the peaks in these spectra are 1.78 and 1.91 Å which are the same as those for bulk WO_3, indicating the presence of only $W(VI)$ on the oxidic (calcined) catalyst. However, the extent of disorder is relatively more.

Fig.5.5 shows the catalyst reduction behaviour as a function of WO_3 content. Each catalyst was reduced in hydrogen for 12 hrs to assure that reduction of the W (VI) species formed on the surface is complete. A slight change is seen in the FT spectra with increasing WO_3 content. The major peak is getting broadened indicating thereby that there is a formation of new species on the surface, which seems to have two W-O distances. This species may be a lower oxidation tungsten species, perhaps $W(V)$-species. The indirect support for the formation of new species on the surface of reduced WO_3/Al_2O_3 catalysts comes from the ESCA studies carried out by Zingg et al [20] on MoO_3/Al_2O_3 catalysts with varying MoO_3 loading in the range 5 - 20 %. These authors have examined the Mo 3d ESCA spectra of reduced MoO_3/Al_2O_3 catalysts. The reduction of the catalytic samples was carried out at 500°C in hydrogen for 12 hours. From their spectra, it is seen that as the loading percentages of MoO_3 increases, a shoulder due to $Mo(V)$ developes gradually at 229.2 eV.

In Fig.5.6 are presented the Fourier transform spectra of WO_3 and 4 and 8% calcined WO_3/TiO_2 catalyst. In this spectra, the peaks observed between 1 - 2.5 Å range correspond to W-O interactions. Around 3.5 Å, (corrected, 3.73 Å) the peak observed is due to W-W bonds. This is similar to that obtained in WO_3 and the structural disorder is similar to those obtained in calcined WO_3/Al_2O_3. In addition, the FT transforms of both the catalytic samples show an extra peak, slightly broad at 2.99 Å, which is not observed in WO_3 or in the FT spectra of other model compounds. This peak may probably be due to W-Ti

139

WO₃

4%WO₃/Al₂O₃
(Calcined)

8%WO₃/Al₂O₃
(Calcined)

12%WO₃/Al₂O₃
(Calcined)
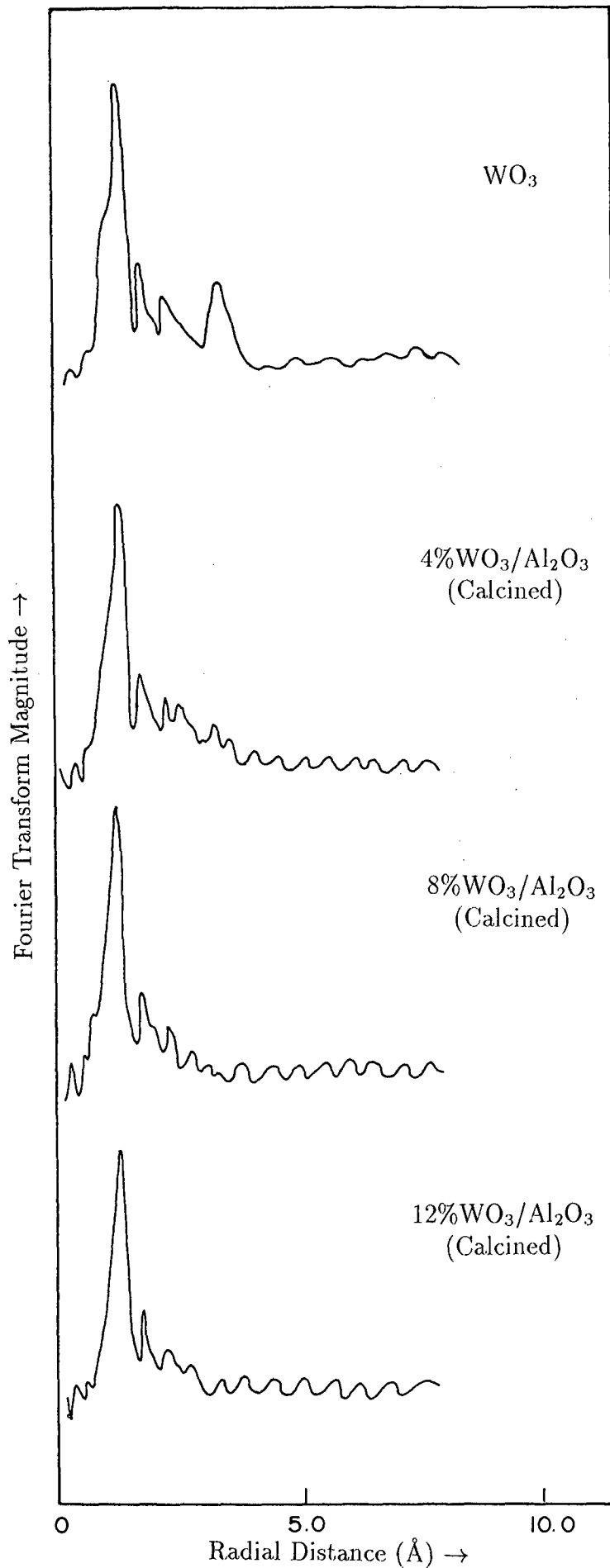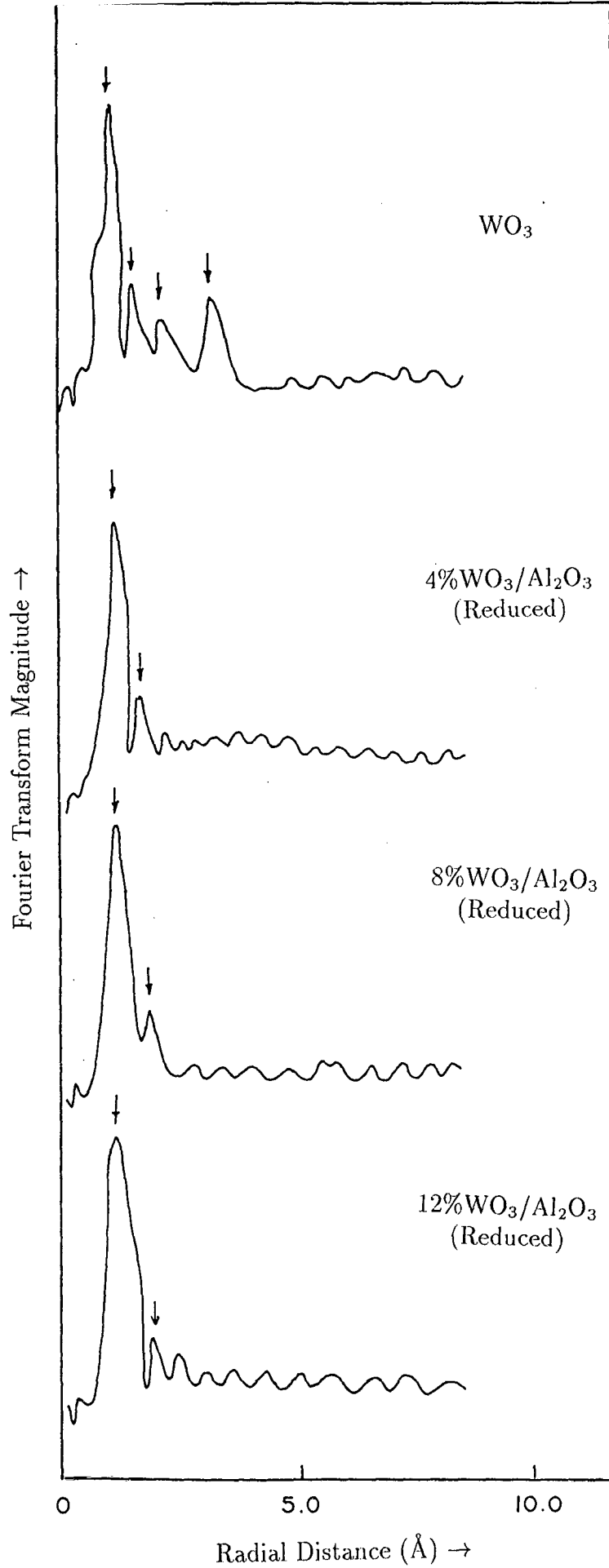
Figure 5.4: Fourier transforms of the L_{III}-edge EXAFS data from calcined 4%,

Figure 5.5: Fourier transforms of the L_{III}-edge EXAFS data from reduced 4%, 8% and 12% WO_3/Al_2O_3 catalysts.
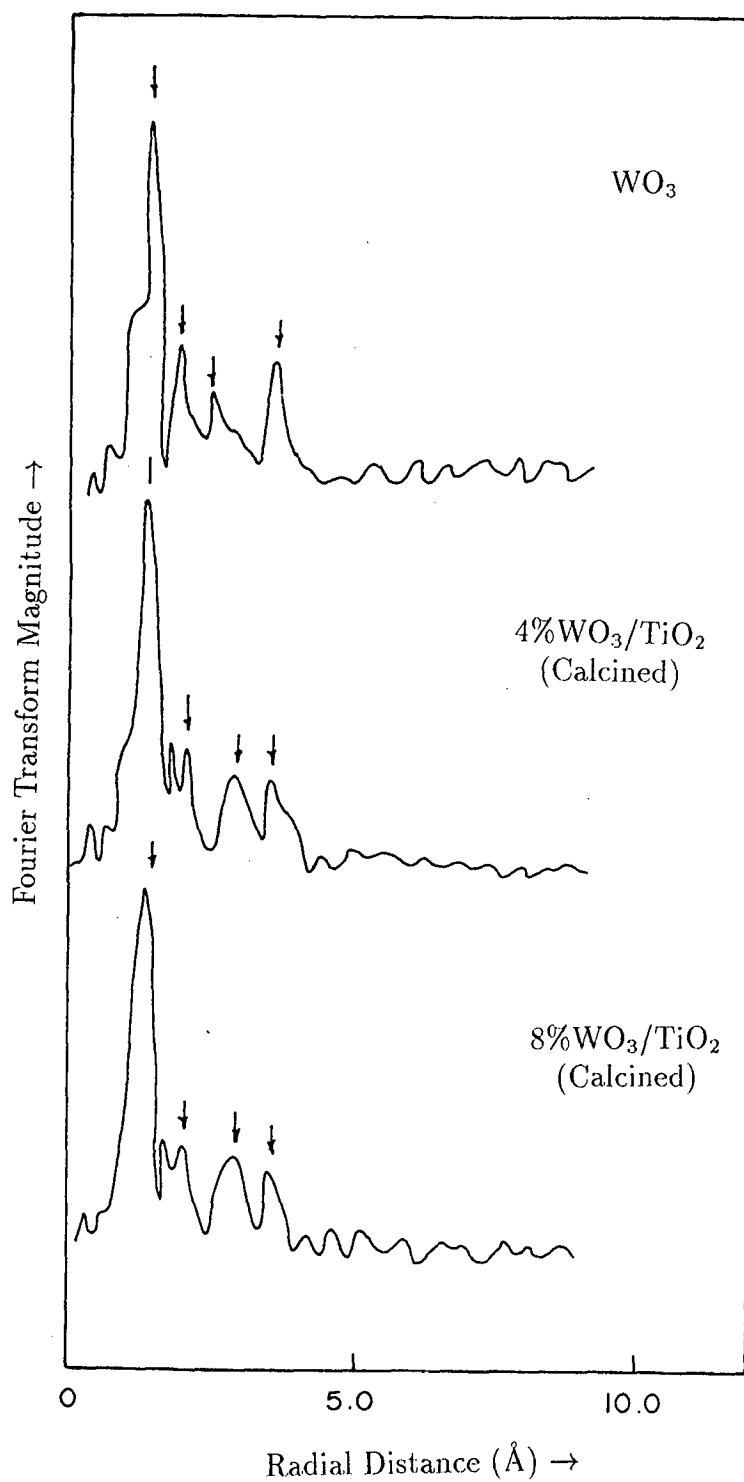
Figure 5.6: Fourier transforms of the L_{III}-edge EXAFS data from WO_3 and calcined 4 and 8% WO_3/TiO_2 catalysts.

bonds. However, in the present investigation, we have not prepared any tungsten compound in which W-Ti bonds are present. Kisfaludi et al [21] observed in their Mo K-edge EXAFS study of MoO_3/Al_2O_3, a peak corresponding to distance 2.99 Å. These coworkers suggested that this peak can be attributed to Mo-Al bonds. In a similar way, the peak at 2.99 Å may be related to a W-Ti distance in these catalysts. In the structure of the species formed, this distance can be attributed to the distance of the centres of edge-connected WO_6 octahedra, since TiO_2 support oxide is built-up by a mixture of edge- and corner-sharing octahedra.

The corrected distance R_j and coordination numbers N_j of the first two W-O shells in the EXAFS of 4% and 8% calcined WO_3/TiO_2 were estimated by a non-linear curve-fitting analysis. The two W-O peaks within 1 - 2.5 Å were isolated with a window and backtransformed to k-space. The results are summarized in Table 5.2. The peak at 1.76 Å, corresponds to the W=O bond in the catalyst spectra. In Raman spectroscopic study of WO_3/TiO_2 catalysts carried out by Hibrig et al [22], the peak at 970 cm^{-1} corresponds to W=O distance of 1.76 Å. The next peak at 1.91 Å with a high Debye-Waller factor presumably correspond to the W-O bonds in the W-O-W and W-O-Ti bridges. From Table 5.2, it can be seen that the coordination numbers obtained in the EXAFS analysis are lower than those expected on the basis of the XANES results. This probably indicates disorder on a large scale, mostly due to the presence of absorbed water on the surface of catalyst or due to a non-Gaussian distance determination as claimed by Hilbrig [22].

On the basis of the structural results described above, one can suggest a nature of the species formed from the tungsten oxide spread on the surface of TiO_2. In these catalysts, from the careful examination of Fourier transforms and Table 5.2, it can be seen that the species formed contains WO_4 units as well as WO_5 units (from the appearance of third peak due to W-O interaction) and their ratio may probably depend upon the degree of the tungsten oxide coverage.

The Fourier transform spectra for 20% calcined and reduced $Ni - W/Al_2O_3$ catalysts are shown in Fig.5.6. In this spectra, for the calcined sample there is only one major peak observed at 1.79 Å corresponding to W-O distance fol-

lowed by a small peak at 1.91 Å. Other peaks seem to have merged with the increased background. These two peaks in the spectra are very similar to those of CaWO4 or $Al_2(WO_4)_3$ and have structural disorder similar to that in calcined WO_3/Al_2O_3.

The spectra in Fig.5.7 correspond to the catalysts that have been reduced at 500°C for 2 hrs and 550°C for 6 hrs respectively. Essentially no change in the FT specta with respect to peak distances and widths of the peaks is observed. It may be interesting to mention here [23] that if WO_2 and WO_3 are reduced under same conditions, the overall FT spectra of the reduced oxides showing only three peaks look very similar to the FT spectra of the L_{III}-edge of tungsten metal. These results leads us to conclude that tungsten forms some kind of a stable interaction complex with the γ-alumina support. The species may perhaps be $Al_2(WO_4)_3$ or some kind of ternary compound of WO_3 and Al_2O_3, as predicted from XANES study.

Ng and Hercules [1] have carried out X-ray photoelectron spectroscopic study on calcined and reduced $Ni - W/Al_2O_3$ with varying percentages of WO_3 (8 - 19%). In the ESCA spectra of calcined and reduced catalysts, the binding energy of W-4$f_{7/2}$ level is found to be at 35.4 eV. This is exactly the value they found for W-4$f_{7/2}$ line in $Al_2(WO_4)_3$. Reduction even for longer period does not change any features of the spectra. Biloen and Pott [24] have also observed from their ESCA studies that species formed on $\gamma - Al_2O_3$ are not reducible at 500°C. Both these studies clearly lend support to our work that suggest a formation of a stable interaction complex of tungsten on the surface of γ-alumina.
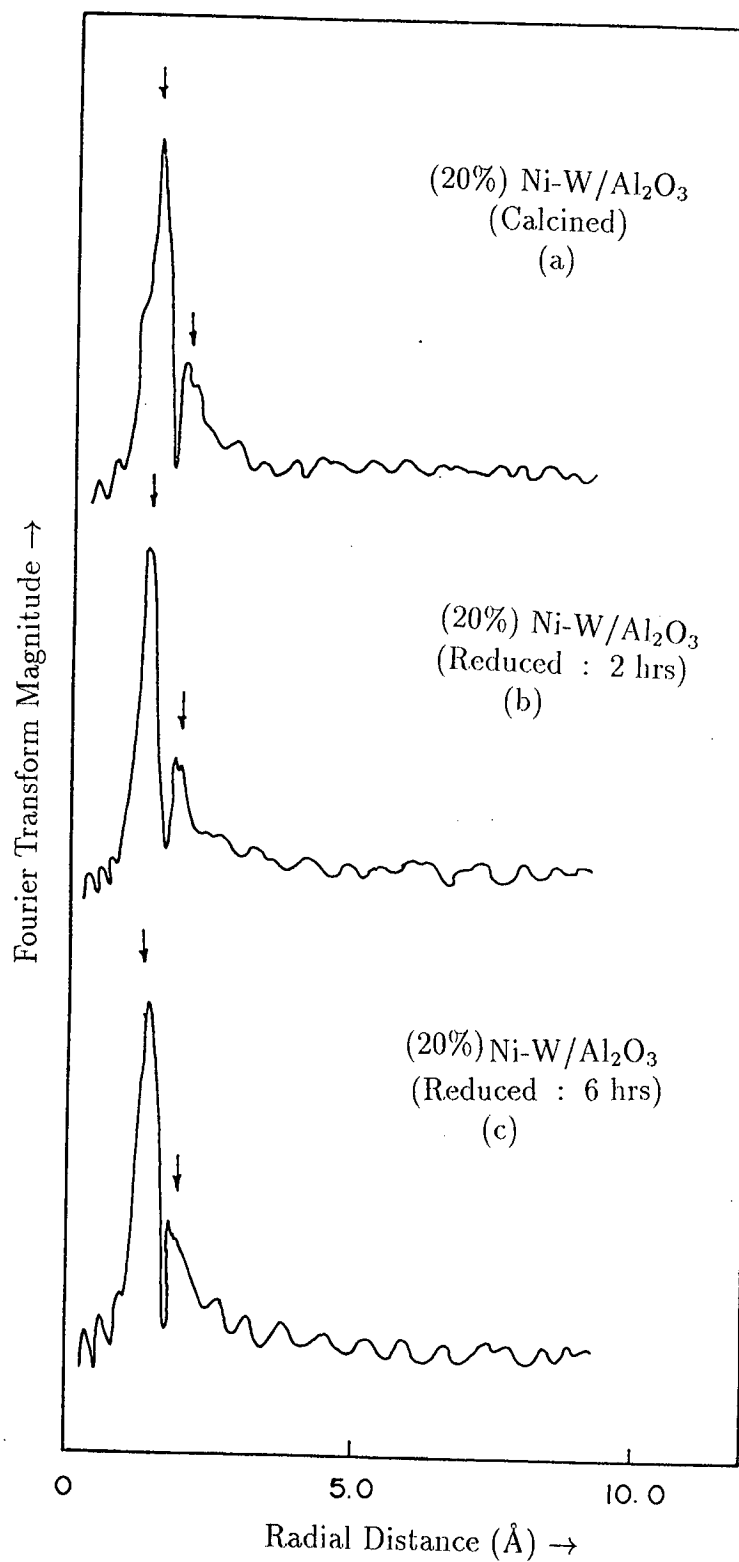
Figure 5.7: Fourier transforms of the L_{III}-edge EXAFS data from 20 % calcined and reduced Ni $-$ W/Al$_2$O$_3$ catalyst.

References

[1] K. T. Ng and D. M. Hercules, J. Phys. Chem., $\underline{80}$, 2094 (1976).

[2] P. A. Lee, P. H. Citrin, P. Eisenberger and B. M. Kincaid, Rev. Mod. Phys., $\underline{53}$, 769 (1981).

[3] D. C. Koningsberger and R. Prins, X-ray Absorption : Principles, Applications, Techniques of EXAFS, SEXAFS and XANES, John Wiley and Sons, New York (1988).

[4] J. H. Sinfelt, G. H. Via and F. W. Lytle, Catal. Rev.-Sci. Eng., $\underline{26}$, 81 (1984).

[5] F. W. Lytle, D. E. Sayers and E. A. Stern, Phys. Rev. B$\underline{11}$, 4825 (1975).

[6] P. A. Lee and G. Beni, Phys. Rev. B$\underline{15}$, 2862 (1977).

[7] B. K. Teo and P. A. Lee, J. Am. Chem. Soc., $\underline{101}$, 2815 (1979).

[8] P. R. Sarode, Computer Programs for EXAFS and XANES Analysis, (1990) (Unpublished).

[9] H. H. Rosenbrock, Comput. J., $\underline{3}$, 175 (1960).

[10] T. E. Eccles, Ph.D. Thesis, Stanford University (1977).

[11] E. A. Stern, D. E. Sayers and F. W. Lytle, Phys. Rev. B$\underline{11}$, 4836 (1975).

[12] R. Greegor and F. W. Lytle, Phys. Rev. B$\underline{20}$, 4902 (1979).

[13] K. J. Rao and J. Wong, J. Chem. Phys., $\underline{81}$, 4832 (1984).

[14] B. K. Teo, P. A. Lee, A. L. Simons, P. Eisenberger and B. M. Kincaid, J. Am. Chem. Soc., $\underline{99}$, 3854 (1977).

[15] P. H. Citrin, P. Eisenberger and B. M. Kincaid, Phys. Rev. Lett., $\underline{36}$, 1346 (1976).

[16] B. Lengeler, J. Phys. Colloq. (France) C8, $\underline{48}$, 75 (1986).

[17] A. R. Chetal, P. Mahto and P. R. Sarode, J. Less-Common Metals, $\underline{167}$, 199 (1991).

[18] A. F. Wells, Structural Inorganic Chemistry, Clarendon Press, Oxford (1986).

[19] F. Hilbrig, H. E. Göbel, H. Knözinger, H. Schmeltz and B. Lengeler, J. Phys. Chem., $\underline{95}$, 6973 (1991).

[20] D. S. Zingg. L. E. Makovsky, R. E. Tischer, F. R. Brown and D. M. Hercules, J. Phys. Chem., $\underline{84}$, 2898 (1980).

[21] G. Kisfaludi, J. Layrer, H. Knözinger and R. Prins. J. Catal., $\underline{130}$, 192 (1991).

[22] F. Hilbrig, Dissertation, Universität, München (1989).

[23] P. R. Sarode, Unpublished results.

[24] P. Biloen and G. T. Pott, J. Catal., $\underline{30}$, 169 (1973).

Table 5.1: Curve-Fitting Phase shift and Amplitude parameters

Optimized function : $\dfrac{C_1}{k^{C_3}}\exp\left(-C_2 k^2\right)\sin\left(C_4 + (2R + C_5)k + C_6 k^2 + \dfrac{C_7}{k^3}\right)$

Convergence limit $=$ 0.000010

Fitting range : $4 - 14$ $(A^{\circ -1})$

Model $\rightarrow$	$CaWO_4$	$(NH_4)_2 WS_4$	WO_3
Atom pair $\rightarrow$	W-O	W-S	W-W
Bond distance	1.78 Å	2.18 Å	3.73 Å
C1	1.692	0.789	0.00456
C2	0.00824	0.01120	0.01560
C3	2.192	1.581	-0.736
C4	1.740	0.230	2.730
C5	2.119	2.786	6.451
C6	0.0360	0.0364	0.0135
C7	1.97×10^{-4}	1.09×10^{-4}	-3.216×10^{-4}
F	3.47×10^{-3}	2.68×10^{-3}	3.02×10^{-3}
E_o (eV)	10204.4 eV	10203.2 eV	10202.0 eV

Table 5.2: Calculation of Bond Distances, disorder and coordination numbers in catalysts using $CaWO_4$ model compound.

Catalyst	Analysis range (A^{o-1})	Curve-fit Distance (Å)	Disorder σ^2 (A^{o2})	Curve-fit Number
Calcined WO$_3$/Al$_2$O$_3$				
4%	4 - 12	1.77	0.0091	1.8
		1.92	0.0098	2.1
8%	4 - 12	1.78	0.0098	1.9
		1.91	0.0094	2.2
12%	4 - 12	1.78	0.0095	2.0
		1.93	0.0099	1.9
Reduced WO$_3$/Al$_2$O$_3$				
4%	4 - 12	1.78	0.0010	1.9
		1.94	0.0018	2.3
8%	4 - 12	1.74	0.0014	1.9
		1.98	0.0020	2.4
12%	4 - 12	1.72	0.0016	2.0
		1.99	0.0023	1.9
Calcined WO$_3$/TiO$_2$				
4%	4 - 12	1.77	0.0090	1.7
8%	4 - 12	1.92	0.0094	2.1
Calcined Ni − W/Al$_2$O$_3$				
20%	4 - 12	1.80	0.0092	1.8
		1.92	0.0097	1.9
Reduced Ni − W/Al$_2$O$_3$				
20% (2 hrs)	4 - 12	1.81	0.0090	1.8
		1.92	0.0099	2.0
20% (6 hrs)	4 - 12	1.80	0.0092	1.8
		1.91	0.0098	2.1

Chapter 6

Resumé

6.1 The Experimental Technique and the Principal Results Obtained

X-ray spectroscopy occupies important place amongst different techniques of investigating the electronic structure of matter. In the recent years, the position, shape and extended fine structure of X-ray absorption discontinuities have been frequently used to deduce useful structural and chemical bonding information on different kind of materials. In the present work, an attempt has been made to observe the changes occurring in the various features of the X-ray L-absorption discontinuities of tungsten in its compounds, complexes, biological complexes, bronzes and catalysts on account of chemical combination and to obtain information on local environment of the excited atom species in these complex systems. In particular, such investigations have been carried out in the systems mentioned below :

1. model compounds including a biocomplex;

2. rare-earth tungsten oxide bronzes;

3. calcined and reduced alumina supported tungsten oxide catalysts with metal oxide loading percentages varying between 4 to 12%;

4. calcined titania supported tungsten oxide catalysts with metal oxide loading percentages varying between 4 to 8% and

5. calcined and reduced alumina supported nickel-tungsten bimetallic catalysts with 20% metal loading.

The thesis is divided into six chapters. Chapter 1 gives an historical perspective of X-ray absorption spectroscopy and briefly reviews the work done on the tungsten compounds, bronzes and supported tungsten oxide catalysts. It also defines the scope and purpose of the present investigation.

Chapter 2 describes the preparation of the model compounds, tungsten bronzes and catalytic compounds of tungsten studied in the present investigation. The

experimental setup and the optimum conditions for obtaining the X-ray absorption spectra with finer details is also given in this Chapter. A single crystal X-ray absorption spectrometer, manufactured by Rigaku Corporation, Japan, having a wide-angle horizontal goniometer and equipped with appropriate electronics has been employed to record the X-ray absorption spectra at room temperature.

Chapter 3 gives the results of our observations on the shape of L_I and L_{III} discontinuities of tungsten in the pure metal and in its model compounds and complexes, wherein the oxidation state of tungsten varies widely. Results obtained on oxide bronzes and catalytic compounds of tungsten are also presented in this Chapter. Splitting of the L_{III}-absorption discontinuity was not observed in the compounds studied. However the L_I discontinuity was found to split into three components viz., pre-edge, that appears at the low energy side of the discontinuity, a shake-down peak and the strong absorption peak. These three features are respectively assigned to electronic transitions $2s \rightarrow 5d$, $2s \rightarrow 6s$ and $2s \rightarrow 6p$ based on a simple atomic model supported by theoretical considerations. The intensities of these components were found to depend primarily on the metal site symmetry. Based on the observations on intensities of the pre-edge features in tetrahedrally and octahedrally coordinated tungsten compounds having oxygen ligand, a method is suggested to determine the local structure of the tungsten ion in bronzes and catalytic compounds of tungsten.

Analysis of energy positions of the L_{III}-edge in tungsten compounds is presented in the Chapter 4. This analysis shows that the absorption discontinuity of tungsten in tungsten compounds shifts to the high energy side with respect to that in pure tungsten metal. When these energy positions are plotted against the coordination charge calculated using Batsanov's formalism, a parabolic relationship is obtained between these two physico-chemical quantities. These findings suggest that the edge positions are determined by the magnitudes of the coordination charges on the absorbing ion. The fractional effective coordination charges obtained from such functional relationship in the case of bronzes and catalysts indicate that there always exists an admixture of two types of bondings, namely, ionic and covalent in any compound. In addition to the above bonding information, the comparison of edge positions in bronzes and catalytic compounds of

tungsten with those in the model compounds suggest that the valence of tungsten ions in the bronzes and catalytic compounds is six. Our results in this respect are in good agreement with those obtained from other experimental techniques. Furthermore, a simple relationship between the edge positions and hardness of the ligating atom is also observed. This correlation is used to predict the nature of ligands in catalyst systems. The results of such correlations indicate that oxygen atoms are ligated to tungsten ion in the complex systems.

Results on EXAFS measurements on model tungsten oxides, sulphide and catalysts are presented in Chapter 5. The EXAFS spectra are analyzed by a method which combines Fourier transform and curve fitting techniques. The parameterized phase shifts and amplitude functions required for describing the W-O, W-S and W-W interactions are obtained from $CaWO_4$, $(NH_4)_2WS_4$ and WO_3. Application of phase shifts and amplitude function for oxygen to the EXAFS spectra of catalysts and bronzes yielded W-O bond distances to an accuracy consistently better than 0.03 $\mathring{A}$. The number and type of coordinating atoms were also determined with a reasonable degree of certainty. This work demonstrates the applicability of EXAFS for providing structural information about a specific absorbing center under complicated crystalline and partially crystalline conditions, and it lays a foundation for analysis of X-ray absorption spectra of industrially important bronzes and complicated catalyst systems.

In Appendix 1, a Rietveld method of crystal structure parameter refinements from powder diffraction patterns is briefly discussed. The crystal structure of the rare-earth tungsten oxide bronzes are not completely known. The structural parameters of the bronzes were deduced and refined using program DBWS 3.2 for Rietveld Analysis of X-ray and Neutron Powder Diffraction Pattern written by Young and coworkers from Georgia Institute of Technology, Atlanta, U.S.A. The results of such refinements are presented in this Appendix.

6.2   Suggestions for future work

This work, which is confined to the L_I and L_{III}-absorption spectra of tungsten, shows that X-ray absorption spectroscopy can be used to obtain fruitful and

direct information regarding the electronic structure and the nature of chemical bonding in different kind of materials. This information is however of a limited value to certain extent because of low intensity X-ray source and the low resolving power of the instrument used. The investigation of the absorption edges using a spectrometer of higher dispersion for recording can no doubt increase the precision of observed results. However, such spectrometer usually of bigger dimensions, enhance the difficulties in recording the spectra with low intensity X-ray source. In this laboratory, an attempt is being made to develop a double-crystal X-ray spectrometer. This spectrometer is proposed to have two detectors, one for measuring the original X-ray beam intensity and the other to measure intensity transmitted through the sample. Such a spectrometer will enable us to obtain more precise and accurate information on the electronic structure of materials. It will be rather interesting then to extend this work to several other rare-earth as well as alkali metal doped tungsten oxide bronzes. The effect of varying percentages of the dopants on the environment of the tungsten metal ion could also be systematized. In situ studies on alumina and titania supported tungsten oxide catalysts and many other bimetallic catalysts, wherein the loading percentages of metal oxides vary in regular or fractional intervals could lead us to many new features which were not covered under this study. In this work, a correlation between coordination charges on the absorbing atoms and the chemical shifts of the absorption discontinuity in different environments has been observed. A systematic extension of this work to study the effect, if any, of atomic number on the liganding atom on the correlation obtained above in the compounds of this investigation and other complex compounds of tungsten could provide us with the role played by the atomic number in determining the X-ray chemical shifts.

In this work, the charges on the absorbing atoms are calculated using the method of Batsanov. Although this model is simple and straightforward and can be applied to any compound, it would be worthwhile to develop a more refined and sophisticated approach to calculate the atomic charges. So also, the chemical parameters like electronegativity and ionicity calculated using the Pauling's formula could be more appropriately determined using such new approaches. A more comprehensive information regarding the electronic structures of the com-

plex oxides concerned could be obtained by recording the X-ray emission and absorption spectra on a double-crystal X-ray spectrometer using synchrotron radiation source or a rotating anode X-ray generator in fluorescence mode.

Further Investigations on the catalytic compounds and the oxide bronzes of tungsten by using various other spectroscopic techniques such as X-ray Photoelectron Spectroscopy (XPS), Auger Electron Spectroscopy (AES), Bremstrahlung Isochromat Spectroscopy (BIS), Laser Raman Spectroscopy, etc. coupled with the results of present X-ray Absorption Spectroscopic (XAS) study may prove to be extremely useful in obtaining detailed information regarding the electronic structure in the compounds studied.

Appendix A

Rietveld Refinement of X-ray Diffraction Data

The detailed crystal structure of rare-earth tungsten bronzes of the form $M_{0.1}WO_3$ (where M is a rare-earth) has not been hitherto reported in literature. The only information on the lattice parameters is presently available. X-ray diffraction patterns of these bronzes have been recorded by Ostertag [1] by using 114-mm Debye-Scherrer camera in the year 1966, and by Ganguly et al [2] in 1986 by using JEOL diffractometer. These authors obtained only the lattice parameters, inter-planar distances and miller indices. The exact intensities and atomic positions of tungsten and oxygen atoms and space group have not been determined. In the year 1993, JCPDS-ICDD published the update of the earlier JCPDS cards with intensities for different Bragg reflections in these compounds. However, no data on atomic coordinates of tungsten and oxygen atoms, crystal angles and space groups for these compounds have been given. In the present work, we thought it interesting to study and analyse in detail the X-ray diffraction patterns of the polycrystalline samples of a few representative rare-earth tungsten oxide bronzes and to obtain all the structural parameters by using recent methods [3, 4] for the analysis of X-ray diffraction patterns.

In the present investigation, X-ray diffraction patterns of two representative compounds of rare-earth tungsten oxide bronzes, namely, $La_{0.1}WO_3$ and $Eu_{0.1}WO_3$ were recorded on a Rigaku X-ray diffractometer (Model D/Max II-C) using monochromatized Cu K_α as well as Fe K_α radiation and a NaI:Tl scintillation detector. This diffractometer is equipped with a curved-crystal graphite monochromator for elimination of undesired K_β radiation. The measurements were carried out in the 2θ range 20°-140°. The powder diffraction pattern was scanned in steps of 0.02 (2θ) and fixed time counting was employed. At the end of data collection the stability of the intensity of the incident beam was checked by recording first few lines of pattern. The whole procedure was repeated three times using different samples prepared from the two bronzes. The diffractograms for these two bronzes are given in Figs. A.1 and A.2. Before giving the details of the analysis, we shall describe in brief the objectives and methods of the Rietveld refinement.
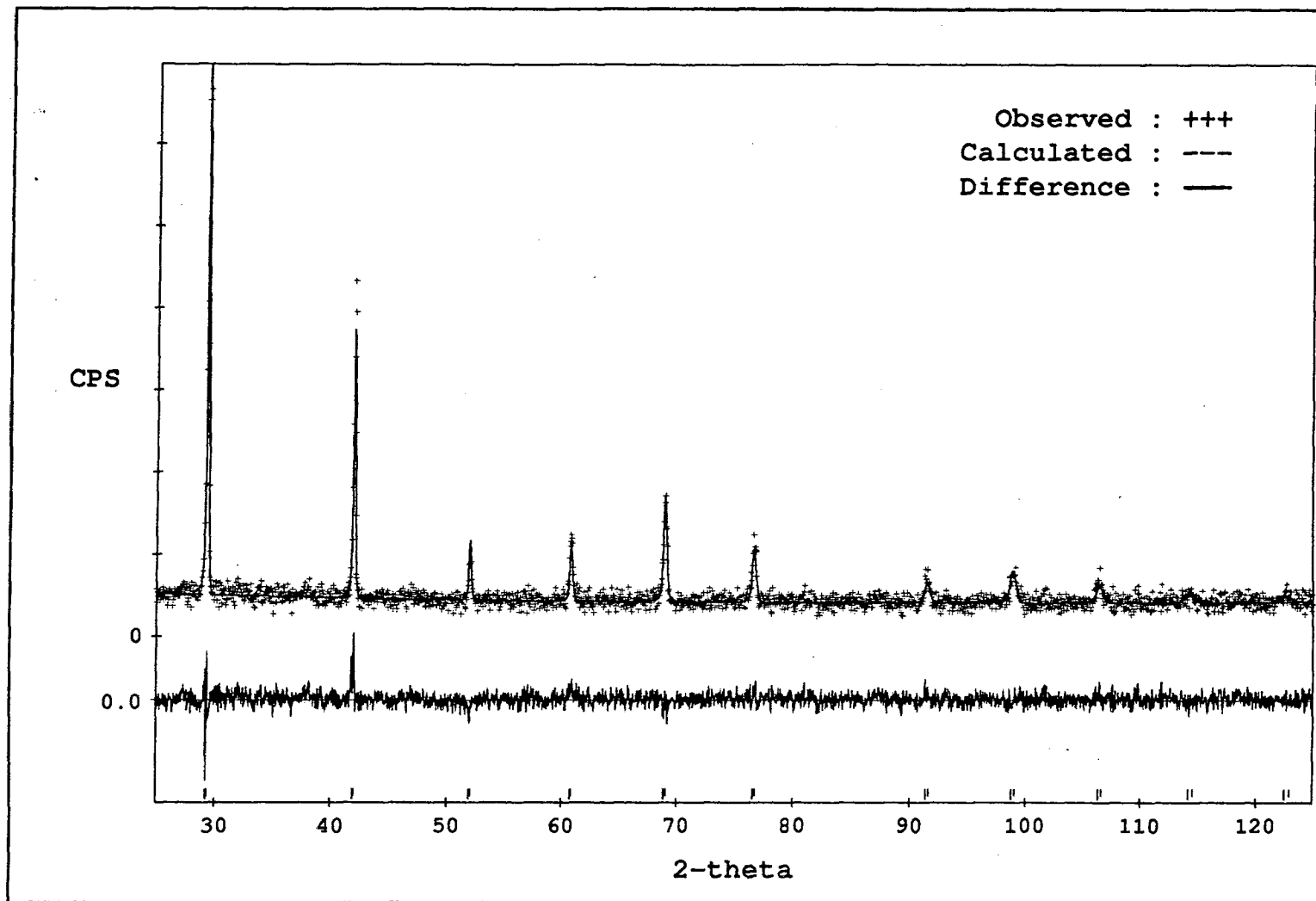
Fig.A.1 : The observed, calculated and difference profiles for lanthanum tungsten bronze.

The object of the Rietveld method is to produce refined values of crystal structure parameters from powder diffraction data. Many materials of great interest cannot be made available for study in the single crystal form. This may be because it is not possible to prepare single crystal form at all or because the single crystal form differ from the polycrystalline form with the properties of interest or due to unavailability of single crystal X-ray diffractometer. Thus, our basic understanding of the atomic scale mechanism is limited on the structural side by the information that can be deduced from the powder diffraction patterns. The Rietveld method has greatly extended the amount of structural details that can be obtained routinely from powder diffraction patterns. In this method, structural parameters such as atom coordinates, thermal motion and site occupancy parameters are adjusted in a least-squares refinement procedure until a best fit is obtained between entire calculated and observed powder diffraction patterns, as a whole. This method of pattern fitting has now been successfully applied to X-ray and Neutron diffraction data by several groups all over the world.

The program developed by Young and coworkers [5] to perform Rietveld analysis of X-ray or Neutron powder diffraction data collected with a θ-2θ diffractometer operated in a step scan mode (equal steps in 2θ) and either one or two (for e.g., Kα doublet) wavelengths. It basically uses Newton-Raphson algorithm to minimize the quantity :

$$S_y = \sum_i w_i \left[Y_i - Y_{ci} \right]^2 \tag{Λ.1}$$

where $w_i = 1/(Y_i)$, Y_i is observed (gross) intensity at i^{th} step, Y_{ci} is calculated intensity at the ith step and the sum is over all data points.

The calculated count Y_{ci} are determined by summing the contribution from the neighbouring Bragg reflections, K, plus the background, y_{bi};

$$Y_{ci} = sS_R A \sum_K \left[|F_K|^2 \Phi(2\theta_i - 2\theta_K) L_K P_K \right] + y_{bi} \tag{A.2}$$

where s is a scale factor, S_R is a function to model the effects of surface roughness, A is an absorption factor, F_K is the structure factor, Φ is a reflection profile function which approximates the effects of both instrumental and, possibly, specimen features. L_K contains the Lorentz, polarization and multiplicity factors, P_K is a preferred orientation function and Y_{bi} is the background contribution.

Observed : +++
Calculated : ---
Difference : ——

CPS

0

0.0

30   40   50   60   70   80   90   100   110   120
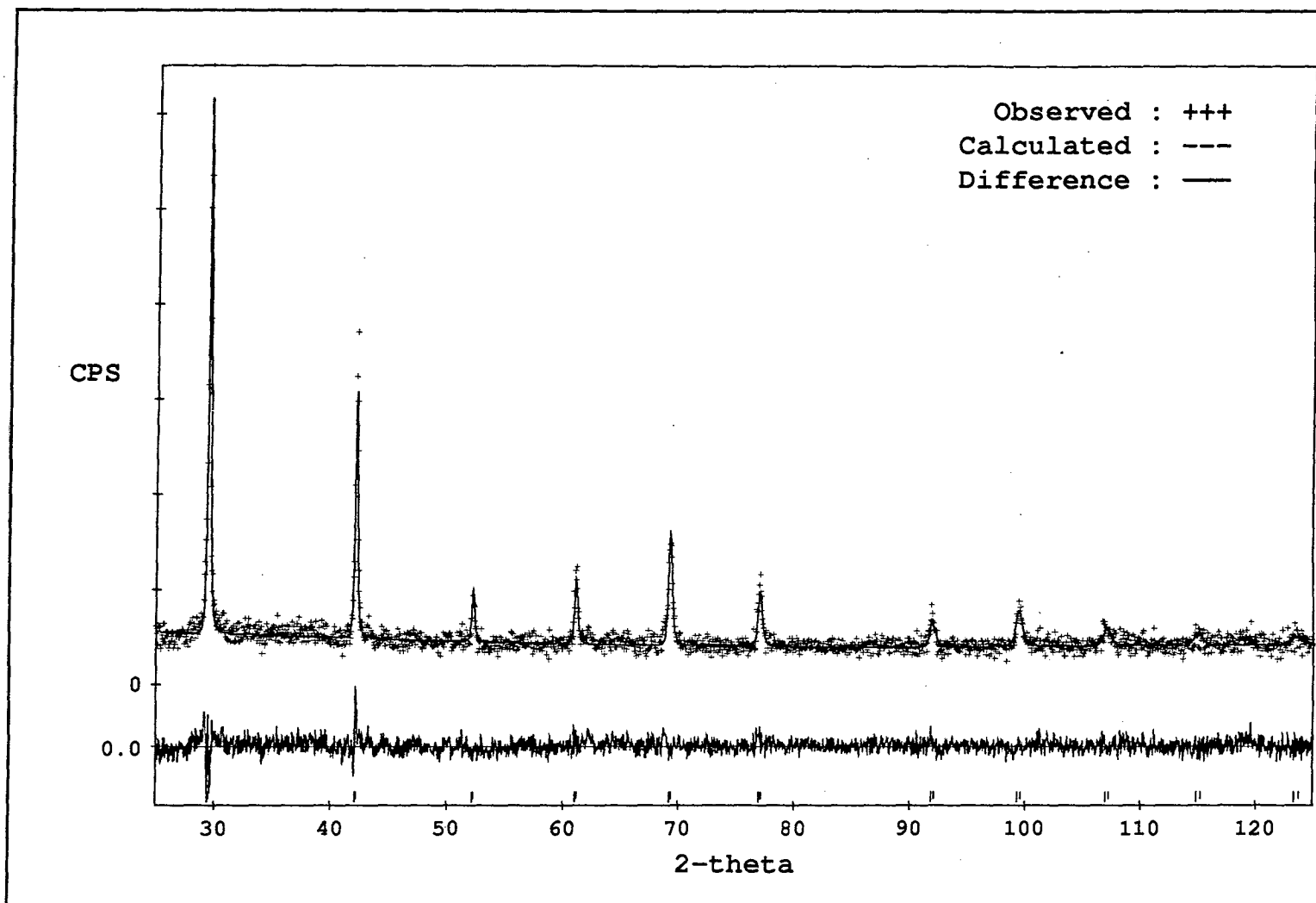
2-theta

Fig.A.2 : The observed, calculated and difference profiles for europium tungsten bronze.

The ratio of intensities for the two α wavelengths is observed in the calculation of $|F_K|^2$, so that only a single scale factor is required. The program uses different profile functions viz. Gaussian, Lorentizian, modified Lorentzian, Split Pearson, Pseudo-Voigt function, etc. depending on the diffraction patterns. At the end of the refinement, the structural parameters are then derived from the best fit. With this brief description about refinement method, we shall now discuss its application to our compounds.

X-ray examination of the samples of bronzes showed that single phase compounds were formed. The patterns of both the bronzes showed sharp diffraction lines corresponding to a simple cubic structure. Indexing of the power pattern was done using the computer program PDP11 (version 1.1) written by Calligaris [6]. From the result of this indexing, lattice parameters were calculated. The estimated values are 3.8245 Å and 3.8088 Å for $La_{0.1}WO_3$ and $Eu_{0.1}WO_3$ respectively. Since the single crystal analysis has not been done on these systems, it was assumed in the present work that the bronze system M_xWO_3 is isostructural with $Li_{0.1}WO_3$. It may be interesting to note that Ostertag [1] also assumed this kind of similarity of bronzes with the structure of $Li_{0.1}WO_3$.

$Li_{0.1}WO_3$ crystallizes in a simple cubic structure with the lattice parameter 3.729 Å and space group Pm3m [7]. For Rietveld analysis of our compounds, we have used [7] the structural parameters viz., space group, atomic coordinates, lattice parameter and thermal parameters of $Li_{0.1}WO_3$ as a starting model for the refinement. The Rietveld refinement were carried out with the help of revised program DBWS 3.2 (Distribution package : DBWS/9411) for Rietveld Analysis of X-ray and Neutron Powder Diffraction Pattern written by Young and coworkers from Georgia Institute of Technology, Atlanta, U.S.A.

A modified Lorentzian function (Mod 2 Lorentzian in the program of Young et al) was used for representation of the individual reflection profiles and the angular dependence of the peak FWHM (full width at half maximum), H_K, described by the usual quadratic form in $\tan(\theta)$:

$$Mod\ 2\ Lorentzian = \frac{\sqrt{C_3}}{2H_K}\left[1 + C_3(2\theta_i - 2\theta_K)^2/H_K^2\right]^{-3/2} \qquad (A.3)$$

where $C_3 = 4\left(\sqrt{2^{2/3}} + 1\right)$ and

$$H_k^2 = U\tan^2\theta + V\tan\theta + W \tag{A.4}$$

where U, V and W are parameters whose values are refined in the program. The background intensity was evaluated by refining a background function y_{bi} :

$$y_{bi} = \sum_{m=0}^{5} B_m[(2\theta_i/BKPOS) - 1]^m \tag{A.5}$$

where B_m are refined and BKPOS is the origin of polynomial for background in 2θ and the background refinements were effected through 90°. It is observed that the inclusion of the lower angle region for the background refinement made the refinements slightly unstable.

Refinement started with the guessing value of scale factor and then followed by the scale factor and lattice parameter. After these had stabilized, the zero correction, the halfwidth and the assymetry parameters were refined separately (three cycles for each group of parameters). Finally all the profile parameters and the scale factor were refined together followed by the refinement of overall isotropic thermal parameter. Reflections collected beyond 110° 2θ were broad and weak and contributed very little to the refinement and therefore the data beyond 125° 2θ were eliminated. The quantities used to estimate the agreement between the observations and the model during the course of Rietveld refinement can be written as

The profile R_p

$$R_p = \frac{\sum |y_i(obs) - (1/c)y_i(calc)|}{\sum y_i(obs)} \tag{A.6}$$

The weighted profile R_{wp}

$$R_{wp} = \left[\frac{\sum w_i[y_i(obs) - (1/c)y_i(calc)]^2}{\sum w_i[y_i(obs)]^2}\right]^{1/2} \tag{A.7}$$

The Bragg R_B

$$R_I = \frac{\sum |I(\text{``}obs\text{''}) - I(calc)|}{\sum I(\text{``}obs\text{''})} \tag{A.8}$$

The structure factor

$$R_F = \frac{\sum |I(\text{``}obs\text{''})^{(1/2)} - I(calc)^{(1/2)}|}{\sum I(\text{``}obs\text{''})^{(1/2)}} \tag{A.9}$$

162

The expected R_{exp}

$$R_E = \left[\frac{N - P}{\sum w_i [y_i(obs)]^2} \right]^{1/2} \qquad (A.10)$$

The goodness of fit GF

$$GF = \left[\frac{R_{wp}}{R_{exp}} \right]^2 \qquad (A.11)$$

The values of various R factors mentioned above are used to judge the quality of the fitted profiles and the quality of structure determination.

The observed, calculated and difference patterns for tungsten oxide bronzes, $La_{0.1}WO_3$ and $Eu_{0.1}WO_3$ are presented in Figs.A.1 and A.2. The observed 2θ values, Miller indices, relative intensities and the interplanar distances calculated are presented in Tables A.1(a) and (b) respectively for $La_{0.1}WO_3$ and $Eu_{0.1}WO_3$. As mentioned above, both the compounds crystallize in simple cubic structure. The application of Rietveld Analysis has fully revealed the details of the structure of the tungsten oxide bronzes studied in this investigation. The atomic coordinates, positional parameters, sites and symmetries for each tungsten and oxygen atoms are given in Table A.2. In Table A.3 are given the summary of Rietveld refined data for $La_{0.1}WO_3$ and $Eu_{0.1}WO_3$.

The similarity between the calculated and the observed profile for $La_{0.1}WO_3$ and $Eu_{0.1}WO_3$ implies that the space group, atomic parameters, thermal parameters and the assymetry parameters of the model $Li_{0.1}WO_3$ are also valid in the case of bronzes studied.

The refined lattice parameter value for $Eu_{0.1}WO_3$ matches very well with that reported by Ostertag [1] and in JCPDS card No. 19-465. For comparison of the lattice parameter of $La_{0.1}WO_3$ lattice parameter data is not available in the literature.

It may be noted that in $Li_{0.1}WO_3$, as shown by Zhong [7], the lithium atoms occupies unknown interstitial sites in the lattice. In rare-earth tungsten oxide bronzes also, the rare-earth ions may possibly go into the interstitial sites. However, it is difficult to confirm the location of the rare-earth ion from the present study. It requires some other experimental techniques to find out such interstitial site occupancy.

The various R factors obtained in the present analysis are consistent with those reported for X-ray Rietveld refinements [8, 9] thereby indicating the correctness of the structure refined. It may be interesting to note that even with less than optimum X-ray diffraction data, the Rietveld method allows a definitive structural solution to be achieved.

References

[1] W. Ostertag, Inorg. Chem., $\underline{5}$, 758 (1966).

[2] P. Ganguly and N. Y. Vasantacharya, Mat. Res. Bull., $\underline{21}$, 479 (1986).

[3] H. M. Rietveld, J. Appl. Crystallogr., $\underline{2}$, 65 (1969).

[4] NBS Spec. Pub. (U.S.) 567, p.143, Nat. Bur. Stand., Washington, D.C. (1980).

[5] R. A. Young, A. Sakthivel, T. S. Moss and C. O. Paisa-Santos, Rietveld Analysis of X-ray and Neurron Powder Diffraction Patterns, Program DBWS-9411 (Dec. 1994).

[6] M. Calligaris, PDP11 version(1.1), Dipartimento di Scienze Chimiche, Università di Trieste (Italy).

[7] Q. Zhong, J. R. Dahn and K. Colbow, Phys. Rev. B, $\underline{46}$, 2554 (1992).

[8] J. L. Hodeau and M. Marezio, J. Solid State Chem., $\underline{45}$, 170 (1982).

[9] L. Eriksson, D. Louer and P. E. Werner, J. Solid State Chem., $\underline{81}$, 9 (1989).

Table A.1: Observed 2θ values, Miller indices, Interplanar distances and Relative intensities for $La_{0.1}WO_3$ and $Eu_{0.1}WO_3$

(a) $La_{0.1}WO_3$

2θ	d	I/I_o	hkl
29.250	3.834	100	100
41.900	2.707	65	110
52.000	2.208	9	111
60.850	1.911	15	200
68.900	1.711	22	210
76.800	1.558	10	211
91.300	1.354	7	220
99.000	1.273	7	300
106.400	1.209	6	31
114.300	1.152	3	311
122.600	1.104	3	222

(b) $Eu_{0.1}WO_3$

2θ	d	I/I_o	hkl
29.450	3.808	100	100
42.150	2.692	55	110
52.250	2.198	9	111
61.100	1.904	15	200
69.300	1.703	20	210
77.000	1.555	13	211
91.900	1.347	6	220
99.450	1.269	8	300
106.800	1.206	5	310
114.750	1.149	3	311
123.400	1.099	3	222

Table A.2: Structure Parameters for cubic $La_{0.1}WO_3$ and $Eu_{0.1}WO_3$

Atom	Wycoff Position	Symmetry	Position
W	a	m3m	0,0,0
O(1)	d	4/mmm	1/2,0,0
O(2)	d	4/mmm	0,1/2,0
O(3)	d	4/mmm	0,,1/2

166

Table A.3: Rietveld Refinement Data for $La_{0.1}WO_3$ and $La_{0.1}WO_3$

Parameter	$La_{0.1}WO_3$	$Eu_{0.1}WO_3$
Cell parameter a ($\text{\AA}$)	3.8230	3.8096
Thermal parameter ($\text{\AA}$)^2	0.524	0.779
Assymetry parameter	1.194	-0.248
Scale factor(s)	0.688×10^{-7}	0.120×10^{-6}
Profile parameters :		
U	0.264	0.279
V	-0.161	-0.145
W	0.047	0.063
Profile shape function	Mod 2 Lorentzian	Mod 2 Lorentzian
Reliability factors :		
R_p	11.92%	10.72%
R_{wp}	14.98%	13.54%
R_{exp}	14.29%	14.16%
R_B	12.13%	11.84%
Goodness of fit	1.05	0.95
Occupancy :		
W	1.24	0.99
O(1)	1.0	1.0
O(2)	1.0	1.0
O(3)	1.0	1.0

ACKNOWLEDGEMENT

LIST OF PUBLICATIONS

1. X-ray Absorption Spectroscopic Study of Some Tungsten Bronzes and Catalytic Compounds

   Shantanu A. Gauns and P. R. Sarode

   Proc. Solid State Physics Symposium, held at S. V. University, Tirupati, Vol.35-C, 105 (December 1992)

2. Structural Investigations on Vanadium Compounds by XANES

   Anjli Chhikara, G. B. Parulekar, B. H. Sonaye, Shantanu A. Gauns, and P. R. Sarode

   Proc. Solid State Physics Symposium, held at University of Rajasthan, Jaipur, Vol.37-C, 113 (1994).

3. X-ray Spectroscopic Study of Vanadium Compounds

   P. R. Sarode, Anjli Chhikara, G. B. Parulekar, K. R. Priolkar, B. H. Sonaye, Shantanu A. Gauns and R. B. Prabhu

   X-ray Spectrometry (communicated).

4. XANES and EXAFS Studies of Alumina and Titania Supported Tungsten Oxide Catalysts

   Shantanu A. Gauns and P. R. Sarode

   J. Catal. (communicated).

170

ERRATUM

1. Page No.: 4, Line No.: 9 - either delocalised at the .....

2. Page No.: 6, Line No.: 3 - magnitude higher than the .....

3. Page No.: 67, Line No.: 16 - We see from these .....

4. Page No.: 68, Line No.: 19 - octahedrally coordinated tungsten ions ......

5. Page No.: 81, Line No.: 28 - since the 5d level ......

6. Page No.: 83, Line No.: 18 - on these complexes and .....

7. Page No.: 83, Line No.: 23 - $4t_2$ and $3a_1$, and .....

8. Page No.: 88, Line No.: 2 - catalysts is not $Al_2(WO_4)_3$.....

9. Page No.: 95, Line No.: 23 - may probably be ascribed .....

10. Page No.: 103, Line No.: 19 - compounds of tungsten suggesting .....

11. Page No.: 111, Line No.: 2 - likely to dominate the others.

12. Page No.: 127, Line No.: 19 - $k = \sqrt{\frac{2m}{\hbar^2}(E - E_o)}$